Local Gouging Detection and Tool Size Determination for 3-Axis Finish Machining of Sculptured Surface Parts

Shahid Hameed Khan

A Thesis

in

the Department

of

Mechanical and Industrial Engineering

Presented in Partial Fulfillment of the Requirements

for the Degree of Master of Applied Science (Mechanical Engineering) at

Concordia University

Montreal, Quebec, Canada

November 2006

Your file Votre référence
ISBN: 978-0-494-28939-6
Our file Notre référence
ISBN: 978-0-494-28939-6

ABSTRACT

Local gouging detection and tool size determination for 3-axis finish machining of sculptured surface parts

Shahid Hameed Khan

Today compound sculptured surfaces have been widely used to design complicated shapes and details of mechanical parts in the automotive, aeronautical, die and mold industries. The technology of machining these surfaces with high quality and efficiency is badly needed in the manufacturing industry. In Computer numerical control (CNC) finish machining of compound sculptured surface parts, local gouging is a major concern due to the geometric mismatch between the engaged regions of the cutting surface and the part surfaces. Specifically, local gouging will occur at a cutter contact point along the tangent direction, in which the normal curvature of the cutting surface is less than that of the part surface. In the past years, some researchers have applied curvature analysis techniques to local gouging detection for a single surface patch; however, a practicable, reliable approach to evaluating the geometric mis/match between the cutting and part surfaces has not yet been available. My research originally proposes an improved approach to detecting potential local gouging for compound surface patches and to determine an optimum tool size for local gouge free machining. This approach applies comprehensive curvature analysis to the engaged regions between the cutting and part surfaces in 3-axis finish machining by using different standard cutters. This research contributes to the research on sculptured surface machining with in-depth understanding about the geometric mis/match between the cutting and part surfaces and has great potential impact to advance CNC machining technique in the manufacturing industry.

ACKNOWLEDGEMENT

I would like to dedicate my thesis to the Department of Mechanical and Industrial Engineering, Concordia University. In hope that sharing my experience will help to enhance my effort in obtaining my goal. I would like to profoundly thank my supervisor **Dr. Chevy Chen,** Department of Mechanical & Industrial engineering, Concordia University, for his kind support, guidance, encouragement and for having trust in me throughout the course of my thesis. Without his help this thesis might not have been completed.

The financial support for this work from the Natural Science and Engineering Research Council of Canada (NSERC) is also thankfully acknowledged.

Table of Contents

List of Figures

List of Tables

Chapter 1 Introduction

1.1 Gouging in CNC Machining

Gouging is defined as an overcut/undercut phenomenon that is occurred by the interaction between model part geometry and cutter geometry or movement. These days in industries there is a high demand for parts with complex shapes mainly because of two reasons. Firstly, because the physical laws require a product to have a special shape in order to have good performance relating to aerodynamic or thermodynamic properties for example the body of a modern day car. Secondly, the consumer tastes tend to favor product of aesthetic appearance. A lot of money is invested in the design and analysis of these kinds of complex parts and if the part is gouged while machining, all the design and analysis part will go in vain. Hence it is very important to check whether the tool used to machine the part will gouge the part surface or not before the actual machining is done. There are mainly two types of gouging namely global and local gouging. A brief description is given below.

1.1.1 Global gouging

If a part surface is being machined by a tool at a point called the cutter contact point (CC point) and if the tool crashes into the part surface at any point other than in the vicinity of

the CC point, then this type of gouging is known as global gouging. This is illustrated with the help of Figure 1.1-Figure 1.2 .In these figures the tool is moving along the part surface at three different CC points namely A, B and C. In Figure 1.1 it can be seen that the tool is machining the CC point A and no portion of the tool is crashing into the part surface but as soon as the tool moves and starts to machine the CC point B, the other end of the tool (see Figure 1.2) touches the part surface at the point D. At this point if the tool follows the path from point D along the part surface. It will leave an uncut portion on the part surface as can be seen from Figure 1.2, but if follows a path from CC point B to CC point C, the other side of the tool will crash into the part surface and hence will overcut the part as can be seen from Figure 1.3 .Hence on both of these cases, gouging will occur and this type of gouging is known as global gouging.

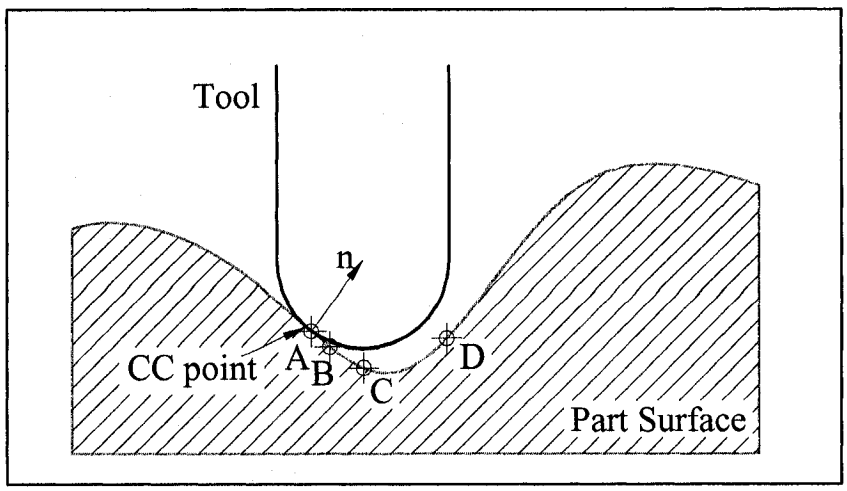

Figure 1.1. Cutter machines the part surface at CC point A.

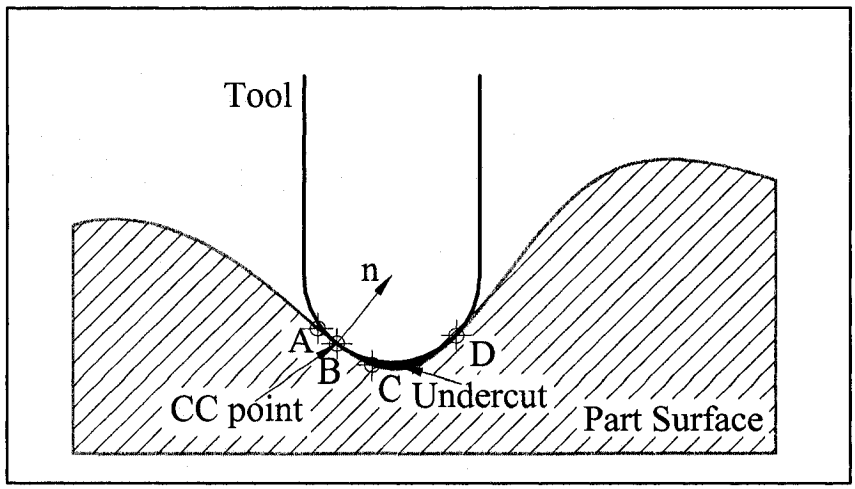

Figure 1.2. Cutter machines the part surface at CC point B.

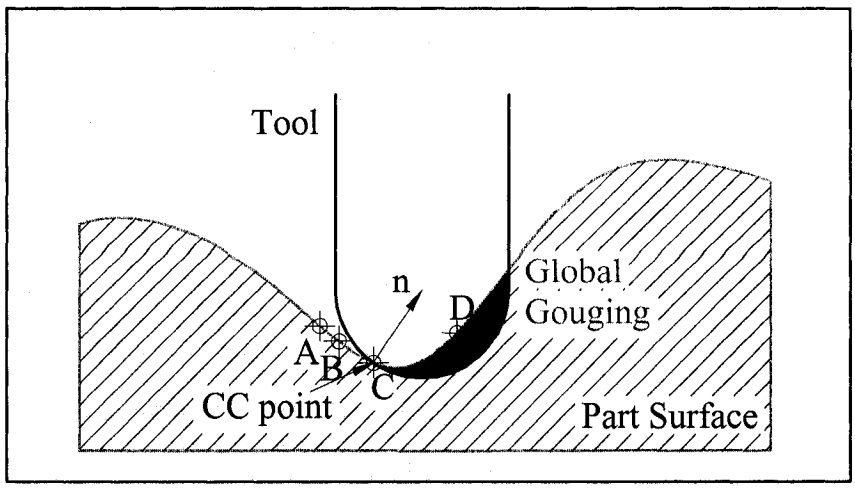

Figure 1.3. Cutter machines the part surface at CC point C.

1.1.2 Local gouging

If gouging occurs in the vicinity of the CC point, then this type of gouging in known as local gouging. It occurs when the normal curvature of the part surface at a CC point is greater than that of the normal curvature of the cutting surface of the tool. It has been illustrated with the help of Figure 1.4. In Figure 1.4 (a), a tool is machining a part surface at a CC point. At this CC point, the tool does not overcut the part in the vicinity of the CC point and hence it can be seen that there is no local gouging. In Figure 1.4 (b), a

bigger tool is used to machine the CC point and tool overcuts the part surface in the vicinity of the tool and therefore local gouging occurs.

In this thesis work local gouging is checked at different CC points on the part surface when being machined with different types of end mills on the 3-Axis CNC Machine. The brief introduction about CNC machines and end mills and the different terminologies involved with them is given in the following sections.

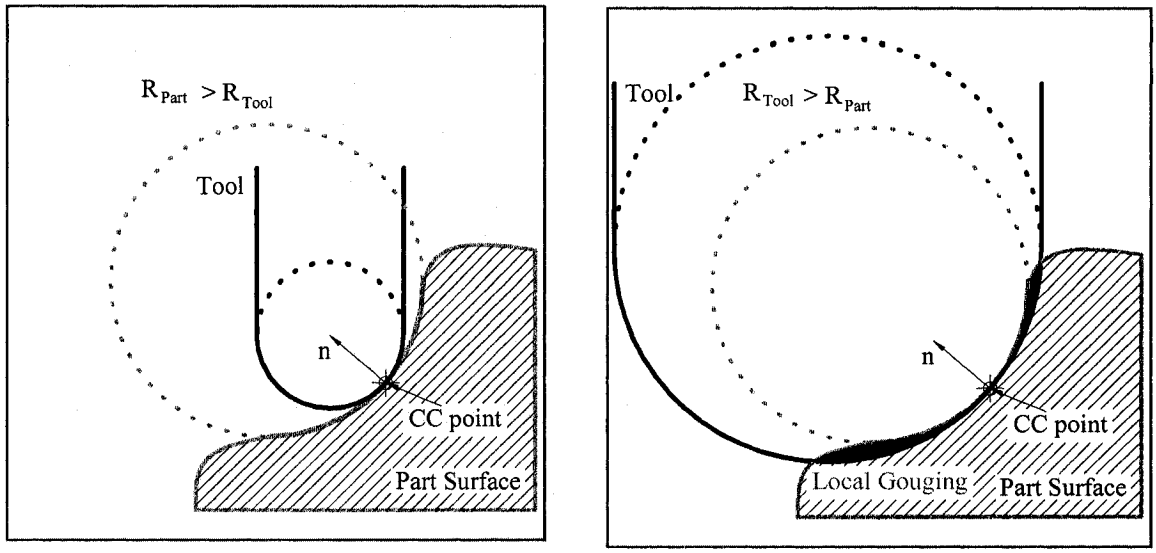

(a) Without local gouging (b) Local gouging

Figure 1.4. Tool and surface interaction at a CC point.

1.2 Computer Numerically-Control Machining

Numerical control (NC) is defined by the Electronic Industries Association (EIA) as "a system in which actions are controlled by the direct insertion of numerical data at some point. The system must automatically interpret at least some portion of this data [14]. CNC is defined as a self-contained numerical control system for a single machine tool that uses a dedicated computer controlled by stored instructions in the memory to implement some or all of the basic NC functions [14]. CNC machining plays an

important role in manufacturing industry. Unlike traditional machining methods, CNC machines can manufacture parts with complex shapes and high precision. Most parts with complex shape are currently machined with CNC machine tools. For example, the turbine blades of airplane engines are machined by CNC machines. Usually CNC machining has higher machining efficiency than traditional machining. They are being widely used in the aeronautical, automotive, and injection mould/die industries.

1.3 CNC Machining Strategies and CNC Machine Types

1.3.1 CNC machining process

Generally, the CNC machining consists of three steps: (1) rough machining, (2) semi-finish and finish machining, and (3) grinding/polishing. Rough machining removes the excess stock material quickly to form a shape slightly larger than the part design, thus high machining productivity or high metal removing rate is its primary concern. Finishing machining produces adequate quality surfaces by cutting the rough shape to the design. Better surface finishing requires costly and labor-intensive manual polishing at the final stage. Adequate quality surfaces, no gouging, and minimum machining time are the objectives of the finishing machining. Different machining strategies and determination of machining parameters lead to variations in machining productivity and surface quality. Gouge free CNC machining is thus one of the most important requirements of finish machining since it results in good surface quality.

1.3.2 CNC machine types

CNC machines are classified into three types: 2½-axis, 3-axis, and 5-axis CNC machines. The cutter on these machines includes three common types: ball, torus, and flat end-mill (see Figure 1.5). According to the different objectives of the rough and finishing machining, normally 2½-axis CNC machines are used for the rough machining, and 3-axis and 5-axis CNC machines are used for the finishing machining. Since this thesis focuses only on 3-axis CNC machining, a brief description is given in the following section.

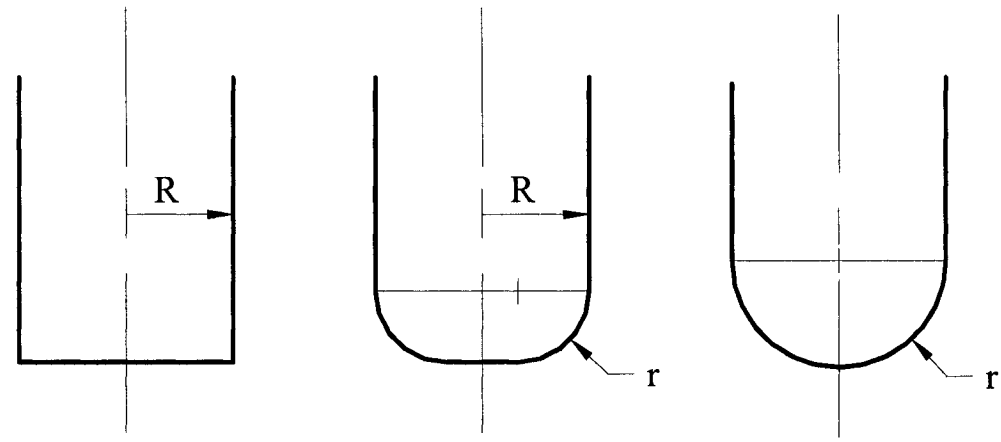

Figure 1.5. Three types of common milling cutters.

1.3.3 Three-axis CNC machining

Three-axis CNC machines are quite popular in the manufacturing industry due to its great features and added advantages. Three-axis CNC machining is exerted when a cutter of a 3-axis CNC machine moves along planned tool paths. This is because a 3-axis CNC machine executes three simultaneous motions including motions of the working table along X- and Y-axis and the cutter motion along Z-axis. Determined by the machine's architecture, the main feature of the machine is that the cutter orientation with

respect to the part is locked after the part is fixed on the worktable. A 3-axis CNC vertical milling machine is shown in Figure 1.7; the cutter orientation is always in the vertical direction.

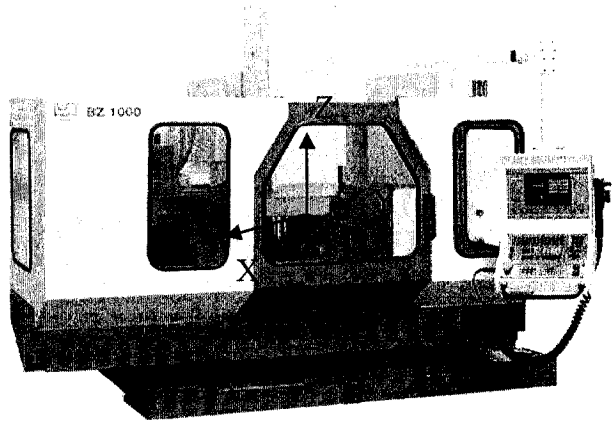

Figure 1.6. Diagram of a 3-axis CNC vertical milling machine.

The 3-axis CNC machining feature enjoys some advantages. These advantages generally are (a) higher stiffness and rigidity of the machine prevents chatter in machining; (b) machine accuracy is high enough for finishing machining; (c) programming for tool paths in 3-axis CNC machining is manageable; and (d) the machine is affordable even for small businesses and its maintenance is not too expensive. Moreover, 3-axis CNC machining is the main metal working operation in the production process. Statistics show that besides the accurate prismatic parts, a majority of sculptured parts in the die/mould industry are made with 3-axis CNC machines. Therefore, 3-axis CNC machining is a major force in manufacturing industry.

While 3-axis CNC machines are popular, they are not universally able to mill all parts. In certain setups, the cutter cannot access some surface regions (or surface patches) of a part without interfering with the part. Three-axis CNC machining for some complex parts is

only practical when all the surface patches to be machined can be accessed by the cutter. This means that for some parts with complex shapes, a preferred solution is 5-axis CNC machining

1.4 Related Work on Gouging Detection and Tool Size Determination for 3-Axis CNC Machining

Gouging is a common problem and has not been well resolved up to the present time. Gouge occurs in NC machining, but it may be caused in the design stage. Gouge can be eliminated either by using a smaller cutter or by revising the original design geometry. Therefore, the outcome of gouge detection is crucial for the consideration of parts modeling.

Among the published, curvature-related works, Glaeser et al. [6] and Pottmann et al. [7] mathematically described the concept of exhaustive curvature comparison and presented local and global conditions for 3-axis collision-free milling of sculptured surfaces. But neither a feasible method to implement these concept and conditions nor a practical example to verify them was provided. Yoon et al. [9] proposed a local condition for 5-axis collision-free milling based on the Taylor's quadratic approximations of the tool and part surfaces in the vicinity of a cutter contact point. Later Yoon [10] introduced the concept of machined region width to optimize the tool orientation for 5-axis machining. Since he assumed that these approximations were accurate in a large area, which is not true, these works are impractical. Rao and Sarma [1] applied the curvature comparison technique to the part and cutter-swept surfaces in order to detect

local gouging when using flat end-mills in 5-axis machining. Wang and Yu [17] determined the tool orientation along the minimum curvature direction for wider machining strips and carried out rough inspection for gouging. Unfortunately, detailed inspection for bull-nose end-mills was not conducted in these two research works.

To detect local gouging and select tool size, many approaches have been proposed without using the curvature-related method. Oliver et al. [11] first identified highly-curved regions on part free-form surfaces and then detected local and global gouging for 3-axis machining of these regions. Yang and Han [3] located iso-phote curves on the sculptured surfaces to find the patches accessible in 3-axis machining and selected a number of cutting tools for the minimum machining time. Yu et al. [5] initialized the tool orientation according to the tangent plane at a CC point on the surface and then determined a final orientation by detecting and eliminating the interference between the cutter and the part surface. George and Babu [12] found the self-intersection curves of the cutter location surface by applying optimization techniques and solving differential equations and deleted the locations that cause local gouging. Hatna and Grieve [2] pre-processed the surface in order to discard the zones of potential interference and generated interference-free tool paths in a simple sweeping process of the surface parametric space. These methods either cannot accurately detect local gouging or are very tedious in computation.

To overcome the drawbacks of the existing local gouging detection approaches, this research work proposes an improved approach to comprehensive curvature analysis for detecting local gouging in 3-axis compound sculptured surface machining. First, the

principal curvatures - the minimum and the maximum normal curvatures - and their corresponding directions - principal directions - of the tool's cutting surface are calculated, and based on the relationship between the tool and the part coordinate systems, these principal directions in the tool coordinate system are transformed to the part coordinate system. Second, the principal curvatures of the part surface and their directions are found in the part coordinate system. Then based on Euler's formulae, the normal curvatures of the cutting and the part surfaces can be calculated and compared in each tangent direction. This new technique is not only applied on the interior points of single surface but also on the interior points as well as on the boundary points of a compound part surfaces Finally, some practical examples are provided to verify this proposed approach. This research provides an in-depth understanding of the tool-surface geometric mismatch and can be readily applied to CNC machining in the manufacturing industry.

The part surface and the cutting surface of the tool is represented mathematically in the form of parametric equation in the Computer Aided Design and Computer Aided Manufacturing Systems (CAD/CAM). A brief introduction to the popular ways of representing curves and surfaces is given in the next chapter.

Chapter 2 Representation of Curves and Surfaces

2.1 Parametric and Non-Parametric Forms

A three dimensional (3D) object is composed of curves and surfaces. These curves and surfaces must be represented in the form of mathematical equation. The two most common methods of representing curves and surfaces in geometric modeling are parametric and non-parametric form. In the parametric form, the *x, y* and *z* coordinates of a point on a curve or surface are related to a parameter whereas in the nonparametric form the *x, y* and *z* coordinates of the point are directly related to a function. The parametric and nonparametric representation of a circle with radius *R* in the *xy* plane is shown in Equation (2.1) and (2.2) respectively.

$$x = R\cos\theta,\ y = R\sin\theta,\ z = 0 \quad \theta \in [0, 2\pi] \tag{2.1}$$

$$x^2 + y^2 - R^2 = 0,\ z = 0 \text{ or } y = \pm\sqrt{R^2 - x^2}, z = 0 \tag{2.2}$$

Both of the forms have their own advantages and disadvantages depending on the application for which the equation is used. Some properties of the parametric and nonparametric form are listed below.

Properties of parametric form:

- Easy to trace a curve or surface.
- Relatively difficult to check whether a point lies on the curve, surface or not.
- Closed (e.g., circles) and multi-valued (e.g., parabolas) curves and surfaces are easy to represent.
- Easy to evaluate tangent line to the curve when the curve has a vertical or near vertical tangent.
- Axis independent (easy to transform to another coordinate system).

Properties of non-parametric form:

- Difficult to trace curves or surfaces.
- Easy to check whether a point lies on the curve or surface.
- Closed (e.g., circles) and multi-valued (e.g., parabolas) curves and surfaces can be represented.
- It is difficult to evaluate tangent line to the curve when the curve has a vertical or near vertical tangent.
- Axis dependent (difficult to transform to another coordinate system).

In parametric form, each of the coordinates of a point on the curve or surface is represented separately as an explicit function of an independent parameter

$$\mathbf{C}(u) = \big(x(u), y(u)\big) \tag{2.3}$$

Thus, $\mathbf{C}(u)$ is a vector-valued function of the independent variable u and the range of u is usually is normalized to $[0,1]$. Therefore, the parametric representation is not

unique. To define a surface, two parameters are required, u and v. A parametric equation of a sphere of radius R is given in Equation (2.4). Holding u fixed and varying v generates the latitudinal lines of a sphere and holding v fixed and varying u generates the longitudinal lines as can be seen in Figure 2.1.

$$\mathbf{S}(u,v)=\begin{bmatrix}\mathbf{x}(u,v)\\ \mathbf{y}(u,v)\\ \mathbf{z}(u,v)\end{bmatrix}=\begin{bmatrix}R\cos(2\pi v)\cos\frac{\pi}{2}(2u-1)\\ R\sin\frac{\pi}{2}(2u-1)\\ -R\sin(2\pi v)\cos\frac{\pi}{2}(2u-1)\end{bmatrix}\left(u\in[0,1],v\in[0,1]\right) \tag{2.4}$$

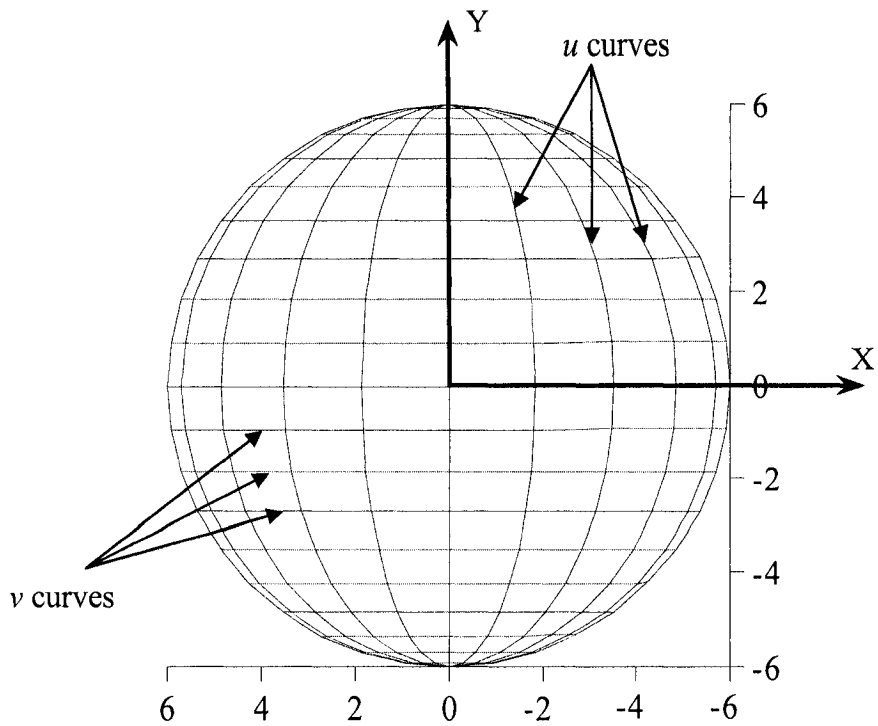

Figure 2.1. Parametric representation of a sphere.

Since interactive graphics is one of the most important feature of CAD/CAM/CAE and it is easy to trace a curve or surface and also because of the added advantages listed

above of using the parametric form, in CAD geometric modeling, the parametric form is used commonly.

2.2 Parametric Representation of Curves

The standard curves (e.g. circle, ellipse, hyperbola etc) are generally not sufficient to meet the functional requirements of the mechanical parts such as car bodies, airplane blades, shoe insoles that require free form curves or surfaces. So curves should be represented in such a way that it is represented with the help of control points and if required, the shape of a curve can be changed by changing the control points. Major CAD/CAM systems provide three types of free form curves namely: Bézier Curve, B-spline and NURBS Curve. A brief description of these curves is given below.

2.2.1 Bézier curves

Bézier curve, named after its inventor Pierre Bézier, is defined by the vertices of a control polygon that enclose the resulting curve. The degree of the curve is one less than the vertices of the polygon. Mathematically, it is expressed as

$$\mathbf{P}(u) = \sum_{i=0}^{n} \mathbf{P}_i \cdot B_{i,n}(n), \quad u \in [0,1] \tag{2.5}$$

where n is the degree of the base functions and u is the parameter. The number of control points is $n+1$. The base function $B_{i,n}(n)$ is the Bernstein Polynomial and is defined as

$$B_{i,n}(u) = \frac{n!}{i!(n-i)!} u^i (1-u)^{n-i} \tag{2.6}$$

The properties of the Bézier curve are listed below

- Bézier curve passes the first and last control points (P_0 and P_n).
- The control points compose a control polygon with $n + 1$ vertices.
- The first-order derivatives (tangent vectors) of a Bézier curve at its ends are

$$\mathbf{P}'_{(u=0)} = n \cdot (\mathbf{P}_1 - \mathbf{P}_0)$$
$$\mathbf{P}'_{(u=1)} = n \cdot (\mathbf{P}_n - \mathbf{P}_{n-1}) \tag{2.7}$$

- The curve is tangent to the first and last edge of the control polygon.
- If one control point is changed, it will affect the shape of the whole curve which is also known as global modification property.
- The sum of all the base functions is equal to one

Despite of the several advantages of the Bézier curve it has some disadvantages such as global modification property and the dependency of degree on the number of control points i.e. if higher number of control points is used, say six, it will result in a curve of degree five which is generally not used in CAD/CAM systems. These disadvantages are dealt with the use of B-spline curve which is discussed below.

2.2.2 B-spline curves

B-spline curve is a generalization of Bézier curve. It shares most of the characteristic of the Bézier curve but has some added advantage such as it provides local control of the curve shape as opposed to global control and it also has the ability to add control points without affecting the degree of the curve. Mathematically, it is expressed as

$$\mathbf{P}(u) = \sum_{i=0}^{n} \mathbf{P}_i \cdot N_{i,k}(u), \quad (t_{k-1} \le u \le t_{n+1}) \tag{2.8}$$

where the base (or blending) functions, $N_{i,k}(u)$, are defined with the recursive formula.

$$N_{i,k}(u) = \frac{(u - t_i)N_{i,k-1}(u)}{t_{i+k-1} - t_i} + \frac{(t_{i+k} - u)N_{i+1,k-1}(u)}{t_{i+k} - t_{i+1}},$$
$$N_{i,1}(u) = \begin{cases} 1 & t_i \le u < t_{i+1} \\ 0 & otherwise \end{cases} \tag{2.9}$$

where k is the order of the base function and is not related with the number of control points. The base function $N_{i,k}(u)$ adjusts the effect of the control point P on the curve shape; strong effect on the closer portion of the curve and weak effect on the farther portion of the curve.

In this definition a sequence of non-decreasing integers, t_i, called a knot vector specifies the range of the parameter u, and defines the base functions. Since there are $(n+1)$ base functions, $N_{0,k}(u), N_{1,k}(u), ...N_{i,k}(u), ...N_{n,k}(u)$, to be determined, the $(n+k+1)$ knot values (t_0 to t_{n+k}) are determined beforehand. In addition 0/0 in Equation (2.9) is pre-assumed to be zero. Basically two types of knot vectors are often used: periodic knot vector and non-periodic knot vector. The periodic knot vector can be determined by the following equation

$$t_i = i - k \quad (0 \le i \le n + k) \tag{2.10}$$

The non-periodic knot vector can be determined as follows,

- When the value of n is greater than or equal to the order of the base functions k,

the non-periodic knot vector are determined by

$$t_i = \begin{cases} 0 & 0 \le i < k \\ i-k+1 & k \le i \le n \\ n-k+2 & n < i \le n+k \end{cases} \tag{2.11}$$

- When the value of n is less than the order of the base functions k, the non-periodic knot vectors are determined by

$$t_i = \begin{cases} 0 & 0 \le i < k \\ 1 & k \le i \le n+k \end{cases} \tag{2.12}$$

Because the parameter intervals defined by the periodic and non-periodic knot vectors by Equations (2.10), (2.11) and (2.12) are uniform, the B-spline curve based on the uniform knots is called a uniform B-spline curve.

Properties of B-spline curves

- The order of the curve can be changed without changing the number of control points as can be seen in Figure 2.2.

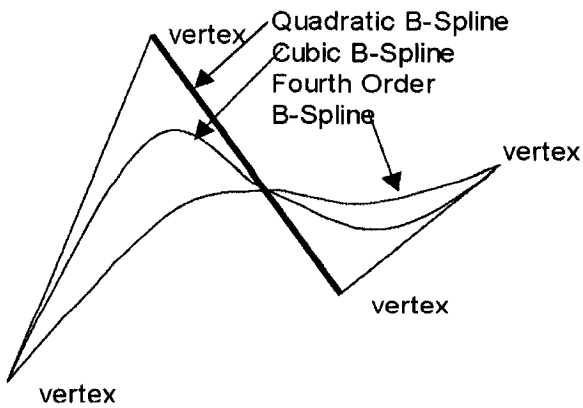

Figure 2.2. Different order B-spline curves with four control points.

- Curve shape can be modified locally by moving the control points. A control point only influences k curve segments of the B-spline curve.

B-spline curves were able to overcome the problems encountered by the Bézier curve i.e. the global modification property and the dependency of the degree on the number of control points. But it still has some disadvantages for example one cannot exactly represent the conic curves (circle, parabola etc.) using the B-spline curves. The conic curves can be exactly represented using NURBS curve which is discussed below.

2.2.3 NURBS curves

NURBS stands for Non-Uniform Rational B-Spline. It is a generalization of all the curves discussed above. Mathematically it can be represented as

$$\mathbf{P}(u) = \frac{\sum_{i=0}^{n} h_i \cdot \mathbf{P}_i \cdot N_{i,k}(u)}{\sum_{i=0}^{n} h_i \cdot N_{i,k}(u)} \tag{2.13}$$

Where $\mathbf{P}_i$ are the control points, and $N_{i,k}(u)$ are the k_{th} degree B-Spline basis functions defined by the non-uniform knot vector.

For NURBS curves, each control point has an associated weight h_i value that affects the shape locally near that point. This weight value is the result of the rational aspect of NURBS, which means that the equation is defined as a fraction or ratio of polynomials. The purposes of the weights are to allow for exact descriptions of conic shapes and to add more user control over the shape of the surface. However, in practice, changing a control point weight value can cause more problems for curve or surface fairing. The best

approach is to apply weight changes only near the end of the design process to achieve very specific local effects.

The NURBS equation can be represented in terms of rational (function) coefficients of the control points:

$$\mathbf{P}(u) = \sum_{i=1}^{n} R_{i,k}(u) \cdot \mathbf{P}_i , \tag{2.14}$$

where

$$R_{i,k}(u) = \frac{N_{i,k}(u) \cdot h_i}{\sum_{j=0}^{n} h_j \cdot N_{j,k}(u)} \tag{2.15}$$

The properties of the (rational) basis functions of NURBS, $R_{i,k}(u)$. Thus, they carry forward nearly all the analytic and geometric characteristics of their non-rational B-Spline counterparts. In particular:

- Non-negativity: each rational basis function is positive or zero for all parameter values, i.e., $R_{i,k}(u) \geq 0$.
- Partition of unity: the sum of the rational B-Spline basis functions is one, i.e. $\sum_{i=1}^{n} R_{i,k}(u) = 1$, for all u in [0, 1].
- Local support: $R_{i,k}(u) = 0$ except in the range $u_i \leq u < u_{i+k+1}$. This property guarantees that changing the location of a given control point will only change the shape of the curve in its neighborhood – not globally.
- Generic case of B-spline: If all the weights, $h_i = 1$, then the NURBS becomes the usual B-spline curve.

From the above definitions and properties, some other properties of the NURBS curve

can be derived:

- $P(0) = P_0$ and $P(1) = P_n$, that is, the curve begins at the first control point, and ends at the last control point.
- Affine invariance: Since the curve depends linearly on each control point – hence the affine transformation can be applied (rotation, translation) to the curve by just applying it to the control points.
- Convex hull property: The curve lies entirely within the convex hull of the control points.
- Local control: A change in position or weight of the i_{th} control point, P_i, will only change the curve in the interval $[u_i, u_{i+k+1}]$. Also note that increasing the weight tends to 'pull' the curve towards the corresponding control point; decreasing the weight 'pushes' the curve away from the control point.

Another big advantage that a NURBS curve has over a B-spline is that NURBS can exactly represent the conic curves- circles, ellipses, parabolas, and hyperbolas. By contrast, these curves can be represented by B-spline equations only in an approximate manner.

2.3 Parametric Representation of Surfaces

2.3.1 Bézier surfaces

The Bezier surface is formed as the Cartesian product of the blending functions of two orthogonal Bezier curves.

$$\mathbf{P}(u,v)=\sum_{i=0}^{n}\sum_{j=0}^{m}\mathbf{P}_{i,j}B_{i,n}(u)B_{j,m}(v) \qquad (u\in[0,1],v\in[0,1])$$

where $\boldsymbol{P}_{i,j}$ is the i,j-th control point. There are $n+1$ and $m+1$ control points in the u and v directions respectively. The corresponding properties of the Bezier curve apply to the Bezier surface:

- The surface does not in general pass through the control points except for the corners of the control point grid.
- The surface is contained within the convex hull of the control points.

Along the edges of the grid patch the Bezier surface matches that of a Bezier curve through the control points along that edge.

Figure 2.3. Convex hull property of Bezier surfaces.

2.3.2 B-spline surfaces

B-spline surface is defined by the following equation:

$$P(u,v)=\sum_{i=0}^{n}\sum_{j=0}^{m}P_{i,j}\cdot N_{i,k}(u)\cdot N_{j,l}(v) \qquad (s_{k-1}\le u\le s_{n+1}, t_{l-1}\le v\le t_{m+1}) \tag{2.16}$$

where $P_{i,j}$ is the i,j-th control point , $N_{i,k}(u)$ and $N_{j,l}(u)$ are B-spline basis functions of degree k and l, respectively. These base functions are defined by the knot vectors, s_0, s_1, ... s_{n+k} and t_0, t_1,... t_{l+m}, respectively. When a B-spline is based on non-periodic knots, it has properties similar to those of a Bézier surface except its strong local control property.

2.3.3 NURBS surfaces

A NURBS surface of order k in the u-direction and l in the v-direction is a piecewise vector function, defined as:

$$\mathbf{P}(u,v)=\frac{\sum_{i=0}^{n}\sum_{j=0}^{m}h_{i,j}\cdot\mathbf{P}_{i,j}\cdot N_{i,k}(u)\cdot N_{j,l}(v)}{\sum_{i=0}^{n}\sum_{j=0}^{m}h_{i,j}\cdot N_{i,k}(u)\cdot N_{j,l}(v)} \qquad (u\in[s_{k-1},s_{n+1}], v\in[t_{l-1},t_{m+1}]) \tag{3.15}$$

$$\mathbf{P}(u,v)=\sum_{i=0}^{n}\sum_{j=0}^{m}R_{i,j}(u,v)\cdot\mathbf{P}_{i,j} \tag{3.16}$$

where

$$R_{i,j}(u,v)=\frac{N_{i,k}(u)\cdot N_{j,l}(v)\cdot h_{i,j}}{\sum_{i=0}^{n}\sum_{j=0}^{m}h_{i,j}\cdot N_{i,k}(u)\cdot N_{j,l}(v)}.$$

As for the B-Splines, the $\mathbf{P}_{i,j}$ form a $(n+1)\times(m+1)$ mesh of control points; each control point is associated with a positive, real weight, $h_{i,j}$; and the $N_{i,k}(u)$ and $N_{j,l}(u)$, are the usual B-spline basis functions.

By and large, all the properties of NURBS curve, such as non-negativity, partition of unity, local support, etc. Furthermore, it is easy to see that when each $h_{i,j}=1$, the summation in the denominator is also equal to 1 (partition of unity property of B-spline basis functions), and therefore the NURBS will become a B-Spline surface. Further, if the knot vectors are restricted to the form {0, ..., 0, 1, ..., 1}, then the basis functions become the Bezier basis functions of degree *n*, and so *P(u,v)* is a Bezier surface.

Since NURBS are piecewise rational polynomials, they allow us exact representations of some important surface/curve types (e.g. sphere/circle). With this characteristic, we can potentially use the same representation scheme for all surfaces of a solid model, without having to write separate "case-based" functions to handle each different surface type in a CAD program.

For most practical designs, NURBS are considered to be fairly powerful – they can be used to represent complex shapes, and allow easy interface for several important CAD functional requirements. These requirements include ease/efficiency of computing the surface coordinates, computing derivatives, changing shape of the surface, local control on the shape using either the control mesh, or the weights, or the degree of the

polynomial etc. Therefore, in this thesis the NURBS surface is used to represent part surface and provide enough accuracy and easy adjustment properties.

Chapter 3 Elementary Computational Differential Geometry

The differential geometry of curves and surfaces is fundamental in Computer Aided Design. In order to detect gouging, the normal curvatures of the part surface and the cutting surface have to be calculated. A brief description of the mathematics involved in determining the normal curvatures of curves and surfaces is discussed below.

3.1 Differential Geometry of Curves

3.1.1 Tangent to a curve

A unit tangent vector $(\mathbf{T})$ to a parametric curve, $\mathbf{r} = \mathbf{r}(u)$ is given by

$$\mathbf{T} = \frac{d\mathbf{r}}{du} \Big/ \left| \frac{d\mathbf{r}}{du} \right| \tag{4.1}$$

provided that $\frac{d\mathbf{r}}{du} \neq 0$. If arc length s is taken as a parameter, then the tangent vector is given by

$$\mathbf{T} = \frac{d\mathbf{r}}{ds} \tag{4.2}$$

From the above two equations and by denoting differentiation with respect to u by a dot

$$\dot{\mathbf{r}} = \dot{s}\mathbf{T} \tag{4.3}$$

3.1.2 The principal normal vector, binormal to a curve

The vector $\dot{\mathbf{T}} = \frac{d\mathbf{T}}{du}$ is normal to the unit tangent vector $\mathbf{T}$. A unit vector $\mathbf{N}$ in the direction of $\dot{\mathbf{T}}$ is known as the principal normal vector. When the parameter is the arc length s, the two vectors are related by the following equation

$$\frac{d\mathbf{T}}{ds} = k \cdot \mathbf{N} \tag{4.4}$$

where k is as the *curvature* of the curve. A third vector defined by the cross product of the unit tangent vector (**T**) and principal normal vector (**N**) is **known** as the binormal vector **B**. Mathematically, it is expressed as

$$\mathbf{B} = \mathbf{T} \times \mathbf{N} \tag{4.5}$$

The three vectors are shown in Figure 4.1.

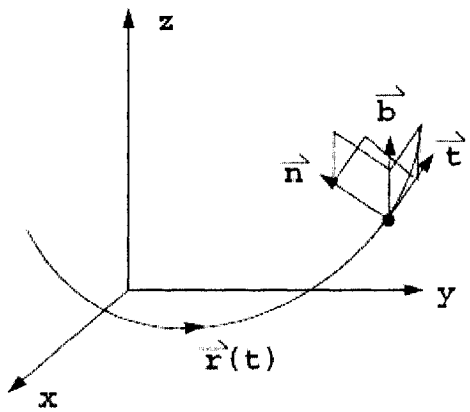

Figure 3.1. The tangent, normal, and bi-normal vectors of a space curve.

The plane defined by normal and binormal vectors is called the *normal plane* and the plane defined by binormal and tangent vector is called the *rectifying plane*. The plane defined by normal and tangent vectors is called the *osculating plane*.

3.1.3 Torsion of a curve and Frenet-Serret formulae

The twisted nature of a curve can be determined by evaluating $\frac{d\mathbf{B}}{ds}$. For a planar curve $\frac{d\mathbf{B}}{ds} = 0$, but for the non-planar curve $\frac{d\mathbf{B}}{ds} = -\tau \cdot \mathbf{N}$, where τ is called the torsion of the curve. Also it can be shown that $\frac{d\mathbf{N}}{ds} = \tau \cdot \mathbf{B} - k \cdot \mathbf{N}$.

These equations are collectively known as the *Frenet-Serret* formulae. They are listed below

$$\frac{d\mathbf{r}}{ds} = \mathbf{T} \tag{4.6}$$

$$\frac{d\mathbf{T}}{ds} = k \cdot \mathbf{N} \tag{4.7}$$

$$\frac{d\mathbf{N}}{ds} = \tau \cdot \mathbf{B} - k \cdot \mathbf{N} \tag{4.8}$$

$$\frac{d\mathbf{B}}{ds} = -\tau \cdot \mathbf{N} \tag{4.9}$$

If the differentiation with respect to s is represented by a prime, the *Frenet-Serret* formulae can be represented in matrix form as

$$\begin{bmatrix} \mathbf{T}' \\ \mathbf{N}' \\ \mathbf{B}' \end{bmatrix} = \begin{bmatrix} 0 & k & 0 \\ -k & 0 & \tau \\ 0 & -\tau & 0 \end{bmatrix} \begin{bmatrix} \mathbf{T} \\ \mathbf{N} \\ \mathbf{B} \end{bmatrix} \tag{4.10}$$

When the parameter is u rather than s, the equivalent equations are

$$\mathbf{T} = \dot{\mathbf{r}} / \dot{s} \tag{4.11}$$

$$k \cdot \mathbf{B} = (\dot{\mathbf{r}} \times \ddot{\mathbf{r}}) / \dot{s}^3 \tag{4.12}$$

$$\mathbf{N} = \mathbf{B} \times \mathbf{T} \tag{4.13}$$

$$\tau = \dot{\mathbf{r}} \cdot (\ddot{\mathbf{r}} \times \dddot{\mathbf{r}}) / \dot{s}^6 k^2 \tag{4.14}$$

$$\dot{s} = |\dot{\mathbf{r}}| \tag{4.15}$$

3.2 Differential Geometry of Surfaces

3.2.1 Tangent plane and surface normal vector

Tangent plane at a point $\mathbf{r} = \mathbf{r}(u_0, v_0)$ is the union of tangent vectors of all curves on the surface that passes through $\mathbf{r} = \mathbf{r}(u_0, v_0)$, as shown in Figure 4.2.

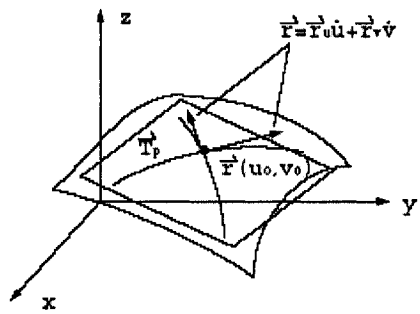

Figure 3.2. The tangent plane at a point on a surface.

A unit surface normal vector $\mathbf{n}$ at point $\mathbf{r} = \mathbf{r}(u_0, v_0)$ is a unit vector perpendicular to the tangent plane, as shown in Figure 3.3 , and is given by

$$\mathbf{n} = \pm\left(\frac{\partial \mathbf{r}}{\partial u} \times \frac{\partial \mathbf{r}}{\partial v}\right) \Big/ \left|\frac{\partial \mathbf{r}}{\partial u} \times \frac{\partial \mathbf{r}}{\partial v}\right| \tag{4.16}$$

The sense of $\mathbf{n}$ must be chosen to suit the application

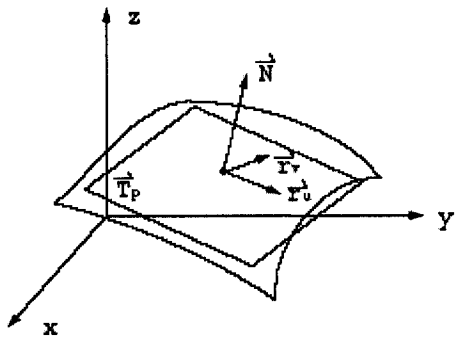

Figure 3.3. The normal to the point on a surface.

3.2.2 Curves on a surface

Let a parametric surface be represented by $\mathbf{r} = \mathbf{r}(u,v)$, then $\mathbf{r} = \mathbf{r}\big(u(t),v(t)\big)$ is a curve lying on the surface. A tangent vector to a curve on a surface is evaluated by differentiating $\mathbf{r} = \mathbf{r}(t)$ with respect to the parameter t by using the chain rule. Representing differentiation with respect to t with a dot, the tangent vector is given by

$$\dot{\mathbf{r}} = \frac{\partial \mathbf{r}}{\partial u}\dot{u} + \frac{\partial \mathbf{r}}{\partial v}\dot{v} = \mathbf{A}\dot{\mathbf{u}} \tag{4.17}$$

where

$$\mathbf{u} = \big[u(t), v(t)\big]^T$$

$$A = \begin{bmatrix} \dfrac{\partial x}{\partial u} & \dfrac{\partial x}{\partial v} \\ \dfrac{\partial y}{\partial u} & \dfrac{\partial y}{\partial v} \\ \dfrac{\partial z}{\partial u} & \dfrac{\partial z}{\partial v} \end{bmatrix} = \begin{bmatrix} \dfrac{\partial \mathbf{r}}{\partial u} & \dfrac{\partial \mathbf{r}}{\partial v} \end{bmatrix}$$

3.2.3 Normal curvature of surfaces

The **normal curvature** k_n of a surface in the direction **Aú** is the curvature of the intersection curve between the surface and the plane containing the surface normal ***n*** and the tangent vector. The normal curvature of the surface is thus a measure of how much a surface is "curving" in a certain direction as shown in Figure 3.4, it is calculated by

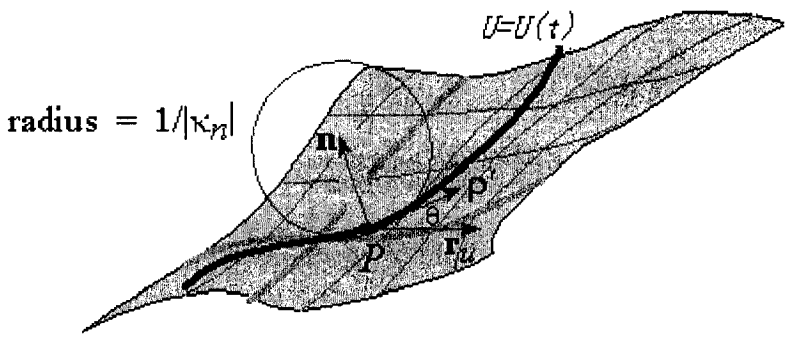

Figure 3.4. Normal curvature of the surface.

$$k_n = \frac{\dot{\mathbf{u}}^{\mathrm{T}} \cdot \mathbf{D} \cdot \dot{\mathbf{u}}}{\dot{\mathbf{u}}^{\mathrm{T}} \cdot \mathbf{G} \cdot \dot{\mathbf{u}}} \tag{4.18}$$

Where **G** is the first fundamental matrix and is given by

$$\mathbf{G} = \begin{bmatrix} g_{11} & g_{12} \\ g_{21} & g_{22} \end{bmatrix} = \begin{bmatrix} \frac{\partial \mathbf{r}^T}{\partial u} \cdot \frac{\partial \mathbf{r}}{\partial u} & \frac{\partial \mathbf{r}^T}{\partial u} \cdot \frac{\partial \mathbf{r}}{\partial v} \\ \frac{\partial \mathbf{r}^T}{\partial v} \cdot \frac{\partial \mathbf{r}}{\partial u} & \frac{\partial \mathbf{r}^T}{\partial v} \cdot \frac{\partial \mathbf{r}}{\partial v} \end{bmatrix} \tag{4.19}$$

D is the second fundamental matrix and is given by

$$\mathbf{D} = \begin{bmatrix} d_{11} & d_{12} \\ d_{21} & d_{22} \end{bmatrix} = \begin{bmatrix} \mathbf{n}^T \cdot \frac{\partial^2 \mathbf{r}}{\partial u^2} & \mathbf{n}^T \cdot \frac{\partial^2 \mathbf{r}}{\partial u \partial v} \\ \mathbf{n}^T \cdot \frac{\partial^2 \mathbf{r}}{\partial v \partial u} & \mathbf{n}^T \cdot \frac{\partial^2 \mathbf{r}}{\partial v^2} \end{bmatrix} \tag{4.20}$$

3.2.4 Principal curvature of surfaces

The maximum and minimum values of the normal curvatures are known as the principal curvatures and the direction in which k_n takes the maximum and minimum values with respect to $\dot{\mathbf{u}}$ is called the principal directions of the normal curvatures. Principal curvatures and directions can be calculated as

From Equation (4.18), we have

$$\dot{\mathbf{u}}^{\mathrm{T}}\mathbf{G}\dot{\mathbf{u}}\cdot k_n = \dot{\mathbf{u}}^{\mathrm{T}}\mathbf{D}\dot{\mathbf{u}}$$

or

$$\mathbf{D}\dot{\mathbf{u}} - \mathbf{G}\dot{\mathbf{u}}\cdot k_n = 0$$

$$\left(\mathbf{D} - \mathbf{G}\cdot k_n\right)\dot{\mathbf{u}} = 0$$

or

$$(d_{11} - k_n g_{11})\dot{\mathbf{u}} + (d_{12} - k_n g_{12})\dot{\mathbf{v}} = 0$$

and

$$(d_{21} - k_n g_{21})\dot{\mathbf{u}} + (d_{22} - k_n g_{22})\dot{\mathbf{v}} = 0 \qquad (4.21)$$

Eliminating $\dot{\mathbf{u}}$ and $\dot{\mathbf{v}}$, we obtain

$$|\mathbf{G}|k_n^{\,2} - (g_{11}d_{22} + d_{11}g_{22} - 2g_{12}d_{12})k_n + |\mathbf{D}| = 0 \qquad (4.22)$$

This equation can be considered as a quadratic equation. So we have the following results:

$$K = k_{\max}k_{\min} = \frac{|\mathbf{D}|}{|\mathbf{G}|}$$

$$H = (k_{\max} + k_{\min})/2 = \frac{(g_{11}d_{22} + d_{11}g_{22} - 2g_{12}d_{12})}{2|\mathbf{G}|} \qquad (4.34)$$

$$\therefore\ k_{\max} = H + \sqrt{H^2 - K}; \qquad k_{\min} = H - \sqrt{H^2 - K}$$

where K is called Gaussian Curvature and H is called Mean Curvature. k_{max} and k_{min} is the maximum normal curvature and minimum normal curvature.

Meanwhile, the principal direction of the maximum curvature $\mathbf{T}_{s,\max}$ is $\mathbf{T}_{s,\max} = du_{\max} \cdot \mathbf{S}_u(u,v) + dv_{\max} \cdot \mathbf{S}_v(u,v)$, where $du_{\max}$ and $dv_{\max}$ are obtained by the solving the system of linear equation given in Equation (4.21)

$$\begin{bmatrix} du_{\max} \\ dv_{\max} \end{bmatrix} = \begin{bmatrix} k_{s,\max} \cdot g_{12} - d_{12} \\ d_{11} - k_{s,\max} \cdot g_{11} \end{bmatrix} \tag{4.35}$$

If Equation (4.35) comes out to be a null matrix, then Equation (4.36) is used to obtain the values of $du_{\max}$ and $dv_{\max}$

$$\begin{bmatrix} du_{\max} \\ dv_{\max} \end{bmatrix} = \begin{bmatrix} k_{s,\max} \cdot g_{22} - d_{22} \\ d_{21} - k_{s,\max} \cdot g_{21} \end{bmatrix} \tag{4.36}$$

Similarly, the principal direction of the minimum curvature $\mathbf{T}_{s,\min}$ is $\mathbf{T}_{s,\min} = du_{\min} \cdot \mathbf{S}_u(u,v) + dv_{\min} \cdot \mathbf{S}_v(u,v)$, where $du_{\max}$ and $dv_{\max}$ are obtained by the solving the system of linear equation given in Equation (4.21).

$$\begin{bmatrix} du_{\max} \\ dv_{\max} \end{bmatrix} = \begin{bmatrix} k_{s,\min} \cdot g_{12} - d_{12} \\ d_{11} - k_{s,\min} \cdot g_{11} \end{bmatrix} \tag{4.35}$$

If Equation (4.35) comes out to be a null matrix, then Equation (4.36) is used to obtain the values of $du_{\max}$ and $dv_{\max}$

$$\begin{bmatrix} du_{\max} \\ dv_{\max} \end{bmatrix} = \begin{bmatrix} k_{s,\min} \cdot g_{22} - d_{22} \\ d_{21} - k_{s,\min} \cdot g_{21} \end{bmatrix} \tag{4.36}$$

Chapter 4 Principal Curvatures and Directions of NURBS Surfaces

In CNC finish machining of sculptured surface parts, which are usually designed with NURBS surfaces, the geometric difference between the cutting tool and the part design surface in the vicinity of a CC point determines the local shape of the machined surface. To represent the shape in the neighborhood at the CC point on the part surface, it is necessary to determine the normal curvatures along different tangent directions and they can be calculated with the principal curvatures. The derivations of the principal curvatures and directions of a NURBS Surface are provided in the following.

Since a part is designed in the part coordinate system, its NURBS surface is generally represented in this system as

$$\mathbf{S}(u,v)=\frac{\sum_{i=0}^{m}\sum_{j=0}^{n} w_{i,j}\cdot\mathbf{P}_{i,j}\cdot N_{i,k}(u)\cdot N_{j,l}(v)}{\sum_{i=0}^{m}\sum_{j=0}^{n} w_{i,j}\cdot N_{i,k}(u)\cdot N_{j,l}(v)} \qquad (u\in[a,b],v\in[c,d]) \tag{4.1}$$

where $\mathbf{P}_{i,j}$ the controls are points and $w_{i,j}$ are their corresponding weights. $N_{i,k}(u)$ and $N_{j,l}(v)$ are the basis functions or order k and l respectively. u and v are the parameters of the basis functions. The first derivatives of $\mathbf{S}(u,v)$ in terms of u and v are denoted as

$\mathbf{S}_u(u,v)$ and $\mathbf{S}_v(u,v)$, respectively. The second derivative in terms of u is denoted as $\mathbf{S}_{uu}(u,v)$, of v as $\mathbf{S}_{vv}(u,v)$, and of u and v as $\mathbf{S}_{uv}(u,v)$.

The above NURBS surface can be represented in the matrix form as

$$S(u,v)=\frac{\begin{bmatrix}N_{0,k}(u) & N_{1,k}(u) & \cdots & N_{m,k}(u)\end{bmatrix}\cdot\begin{bmatrix}w_{0,0}\cdot P_{0,0} & w_{0,1}\cdot P_{0,1} & \cdots & w_{0,n}\cdot P_{0,n}\\ w_{1,0}\cdot P_{1,0} & w_{1,1}\cdot P_{1,1} & \cdots & w_{1,n}\cdot P_{1,n}\\ \vdots & \vdots & \ddots & \vdots\\ w_{m,0}\cdot P_{m,0} & w_{m,1}\cdot P_{m,1} & \cdots & w_{m,n}\cdot P_{m,n}\end{bmatrix}\cdot\begin{bmatrix}N_{0,l}(v)\\ N_{1,l}(v)\\ \vdots\\ N_{n,l}(v)\end{bmatrix}}{\begin{bmatrix}N_{0,k}(u) & N_{1,k}(u) & \cdots & N_{m,k}(u)\end{bmatrix}\cdot\begin{bmatrix}w_{0,0} & w_{0,1} & \cdots & w_{0,n}\\ w_{1,0} & w_{1,1} & \cdots & w_{1,n}\\ \vdots & \vdots & \ddots & \vdots\\ w_{m,0} & w_{m,1} & \cdots & w_{m,n}\end{bmatrix}\cdot\begin{bmatrix}N_{0,l}(v)\\ N_{1,l}(v)\\ \vdots\\ N_{n,l}(v)\end{bmatrix}} \quad (4.2)$$

This equation can further be simplified by assigning **U** and **V** for the base function matrices

$$\mathbf{U}=\begin{bmatrix}N_{0,k}(u) & N_{1,k}(u) & \cdots & N_{m,k}(u)\end{bmatrix} \quad (4.3)$$

$$\mathbf{V}=\begin{bmatrix}N_{0,l}(u) & N_{1,l}(u) & \cdots & N_{n,l}(u)\end{bmatrix} \quad (4.4)$$

The scalar form of matrix $\begin{bmatrix}w_{0,0}\cdot P_{0,0} & w_{0,1}\cdot P_{0,1} & \cdots & w_{0,n}\cdot P_{0,n}\\ w_{1,0}\cdot P_{1,0} & w_{1,1}\cdot P_{1,1} & \cdots & w_{1,n}\cdot P_{1,n}\\ \vdots & \vdots & \ddots & \vdots\\ w_{m,0}\cdot P_{m,0} & w_{m,1}\cdot P_{m,1} & \cdots & w_{m,n}\cdot P_{m,n}\end{bmatrix}$ is represented using **X,** **Y,** and **Z** matrices, and the weight matrix is denoted as **W.**

$$\mathbf{X}=\begin{bmatrix}w_{0,0}\cdot x_{0,0} & w_{0,1}\cdot x_{0,1} & \cdots & w_{0,n}\cdot x_{0,n}\\ w_{1,0}\cdot x_{1,0} & w_{1,1}\cdot x_{1,1} & \cdots & w_{1,n}\cdot x_{1,n}\\ \vdots & \vdots & \ddots & \vdots\\ w_{m,0}\cdot x_{m,0} & w_{m,1}\cdot x_{m,1} & \cdots & w_{m,n}\cdot x_{m,n}\end{bmatrix} \quad (4.5)$$

$$\mathbf{Y}=\begin{bmatrix} w_{0,0}\cdot y_{0,0} & w_{0,1}\cdot y_{0,1} & \cdots & w_{0,n}\cdot y_{0,n} \\ w_{1,0}\cdot y_{1,0} & w_{1,1}\cdot y_{1,1} & \cdots & w_{1,n}\cdot y_{1,n} \\ \vdots & \vdots & \ddots & \vdots \\ w_{m,0}\cdot y_{m,0} & w_{m,1}\cdot y_{m,1} & \cdots & w_{m,n}\cdot y_{m,n} \end{bmatrix} \tag{4.6}$$

$$\mathbf{Z}=\begin{bmatrix} w_{0,0}\cdot z_{0,0} & w_{0,1}\cdot z_{0,1} & \cdots & w_{0,n}\cdot z_{0,n} \\ w_{1,0}\cdot z_{1,0} & w_{1,1}\cdot z_{1,1} & \cdots & w_{1,n}\cdot z_{1,n} \\ \vdots & \vdots & \ddots & \vdots \\ w_{m,0}\cdot z_{m,0} & w_{m,1}\cdot z_{m,1} & \cdots & w_{m,n}\cdot z_{m,n} \end{bmatrix} \tag{4.7}$$

$$\mathbf{W}=\begin{bmatrix} w_{0,0} & w_{0,1} & \cdots & w_{0,n} \\ w_{1,0} & w_{1,1} & \cdots & w_{1,n} \\ \vdots & \vdots & \ddots & \vdots \\ w_{m,0} & w_{m,1} & \cdots & w_{m,n} \end{bmatrix} \tag{4.8}$$

Substituting the above equations into the equations of the NURBS surface to obtain the scalar form.

$$S(u,v)=\begin{bmatrix} x(u,v) \\ y(u,v) \\ z(u,v) \end{bmatrix}=\begin{bmatrix} \dfrac{xw(u,v)}{w(u,v)} \\ \dfrac{yw(u,v)}{w(u,v)} \\ \dfrac{zw(u,v)}{w(u,v)} \end{bmatrix}=\begin{bmatrix} \dfrac{\mathbf{U}\cdot\mathbf{X}\cdot\mathbf{V}^{\mathrm{T}}}{\mathbf{U}\cdot\mathbf{W}\cdot\mathbf{V}^{\mathrm{T}}} \\ \dfrac{\mathbf{U}\cdot\mathbf{Y}\cdot\mathbf{V}^{\mathrm{T}}}{\mathbf{U}\cdot\mathbf{W}\cdot\mathbf{V}^{\mathrm{T}}} \\ \dfrac{\mathbf{U}\cdot\mathbf{Z}\cdot\mathbf{V}^{\mathrm{T}}}{\mathbf{U}\cdot\mathbf{W}\cdot\mathbf{V}^{\mathrm{T}}} \end{bmatrix} \tag{4.9}$$

4.1 The First and Second Derivative of Base Function of B-Spline

According to [13] ,appendix I, the first derivative of B-spline base function:

$$N'_{i,k} = (k-1)\left(\frac{N_{i,k-1}}{t_{i+k-1}-t_i}-\frac{N_{i+1,k-1}}{t_{i+k}-t_{i+1}}\right) \tag{4.10}$$

and

$$N'_{i,k-1} = (k-2)\left(\frac{N_{i,k-2}}{t_{i+k-2}-t_i} - \frac{N_{i+1,k-2}}{t_{i+k-1}-t_{i+1}}\right) \tag{4.11}$$

Second derivative:

$$N''_{i,k} = (k-1)\left(\frac{N'_{i,k-1}}{t_{i+k-1}-t_i} - \frac{N'_{i+1,k-1}}{t_{i+k}-t_{i+1}}\right) \tag{4.12}$$

4.2 The First and Second Derivative of NURBS Surfaces

In order to simplify the calculation, the NURBS surface can be represented as

$$S(u,v) = \frac{N(u,v)}{D(u,v)} \tag{4.13}$$

where

$$N(u,v) = \sum_{i=0}^{n}\sum_{j=0}^{m} w_{i,j} \cdot \mathbf{P}_{i,j} \cdot N_{i,k}(u) \cdot N_{j,l}(v)$$

$$D(u,v) = \sum_{i=0}^{n}\sum_{j=0}^{m} w_{i,j} \cdot N_{i,k}(u) \cdot N_{j,l}(v)$$

With the help of Equations (4.5) and (4.6), the first derivative with respect to u of the NURBS surface can be calculated as shown in the following equations

$$S_u(u,v) = \frac{\partial}{\partial u}\left(N(u,v)/D(u,v)\right) = \left(\frac{N_u(u,v)}{D(u,v)}\right) - \left(\frac{N(u,v)\cdot D_u(u,v)}{D^2(u,v)}\right) \tag{4.14}$$

where

$$N_u(u,v) = \frac{\partial}{\partial u}\left(\sum_{i=0}^{n}\sum_{j=0}^{m} w_{i,j}\mathbf{P}_{i,j}N_{i,k}(u)N_{j,l}(v)\right)$$

$$= \sum_{i=0}^{n}\sum_{j=0}^{m} w_{i,j} \cdot \mathbf{P}_{i,j} \cdot N'_{i,k}(u) \cdot N_{j,l}(v) = \sum_{i=0}^{n} N'_{i,k}(u)\sum_{j=0}^{m} w_{i,j} \cdot \mathbf{P}_{i,j} \cdot N_{j,l}(v)$$

In the matrix form the above equation can be represented as

$$N_u(u,v)=\left[N'_{i,k}(u)\right]\cdot\left(\left[w_{i,j}\right]\times\left[\mathbf{P}_{i,j}\right]\right)\cdot\left[N_{j,l}(v)\right]=$$

$$\left[N'_{0,k}(u)\quad N'_{1,k}(u)\quad\cdots\quad N'_{m,k}(u)\right]\begin{bmatrix} w_{0,0}\cdot P_{0,0} & w_{0,1}\cdot P_{0,1} & \cdots & w_{0,n}\cdot P_{0,n}\\ w_{1,0}\cdot P_{1,0} & w_{1,1}\cdot P_{1,1} & \cdots & w_{1,n}\cdot P_{1,n}\\ \vdots & \vdots & \ddots & \vdots\\ w_{m,0}\cdot P_{m,0} & w_{m,1}\cdot P_{m,1} & \cdots & w_{m,n}\cdot P_{m,n}\end{bmatrix}\begin{bmatrix}N_{0,l}(v)\\ N_{1,l}(v)\\ \vdots\\ N_{n,l}(v)\end{bmatrix}$$

and

$$D_u(u,v)=\frac{\partial}{\partial u}\left[\sum_{i=0}^{n}\sum_{j=0}^{m}w_{i,j}\cdot N_{i,k}(u)\cdot N_{j,l}(v)\right]$$

$$=\sum_{i=0}^{n}\sum_{j=0}^{m}w_{i,j}\cdot N'_{i,k}(u)\cdot N_{j,l}(v)=\sum_{i=0}^{n}N'_{i,k}(u)\sum_{j=0}^{m}w_{i,j}\cdot N_{j,l}(v)$$

In matrix form, the above equation can be represented as

$$D_u(u,v)=\left[N'_{i,k}(u)\right]\cdot\left[w_{i,j}\right]\cdot\left[N_{j,l}(v)\right]$$

$$=\left[N'_{0,k}(u)\quad N'_{1,k}(u)\quad\cdots\quad N'_{m,k}(u)\right]\cdot\begin{bmatrix} w_{0,0} & w_{0,1} & \cdots & w_{0,n}\\ w_{1,0} & w_{1,1} & \cdots & w_{1,n}\\ \vdots & \vdots & \ddots & \vdots\\ w_{m,0} & w_{m,1} & \cdots & w_{m,n}\end{bmatrix}\cdot\begin{bmatrix}N_{0,l}(v)\\ N_{1,l}(v)\\ \vdots\\ N_{n,l}(v)\end{bmatrix}$$

Similarly the first derivative of the NURBS surface with respect to the parameter v can be calculated as shown in the following equation

$$S_v(u,v)=\frac{\partial(N/D)}{\partial v}=\left(\frac{N_v}{D}\right)-\left(\frac{N\cdot D_v}{D^2}\right)\qquad(4.15)$$

where

$$N_v(u,v)=\frac{\partial}{\partial v}\left[\sum_{i=0}^{n}\sum_{j=0}^{m}w_{i,j}\mathbf{P}_{i,j}\cdot N_{i,k}(u)\cdot N_{j,l}(v)\right]$$

$$=\sum_{i=0}^{n}\sum_{j=0}^{m}w_{i,j}\cdot\mathbf{P}_{i,j}\cdot N_{i,k}(u)\cdot N'_{j,l}(v)=\sum_{i=0}^{n}N_{i,k}(u)\cdot w_{i,j}\cdot\mathbf{P}_{i,j}\sum_{j=0}^{m}N'_{j,l}(v)$$

In the matrix form

$$N_v(u,v)=\left[N_{i,k}(u)\right]\cdot\left(\left[w_{i,j}\right]\cdot\times\left[\mathbf{P}_{i,j}\right]\right)\cdot\left[N'_{j,l}(v)\right]$$

$$=\left[N_{0,k}(u)\quad N_{1,k}(u)\quad\cdots\quad N_{m,k}(u)\right]\cdot\begin{bmatrix} w_{0,0}\cdot\mathbf{P}_{0,0} & w_{0,1}\cdot\mathbf{P}_{0,1} & \cdots & w_{0,n}\cdot\mathbf{P}_{0,n} \\ w_{1,0}\cdot\mathbf{P}_{1,0} & w_{1,1}\cdot\mathbf{P}_{1,1} & \cdots & w_{1,n}\cdot\mathbf{P}_{1,n} \\ \vdots & \vdots & \ddots & \vdots \\ w_{m,0}\cdot\mathbf{P}_{m,0} & w_{m,1}\cdot\mathbf{P}_{m,1} & \cdots & w_{m,n}\cdot\mathbf{P}_{m,n} \end{bmatrix}\cdot\begin{bmatrix} N'_{0,l}(v) \\ N'_{1,l}(v) \\ \vdots \\ N'_{n,l}(v) \end{bmatrix}$$

and

$$D_v(u,v)=\frac{\partial}{\partial v}\left[\sum_{i=0}^{n}\sum_{j=0}^{m}w_{i,j}N_{i,k}(u)N_{j,l}(v)\right]$$

$$=\sum_{i=0}^{n}\sum_{j=0}^{m}w_{i,j}\cdot N_{i,k}(u)\cdot N'_{j,l}(v)=\sum_{i=0}^{n}N_{i,k}(u)\sum_{j=0}^{m}w_{i,j}\cdot N'_{j,l}(v)$$

In the matrix form, the above equation can be written as

$$\mathrm{D}_v(u,v)=\left[N_{i,k}(u)\right]\cdot\left[h_{i,j}\right]\cdot\left[N'_{j,l}(v)\right]$$

$$=\left[N_{0,k}(u)\quad N_{1,k}(u)\quad\cdots\quad N_{m,k}(u)\right]\cdot\begin{bmatrix} w_{0,0} & w_{0,1} & \cdots & w_{0,n} \\ w_{1,0} & w_{1,1} & \cdots & w_{1,n} \\ \vdots & \vdots & \ddots & \vdots \\ w_{m,0} & w_{m,1} & \cdots & w_{m,n} \end{bmatrix}\cdot\begin{bmatrix} N'_{0,l}(v) \\ N'_{1,l}(v) \\ \vdots \\ N'_{n,l}(v) \end{bmatrix}$$

The double derivative of the NURBS surface with respect to the parameter u and v can be calculated as shown in the following equation.

$$S_{uv}(u,v)=\frac{\partial^2}{\partial u\cdot\partial v}\left(\frac{N}{D}\right)=\frac{\partial}{\partial v}\left(\frac{\partial}{\partial u}\left(\frac{N}{D}\right)\right)=\frac{\partial}{\partial v}\left(\frac{N_u}{D}-\frac{N\cdot D_u}{D^2}\right)$$

$$=\left(-\frac{D_v\cdot N_u}{D^2}\right)+\left(\frac{N_{uv}}{D}\right)-\left(-2\frac{N\cdot D_v\cdot D_u}{D^3}+\frac{\partial(N\cdot D_u)/\partial v}{D^2}\right)$$

$$\Rightarrow S_{uv}(u,v)=-\left(\frac{D_v\cdot N_u}{D^2}\right)+\left(\frac{N_{uv}}{D}\right)+2\cdot\left(\frac{N\cdot D_v\cdot D_u}{D^3}\right)-\left(\frac{D_{uv}\cdot N}{D^2}\right)-\left(\frac{N_v\cdot D_u}{D^2}\right)\qquad(4.16)$$

where

$$N_{uv}(u,v)=\sum_{i=0}^{n}\sum_{j=0}^{m}w_{i,j}\cdot\mathbf{P}_{i,j}\cdot N'_{i,j}(u)\cdot N'_{j,l}(v)=\sum_{i=0}^{n}N'_{i,j}(u)\sum_{j=0}^{m}w_{i,j}\cdot\mathbf{P}_{i,j}\cdot N'_{j,l}(v)$$

The above equation can be represented in matrix form as follows

$$N_{uv}(u,v)=\left[N'_{i,j}(u)\right]\cdot\left(\left[w_{i,j}\right]\cdot\times\left[\mathbf{P}_{i,j}\right]\right)\cdot\left[N'_{j,l}(v)\right]$$

$$=\left[N'_{0,k}(u)\quad N'_{1,k}(u)\quad\cdots\quad N'_{m,k}(u)\right]\cdot\begin{bmatrix} w_{0,0}\cdot\mathbf{P}_{0,0} & w_{0,1}\cdot\mathbf{P}_{0,1} & \cdots & w_{0,n}\cdot\mathbf{P}_{0,n} \\ w_{1,0}\cdot\mathbf{P}_{1,0} & w_{1,1}\cdot\mathbf{P}_{1,1} & \cdots & w_{1,n}\cdot\mathbf{P}_{1,n} \\ \vdots & \vdots & \ddots & \vdots \\ w_{m,0}\cdot\mathbf{P}_{m,0} & w_{m,1}\cdot\mathbf{P}_{m,1} & \cdots & w_{m,n}\cdot\mathbf{P}_{m,n} \end{bmatrix}\cdot\begin{bmatrix} N'_{0,l}(v) \\ N'_{1,l}(v) \\ \vdots \\ N'_{n,l}(v) \end{bmatrix}$$

and

$$D_{uv}(u,v)=\sum_{i=0}^{n}\sum_{j=0}^{m}w_{i,j}\cdot N'_{i,k}(u)\cdot N'_{j,l}(v)=\sum_{i=0}^{n}N'_{i,k}(u)\sum_{j=0}^{m}w_{i,j}\cdot N'_{j,l}(v)$$

The above equation can be represented in matrix form as follows

$$D_{uv}(u,v)=\left[N'_{i,k}(u)\right]\cdot\left[w_{i,j}\right]\cdot\left[N'_{j,l}(v)\right]$$

$$=\left[N'_{0,k}(u)\quad N'_{1,k}(u)\quad\cdots\quad N'_{m,k}(u)\right]\cdot\begin{bmatrix} w_{0,0} & w_{0,1} & \cdots & w_{0,n} \\ w_{1,0} & w_{1,1} & \cdots & w_{1,n} \\ \vdots & \vdots & \ddots & \vdots \\ w_{m,0} & w_{m,1} & \cdots & w_{m,n} \end{bmatrix}\cdot\begin{bmatrix} N'_{0,l}(v) \\ N'_{1,l}(v) \\ \vdots \\ N'_{n,l}(v) \end{bmatrix}$$

Similarly the second derivative with respect to u of the NURBS surface can be calculated as shown in the following equations

$$S_{uu}(u,v)=\frac{\partial^2}{\partial u^2}\left(\frac{N}{D}\right)=\frac{\partial}{\partial u}\left(\frac{\partial}{\partial u}\left(\frac{N}{D}\right)\right)=\frac{\partial}{\partial u}\left(\frac{N_u}{D}-\frac{N\cdot D_u}{D^2}\right)$$

$$=-\frac{D_u\cdot N_u}{D^2}+\frac{N_{uu}}{D}-\left(-2\frac{N\cdot D_u\cdot D_u}{D^3}+\frac{\partial(N\cdot D_u)/\partial u}{D^2}\right)$$

$$\Rightarrow S_{uu}(u,v)=-\left(2\frac{D_u\cdot N_u}{D^2}\right)+\left(\frac{N_{uu}}{D}\right)+2\left(\frac{N\cdot D_u\cdot D_u}{D^3}\right)-\left(\frac{D_{uu}\cdot N}{D^2}\right) \qquad (4.17)$$

where

$$N_{uu}(u,v)=\sum_{i=0}^{n}\sum_{j=0}^{m}w_{i,j}\cdot\mathbf{P}_{i,j}\cdot N''_{i,j}(u)\cdot N_{j,l}(v)=\sum_{i=0}^{n}N''_{i,j}(u)\sum_{j=0}^{m}w_{i,j}\cdot\mathbf{P}_{i,j}\cdot N_{j,l}(v)$$

The above equation can be represented in matrix form as follows

$$N_{uu}(u,v)=\left[N''_{i,j}(u)\right]\cdot\left(\left[w_{i,j}\right]\cdot\times\left[\mathbf{P}_{i,j}\right]\right)\cdot\left[N_{j,l}(v)\right]$$

$$=\left[N''_{0,k}(u)\quad N''_{1,k}(u)\quad\cdots\quad N''_{m,k}(u)\right]\cdot\begin{bmatrix} w_{0,0}\cdot\mathbf{P}_{0,0} & w_{0,1}\cdot\mathbf{P}_{0,1} & \cdots & w_{0,n}\cdot\mathbf{P}_{0,n} \\ w_{1,0}\cdot\mathbf{P}_{1,0} & w_{1,1}\cdot\mathbf{P}_{1,1} & \cdots & w_{1,n}\cdot\mathbf{P}_{1,n} \\ \vdots & \vdots & \ddots & \vdots \\ w_{m,0}\cdot\mathbf{P}_{m,0} & w_{m,1}\cdot\mathbf{P}_{m,1} & \cdots & w_{m,n}\cdot\mathbf{P}_{m,n} \end{bmatrix}\cdot\begin{bmatrix} N_{0,l}(v) \\ N_{1,l}(v) \\ \vdots \\ N_{n,l}(v) \end{bmatrix}$$

and

$$D_{uu}(u,v)=\sum_{i=0}^{n}\sum_{j=0}^{m}w_{i,j}N''_{i,k}(u)N_{j,l}(v)=\sum_{i=0}^{n}N''_{i,k}(u)\sum_{j=0}^{m}w_{i,j}N_{j,l}(v)$$

$$=\left[N''_{i,k}(u)\right]\cdot\left[w_{i,j}\right]\cdot\left[N_{j,l}(v)\right]$$

$$=\left[N''_{0,k}(u)\quad N''_{1,k}(u)\quad\cdots\quad N''_{m,k}(u)\right]\cdot\begin{bmatrix} w_{0,0} & w_{0,1} & \cdots & w_{0,n} \\ w_{1,0} & w_{1,1} & \cdots & w_{1,n} \\ \vdots & \vdots & \ddots & \vdots \\ w_{m,0} & w_{m,1} & \cdots & w_{m,n} \end{bmatrix}\cdot\begin{bmatrix} N_{0,l}(v) \\ N_{1,l}(v) \\ \vdots \\ N_{n,l}(v) \end{bmatrix}$$

and the second derivative of the NURBS surface with respect to v can be calculated as shown in the following equations

$$S_{vv}(u,v)=\frac{\partial^2}{\partial v^2}\left(\frac{N}{D}\right)=\frac{\partial}{\partial v}\left(\frac{\partial}{\partial v}\left(\frac{N}{D}\right)\right)=\frac{\partial}{\partial v}\left(\frac{N_v}{D}-\frac{N\cdot D_v}{D^2}\right)$$

$$=-\frac{D_v\cdot N_v}{D^2}+\frac{N_{vv}}{D}-\left(-2\frac{N\cdot D_v\cdot D_v}{D^3}+\frac{\partial(N\cdot D_v)/\partial v}{D^2}\right)$$

$$\Rightarrow S_{vv}=-\left(2\frac{D_v\cdot N_v}{D^2}\right)+\left(\frac{N_{vv}}{D}\right)+2\left(\frac{N\cdot D_v\cdot D_v}{D^3}\right)-\left(\frac{D_{vv}\cdot N}{D^2}\right)\qquad(4.18)$$

where

$$N_{vv}(u,v)=\sum_{i=0}^{n}\sum_{j=0}^{m}w_{i,j}\cdot\mathbf{P}_{i,j}\cdot N_{i,j}(u)\cdot N''_{j,l}(v)=\sum_{i=0}^{n}N_{i,j}(u)\cdot w_{i,j}\cdot\mathbf{P}_{i,j}\sum_{j=0}^{m}N''_{j,l}(v)$$

The above equation can be represented in matrix form as follows

$$N_{vv}(u,v)=\left[N_{i,j}(u)\right]\cdot\left(\left[w_{i,j}\right]\cdot\times\left[\mathbf{P}_{i,j}\right]\right)\cdot\left[N''_{j,l}(v)\right]$$

$$=\begin{bmatrix}N_{0,k}(u) & N_{1,k}(u) & \cdots & N_{m,k}(u)\end{bmatrix}\cdot\begin{bmatrix}w_{0,0}\cdot\mathbf{P}_{0,0} & w_{0,1}\cdot\mathbf{P}_{0,1} & \cdots & w_{0,n}\cdot\mathbf{P}_{0,n}\\ w_{1,0}\cdot\mathbf{P}_{1,0} & w_{1,1}\cdot\mathbf{P}_{1,1} & \cdots & w_{1,n}\cdot\mathbf{P}_{1,n}\\ \vdots & \vdots & \ddots & \vdots\\ w_{m,0}\cdot\mathbf{P}_{m,0} & w_{m,1}\cdot\mathbf{P}_{m,1} & \cdots & w_{m,n}\cdot\mathbf{P}_{m,n}\end{bmatrix}\cdot\begin{bmatrix}N''_{0,l}(v)\\ N''_{1,l}(v)\\ \vdots\\ N''_{n,l}(v)\end{bmatrix}$$

and

$$D_{vv}(u,v)=\sum_{i=0}^{n}\sum_{j=0}^{m}w_{i,j}N_{i,k}(u)N''_{j,l}(v)=\sum_{i=0}^{n}N_{i,k}(u)\cdot w_{i,j}\sum_{j=0}^{m}N_{j,l}(v)$$

$$=\left[N_{i,k}(u)\right]\cdot\left[w_{i,j}\right]\cdot\left[N''_{j,l}(v)\right]$$

$$=\begin{bmatrix}N_{0,k}(u) & N_{1,k}(u) & \cdots & N_{m,k}(u)\end{bmatrix}\cdot\begin{bmatrix}w_{0,0} & w_{0,1} & \cdots & w_{0,n}\\ w_{1,0} & w_{1,1} & \cdots & w_{1,n}\\ \vdots & \vdots & \ddots & \vdots\\ w_{m,0} & w_{m,1} & \cdots & w_{m,n}\end{bmatrix}\cdot\begin{bmatrix}N''_{0,l}(v)\\ N''_{1,l}(v)\\ \vdots\\ N''_{n,l}(v)\end{bmatrix}$$

Based on the derivative formulas of a NURBS surface $\mathbf{S}(u,v)$, the first and the second fundamental matrices of this surface, denoted as **G** and **D** respectively, can be calculated. Specifically, **G** is

$$\mathbf{G}=\begin{bmatrix}g_{11} & g_{12}\\ g_{21} & g_{22}\end{bmatrix}=\begin{bmatrix}\mathbf{S}_u(u,v)^T\cdot\mathbf{S}_u(u,v) & \mathbf{S}_u(u,v)^T\cdot\mathbf{S}_v(u,v)\\ \mathbf{S}_v(u,v)^T\cdot\mathbf{S}_u(u,v) & \mathbf{S}_v(u,v)^T\cdot\mathbf{S}_v(u,v)\end{bmatrix} \tag{4.19}$$

and **D** is

$$\mathbf{D}=\begin{bmatrix}d_{11} & d_{12}\\ d_{21} & d_{22}\end{bmatrix}=\begin{bmatrix}\mathbf{n}\cdot\mathbf{S}_{uu}(u,v) & \mathbf{n}\cdot\mathbf{S}_{uv}(u,v)\\ \mathbf{n}\cdot\mathbf{S}_{uv}(u,v) & \mathbf{n}\cdot\mathbf{S}_{vv}(u,v)\end{bmatrix} \tag{4.20}$$

where the unit surface normal is defined as $\mathbf{n}=\left[n_x,n_y,n_z\right]^T=\mathbf{S}_u(u,v)\times\mathbf{S}_v(u,v)\Big/\sqrt{g_{11}\cdot g_{22}-g_{12}^2}$. The maximum and the minimum

curvatures of the part surface are represented as $k_{s,\max}$ and $k_{s,\min}$, respectively. The Gauss curvature K and mean curvature H can be calculated as

$$K = k_{s,\max} \cdot k_{s,\min} = \frac{d_{11} \cdot d_{22} - d_{12}^2}{g_{11} \cdot g_{22} - g_{12}^2} \tag{4.21}$$

and

$$H = \frac{1}{2} \cdot (k_{s,\max} + k_{s,\min}) = \frac{1}{2} \cdot \frac{g_{11} \cdot d_{22} - 2 \cdot g_{12} \cdot d_{12} + g_{22} \cdot d_{11}}{g_{11} \cdot g_{22} - g_{12}^2} \tag{4.22}$$

Hence, the maximum curvature is $k_{s,\max} = H + \sqrt{H^2 - K}$, and the minimum curvature is $k_{s,\min} = H - \sqrt{H^2 - K}$.

Meanwhile, the principal direction of the maximum curvature $\mathbf{T}_{s,\max}$ is $\mathbf{T}_{s,\max} = du_{\max} \cdot \mathbf{S}_u(u,v) + dv_{\max} \cdot \mathbf{S}_v(u,v)$, where

$$\begin{bmatrix} du_{\max} \\ dv_{\max} \end{bmatrix} = \begin{bmatrix} k_{s,\max} \cdot g_{21} - d_{21} \\ d_{11} - k_{s,\max} \cdot g_{11} \end{bmatrix} \tag{4.23}$$

Similarly, the principal direction of the minimum curvature $\mathbf{T}_{s,\min}$ is $\mathbf{T}_{s,\min} = du_{\min} \cdot \mathbf{S}_u(u,v) + dv_{\min} \cdot \mathbf{S}_v(u,v)$, where

$$\begin{bmatrix} du_{\min} \\ dv_{\min} \end{bmatrix} = \begin{bmatrix} k_{s,\min} \cdot g_{21} - d_{21} \\ d_{11} - k_{s,\min} \cdot g_{11} \end{bmatrix} \tag{4.24}$$

According to Euler's equation, the normal curvature in a tangent direction at an interior surface point can be calculated as

$$k_s(\beta) = k_{s,\max} \cdot \cos^2 \beta + k_{s,\min} \cdot \sin^2 \beta \qquad \beta \in [0, 2\pi] \tag{4.25}$$

Where angle β represents this tangent direction in terms of direction $\mathbf{T}_{s,\max}$ in counter-clockwise. At a convex point, all normal curvatures are negative; at a concave point, they

are positive; and at a saddle point, they are either positive or negative. Figure 4.1 shows the curvature curves along different tangent directions at these points. For a point on the boundary of the surface, the formula of normal curvatures is the same as Eq. (4.20); however, the range of angle β is determined by the tangents of the boundary at this point, instead of being $[0, 2\pi]$.

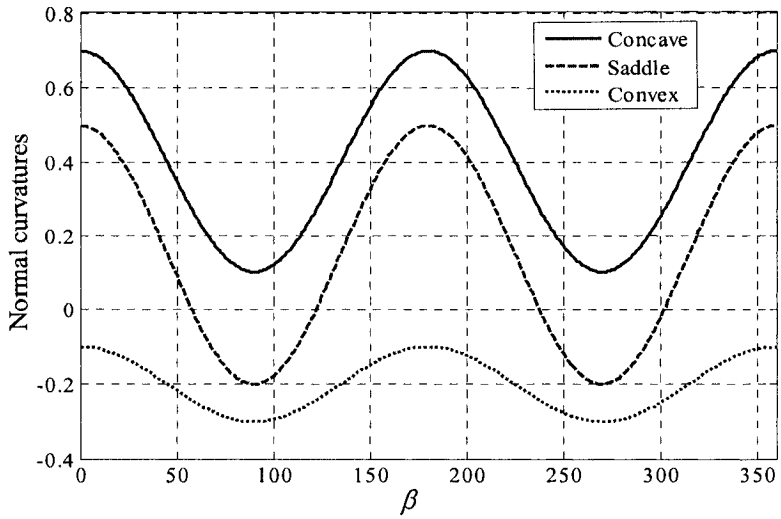

Figure 4.1. NURBS surface curvatures along all the tangent directions at a convex, a concave, and a saddle points.

Chapter 5 Principal Curvatures and Directions of Bull- and Ball-Nose End-Mills

In 3-axis milling on a vertical CNC machine, in which the cutting tool is vertically oriented, a NURBS-surface part is set up on the machine table. Among the three different common types of cutting tools available in the market, namely bull-nose, ball-end and flat end mill, the bull-nose end mill represents a generic case. The shank and corner radii of this end-mill are denoted as R and r, respectively; and $R \geq r$. When $R=r$, it represents a ball-end mill and when $r=0$ it represents a flat end mill. Therefore in order to build a generic model, a bull-nose end-mill which is represented by a toroidal shape is used to machine the surface at each CC point. (see Figure 5.1). In this work, the part coordinate system (X-Y-Z), in which the NURBS-part surface is represented, is assumed to be the reference coordinate system. A CC point P_0 on the NURBS surface $\mathbf{S}(u,v)$, and the tool axis is along the direction $[0, \ 0, \ 1]^T$ are represented in this coordinate system. To facilitate finding the principal curvatures and principal directions of the cutting surface of the tool, a new coordinate system called the tool coordinate system is established in the following.

5.1 Tool Coordinate System

To establish the tool coordinate system (x-y-z) for the bull-nose end-mill at CC point P_0, four steps are involved: (1) the tool tip (the center of the bottom circle) is set as the origin of this coordinate system; (2) its z-axis is aligned with the tool axis; (3) its x-axis is perpendicular to its z-axis and is on the plane formed by this z-axis and the surface normal **n** at this CC point; and (4) its y-axis is the cross-product of these z- and x-axes (see Figure 5.2)

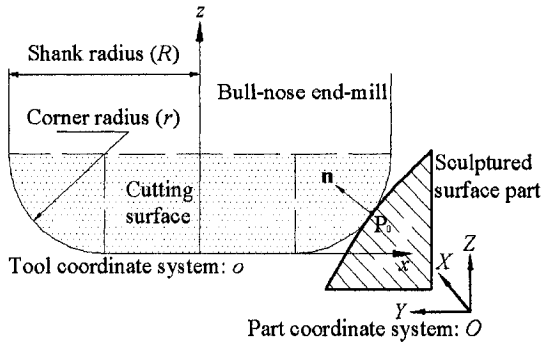

Figure 5.1. Bull-nose end-mill cuts the NURBS surface at CC point P_0 in the part coordinate system.

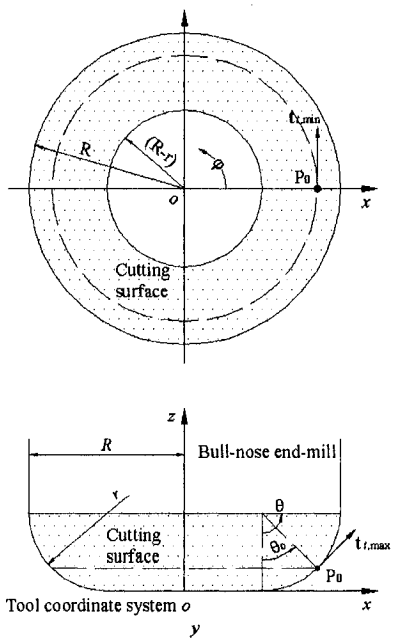

Figure 5.2. Toroidal cutting surface of the bull-nose end-mill in the tool coordinate system.

Thus, the equation of the cutting surface of the bull-nose end mill in terms of the tool coordinate system can be derived as follows. Consider a point P_0 on a curve as shown in Figure 5.2 which makes an angle θ_0 with the vertical direction. The location of this point in terms of the tool coordinate system is

$$P_0 = \begin{bmatrix} x_0 \\ y_0 \\ z_0 \end{bmatrix} = \begin{bmatrix} R - r + r \cdot \sin\theta_0 \\ 0 \\ r - r \cdot \cos\theta_0 \end{bmatrix} \tag{5.1}$$

The parametric equation of the curve can be represented by varying the parameter, $\theta \in [0, \pi/2]$. Hence the equation of the curve is given by

$$\mathbf{P} = \begin{bmatrix} x \\ y \\ z \end{bmatrix} = \begin{bmatrix} R - r + r \cdot \sin\theta \\ 0 \\ r - r \cdot \cos\theta \end{bmatrix} \tag{5.2}$$

where $\theta \in [0, \pi/2]$.

Rotating the curve about the z-axis by an angle φ gives the equation of the cutting surface of the bull-nose end mill. Mathematically,

$$\mathbf{CS}(\varphi, \theta) = R(z, \varphi) \cdot \mathbf{P}(\boldsymbol{\theta}) = \begin{bmatrix} \cos\varphi & -\sin\varphi & 0 \\ \sin\varphi & \cos\varphi & 0 \\ 0 & 0 & 1 \end{bmatrix} \cdot \begin{bmatrix} R - r + r \cdot \sin\theta \\ 0 \\ r - r \cdot \cos\theta \end{bmatrix}$$

$$\Rightarrow \mathbf{CS}(\varphi, \theta) = \begin{bmatrix} (R - r + r \cdot \sin\theta) \cdot \cos\varphi \\ (R - r + r \cdot \sin\theta) \cdot \sin\varphi \\ r \cdot (1 - \cos\theta) \end{bmatrix} \tag{5.3}$$

where $\theta \in [0, \pi/2]$ and $\varphi \in [0, 2\pi]$. These parameters are illustrated in Figure 5.2

5.2 Principal Curvatures of the Toroidal Cutting Surface

For a CC point P_0 on the toroidal cutting surface of the tool in the tool coordinate system, the principal curvatures and their directions need to be calculated. At this CC point, the values of its parameters φ and θ are 0 and θ_0 respectively as can be seen from Figure 5.2. First the elements of the D and G are calculated.

In the cutter coordinate system, the parametric equation of the cutting surface is

$$\mathbf{CS}(\varphi,\theta) = \begin{bmatrix} (R-r+r\cdot\sin\theta)\cdot\cos\varphi \\ (R-r+r\cdot\sin\theta)\cdot\sin\varphi \\ r\cdot(1-\cos\theta) \end{bmatrix} \tag{5.4}$$

The first derivative with respect to φ is calculated to be

$$\frac{\partial \mathbf{CS}(\varphi,\theta)}{\partial\varphi} = \begin{bmatrix} -(R-r+r\cdot\sin\theta)\cdot\sin\varphi \\ (R-r+r\cdot\sin\theta)\cdot\cos\varphi \\ 0 \end{bmatrix} \tag{5.5}$$

At a CC point $(\varphi = 0, \theta = \theta_0)$, the value of the first derivative is calculated to be

$$\left.\frac{\partial \mathbf{CS}(\varphi,\theta)}{\partial\varphi}\right|_{\substack{\varphi=0 \\ \theta=\theta_0}} = \begin{bmatrix} 0 \\ R-r+r\cdot\sin\theta_0 \\ 0 \end{bmatrix} \tag{5.6}$$

The second derivative with respect to φ is calculated to be

$$\frac{\partial^2 \mathbf{CS}(\varphi,\theta)}{\partial\varphi^2} = \begin{bmatrix} -(R-r+r\cdot\sin\theta)\cdot\cos\varphi \\ -(R-r+r\cdot\sin\theta)\cdot\sin\varphi \\ 0 \end{bmatrix} \tag{5.7}$$

At a CC point $(\varphi = 0, \theta = \theta_0)$, the value of the second derivative is calculated to be

$$\left.\frac{\partial^2 \mathbf{CS}(\varphi,\theta)}{\partial \varphi^2}\right|_{\substack{\varphi=0 \\ \theta=\theta_0}} = \begin{bmatrix} -(R - r + r \cdot \sin\theta_0) \\ 0 \\ 0 \end{bmatrix} \tag{5.8}$$

The first derivative with respect to θ is calculated to be

$$\frac{\partial \mathbf{CS}(\varphi,\theta)}{\partial \theta} = \begin{bmatrix} r.\cos\varphi.\cos\theta \\ r.\sin\varphi.\cos\theta \\ r\sin\theta \end{bmatrix} \tag{5.9}$$

At a CC point $(\varphi = 0, \theta = \theta_0)$, the value of the first derivative is calculated to be

$$\left.\frac{\partial \mathbf{CS}(\varphi,\theta)}{\partial \theta}\right|_{\substack{\varphi=0 \\ \theta=\theta_0}} = \begin{bmatrix} r \cdot \cos\theta_0 \\ 0 \\ r \cdot \sin\theta_0 \end{bmatrix} \tag{5.10}$$

The second derivative with respect to θ is calculated to be

$$\frac{\partial^2 \mathbf{CS}(\varphi,\theta)}{\partial \theta^2} = \begin{bmatrix} -r.\cos\varphi.\sin\theta \\ -r.\sin\varphi.\sin\theta \\ r\cos\theta \end{bmatrix} \tag{5.11}$$

At a CC point $(\varphi = 0, \theta = \theta_0)$, the value of the second derivative is calculated to be

$$\left.\frac{\partial^2 \mathbf{CS}(\varphi,\theta)}{\partial \theta^2}\right|_{\substack{\varphi=0 \\ \theta=\theta_0}} = \begin{bmatrix} -r \cdot \sin\theta_0 \\ 0 \\ r \cdot \cos\theta_0 \end{bmatrix} \tag{5.12}$$

The mixed second derivative is calculated to be

$$\frac{\partial^2 \mathbf{CS}(\varphi,\theta)}{\partial \varphi \partial \theta} = \begin{bmatrix} -r \cdot \sin\varphi \cdot \cos\theta \\ r \cdot \cos\varphi \cdot \cos\theta \\ 0 \end{bmatrix} \tag{5.13}$$

At a CC point $(\varphi = 0, \theta = \theta_0)$, the value of the mixed second derivative is calculated to be

$$\left.\frac{\partial^2 \mathbf{CS}(\varphi,\theta)}{\partial\varphi\partial\theta}\right|_{\substack{\varphi=0\\ \theta=\theta_0}} = \begin{bmatrix} 0 \\ r\cdot\cos\theta_0 \\ 0 \end{bmatrix} \tag{5.14}$$

The next step is to find the surface normal $(\mathbf{n}_t)$ of the cutting surface in terms of the tool coordinate system at a CC point. The surface normal is given by

$$\mathbf{n}_t = \left(\frac{\partial \mathbf{CS}(\varphi,\theta)}{\partial\varphi} \times \frac{\partial \mathbf{CS}(\varphi,\theta)}{\partial\theta}\right) \tag{5.15}$$

At a CC point, the surface normal can be calculated by the following equation

$$\left.\mathbf{n}_t\right|_{\substack{\varphi=0\\ \theta=\theta_0}} = \left(\left.\frac{\partial \mathbf{CS}(\varphi,\theta)}{\partial\varphi}\right|_{\substack{\varphi=0\\ \theta=\theta_0}} \times \left.\frac{\partial \mathbf{CS}(\varphi,\theta)}{\partial\theta}\right|_{\substack{\varphi=0\\ \theta=\theta_0}}\right)$$

$$\left.\mathbf{n}_t\right|_{\substack{\varphi=0\\ \theta=\theta_0}} = \begin{vmatrix} i & j & k \\ r\cdot\cos\theta_0 & 0 & r\cdot\sin\theta_0 \\ 0 & R-r+r\sin\theta_0 & 0 \end{vmatrix}$$

Hence, the surface normal of the cutting surface at a CC point is calculated to be

$$\Rightarrow \left.\mathbf{n}_t\right|_{\substack{\varphi=0\\ \theta=\theta_0}} = \begin{bmatrix} (R-r+r\sin\theta_0)\cdot r\cdot\sin\theta_0 \\ 0 \\ -(R-r+r\sin\theta_0)\cdot r\cdot\cos\theta_0 \end{bmatrix} \tag{5.16}$$

The unit normal at a CC point in terms of the tool coordinate system will be

$$\left.\hat{\mathbf{n}}_t\right|_{\substack{\varphi=0\\ \theta=\theta_0}} = \frac{\mathbf{n}_t}{|\mathbf{n}_t|} = \frac{\begin{bmatrix} (R-r+r\sin\theta_0)(r\sin\theta_0) \\ 0 \\ -(R-r+r\sin\theta_0)(r\cos\theta_0) \end{bmatrix}}{\sqrt{\{(R-r+r\sin\theta_0)(r\sin\theta_0)\}^2 + \{(R-r+r\sin\theta_0)(r\cos\theta_0)\}^2}}$$

$$\Rightarrow \left.\hat{\mathbf{n}}_t\right|_{\substack{\varphi=0\\ \theta=\theta_0}} = \begin{bmatrix} -\sin\theta_0 \\ 0 \\ \cos\theta_0 \end{bmatrix} \tag{5.17}$$

The D and G matrix are represented as

$$D=\begin{bmatrix} \hat{\mathbf{n}}_t^{\,T}\cdot\dfrac{\partial^2\mathbf{CS}(\varphi,\theta)}{\partial\varphi^2} & \hat{\mathbf{n}}_t^{\,T}\cdot\dfrac{\partial^2\mathbf{CS}(\varphi,\theta)}{\partial\varphi\cdot\partial\theta} \\ \hat{\mathbf{n}}_t^{\,T}\cdot\dfrac{\partial^2\mathbf{CS}(\varphi,\theta)}{\partial\theta\cdot\partial\varphi} & \hat{\mathbf{n}}_t^{\,T}\cdot\dfrac{\partial^2\mathbf{CS}(\varphi,\theta)}{\partial\theta^2} \end{bmatrix}=\begin{bmatrix} d_{11} & d_{12} \\ d_{21} & d_{22} \end{bmatrix}$$

$$G=\begin{bmatrix} \left(\dfrac{\partial\mathbf{CS}(\varphi,\theta)}{\partial\varphi}\right)^T\cdot\left(\dfrac{\partial\mathbf{CS}(\varphi,\theta)}{\partial\varphi}\right) & \left(\dfrac{\partial\mathbf{CS}(\varphi,\theta)}{\partial\varphi}\right)^T\cdot\left(\dfrac{\partial\mathbf{CS}(\varphi,\theta)}{\partial\theta}\right) \\ \left(\dfrac{\partial\mathbf{CS}(\varphi,\theta)}{\partial\theta}\right)^T\cdot\left(\dfrac{\partial\mathbf{CS}(\varphi,\theta)}{\partial\varphi}\right) & \left(\dfrac{\partial\mathbf{CS}(\varphi,\theta)}{\partial\theta}\right)^T\cdot\left(\dfrac{\partial\mathbf{CS}(\varphi,\theta)}{\partial\theta}\right) \end{bmatrix}=\begin{bmatrix} g_{11} & g_{12} \\ g_{21} & g_{22} \end{bmatrix}$$

The elements of D matrix at a CC point can be calculated as

$$d_{11}\Big|_{\substack{\varphi=0\\ \theta=\theta_0}}=\hat{\mathbf{n}}_t^{\,T}\Big|_{\substack{\varphi=0\\ \theta=\theta_0}}\cdot\frac{\partial^2\mathbf{CS}(\varphi,\theta)}{\partial\varphi^2}\Big|_{\substack{\varphi=0\\ \theta=\theta_0}}=\begin{bmatrix}-\sin\theta_0 & 0 & \cos\theta_0\end{bmatrix}\cdot\begin{bmatrix}-(R-r+r.\sin\theta_0)\\ 0\\ 0\end{bmatrix}$$

$$\Rightarrow d_{11}\Big|_{\substack{\varphi=0\\ \theta=\theta_0}}=(R-r+r.\sin\theta_0)\cdot\sin\theta_0 \tag{5.18}$$

Similarly the second element of the second fundamental matrix D can be calculated

$$d_{12}\Big|_{\substack{\varphi=0\\ \theta=\theta_0}}=\hat{\mathbf{n}}_t^{\,T}\Big|_{\substack{\varphi=0\\ \theta=\theta_0}}\cdot\frac{\partial^2\mathbf{CS}(\varphi,\theta)}{\partial\varphi\cdot\partial\theta}\Big|_{\substack{\varphi=0\\ \theta=\theta_0}}=\begin{bmatrix}\sin\theta_0 & 0 & \cos\theta_0\end{bmatrix}\cdot\begin{bmatrix}0\\ r\cdot\cos\theta_0\\ 0\end{bmatrix}$$

$$\Rightarrow d_{12}\Big|_{\substack{\varphi=0\\ \theta=\theta_0}}=0=d_{21}\Big|_{\substack{\varphi=0\\ \theta=\theta_0}} \tag{5.19}$$

and

$$d_{22}\Big|_{\substack{\varphi=0\\ \theta=\theta_0}} = \hat{\mathbf{n}}_t{}^{\mathrm{T}}\Big|_{\substack{\varphi=0\\ \theta=\theta_0}} \cdot \frac{\partial^2 CS(\varphi,\theta)}{\partial\theta^2}\Big|_{\substack{\varphi=0\\ \theta=\theta_0}} = \begin{bmatrix}-\sin\theta_0 & 0 & \cos\theta_0\end{bmatrix}\cdot\begin{bmatrix}-r\cdot\sin\theta_0\\ 0\\ r\cdot\cos\theta_0\end{bmatrix}$$

$$= r\cdot(\sin^2\theta_0+\cos^2\theta_0)$$

$$\Rightarrow d_{22}\Big|_{\substack{\varphi=0\\ \theta=\theta_0}} = r \tag{5.20}$$

Similarly the elements of the G matrix at a CC point can be calculated

$$g_{11}\Big|_{\substack{\varphi=0\\ \theta=\theta_0}} = \left(\frac{\partial \mathbf{CS}(\varphi,\theta)}{\partial\varphi}\right)^T\cdot\left(\frac{\partial \mathbf{CS}(\varphi,\theta)}{\partial\varphi}\right) = \begin{bmatrix}0 & R-r+r.\sin\theta_0 & 0\end{bmatrix}\cdot\begin{bmatrix}0\\ R-r+r.\sin\theta_0\\ 0\end{bmatrix}$$

$$\Rightarrow g_{11}\Big|_{\substack{\varphi=0\\ \theta=\theta_0}} = \left(R-r+r.\sin\theta_0\right)^2 \tag{5.21}$$

Similarly,

$$g_{12}\Big|_{\substack{\varphi=0\\ \theta=\theta_0}} = \left(\frac{\partial \mathbf{CS}(\varphi,\theta)}{\partial\varphi}\right)^T\cdot\left(\frac{\partial \mathbf{CS}(\varphi,\theta)}{\partial\theta}\right) = \begin{bmatrix}0 & R-r+r.\sin\theta_0 & 0\end{bmatrix}\cdot\begin{bmatrix}r\cdot\cos\theta_0\\ 0\\ r\cdot\sin\theta_0\end{bmatrix}$$

$$\Rightarrow \quad g_{12}\Big|_{\substack{\varphi=0\\ \theta=\theta_0}} = 0 = g_{21}\Big|_{\substack{\varphi=0\\ \theta=\theta_0}} \tag{5.22}$$

and

$$g_{22}\Big|_{\substack{\varphi=0\\ \theta=\theta_0}} = \left(\frac{\partial CS(\varphi,\theta)}{\partial\theta}\right)^T\cdot\left(\frac{\partial CS(\varphi,\theta)}{\partial\theta}\right) = \begin{bmatrix}r\cdot\cos\theta_0 & 0 & r\cdot\sin\theta_0\end{bmatrix}\cdot\begin{bmatrix}r\cdot\cos\theta_0\\ 0\\ r\cdot\sin\theta_0\end{bmatrix}$$

$$= r^2\cdot(\cos^2\theta_0+\sin^2\theta_0)$$

$$\Rightarrow \left. g_{22} \right|_{\substack{\varphi=0 \\ \theta=\theta_0}} = r^2 \tag{5.23}$$

Hence the D and G matrix at a CC point on the cutting surface of the tool is

$$D = \begin{bmatrix} (R - r + r.\sin\theta_0)\cdot\sin\theta_0 & 0 \\ 0 & r \end{bmatrix}$$

$$G = \begin{bmatrix} (R - r + r.\sin\theta_0)^2 & 0 \\ 0 & r^2 \end{bmatrix}$$

Substituting the above calculated values in Equation (5.16) and (5.17), the Gaussian curvature K and mean curvature H at a CC point on the cutting surface of the tool can be calculated as follows

$$K = \frac{d_{11}\cdot d_{22} - d_{12}^2}{g_{11}\cdot g_{22} - g_{12}^2} = \frac{\left((R - r + r\cdot\sin\theta_0)\cdot\sin\theta_0\right)\cdot(r) - 0^2}{(R - r + r\cdot\sin\theta_0)^2\cdot r^2 - 0^2}$$

$$\Rightarrow K = \frac{\sin\theta_0}{r\cdot(R - r + r\cdot\sin\theta_0)} \tag{5.24}$$

and

$$H = \frac{1}{2}\cdot\left(\frac{g_{11}\cdot d_{22} - 2\cdot g_{12}\cdot d_{12} + g_{22}\cdot d_{11}}{g_{11}\cdot g_{22} - g_{12}^2}\right)$$

$$= \frac{1}{2}\cdot\left(\frac{(R - r + r.\sin\theta_0)^2\cdot(r) - 2\cdot 0\cdot 0 + (r^2)\cdot\left((R - r + r\cdot\sin\theta_0)\cdot\sin\theta_0\right)}{(R - r + r\cdot\sin\theta_0)^2(r^2) - 0^2}\right)$$

$$= \frac{1}{2}\cdot\left(\frac{(R - r + r\cdot\sin\theta_0) + (r)\cdot\sin\theta_0}{(R - r + r.\sin\theta_0)\cdot r}\right)$$

$$\Rightarrow H = \frac{1}{2}\cdot\left(\frac{(R - r + r\cdot\sin\theta_0) + r\cdot\sin\theta_0}{(R - r + r\cdot\sin\theta_0)\cdot r}\right) \tag{5.25}$$

The maximum curvature is $k_{s,\max} = H + \sqrt{H^2 - K}$, and the minimum curvature is $k_{s,\min} = H - \sqrt{H^2 - K}$. So,

$$\sqrt{H^2 - K} = \sqrt{\left(\frac{(R - r + r\cdot\sin\theta_0) + r\cdot\sin\theta_0}{2\cdot(R - r + r.\sin\theta_0)\cdot r}\right)^2 - \left(\frac{\sin\theta_0}{r\cdot(R - r + r.\sin\theta_0)}\right)}$$

$$= \sqrt{\frac{(R - r + r\cdot\sin\theta_0)^2 + (r\cdot\sin\theta_0)^2 + 2\cdot(R - r + r.\sin\theta_0)\cdot r\cdot\sin\theta_0}{4\cdot(R - r + r\cdot\sin\theta_0)^2\cdot r^2} - \frac{4\cdot(R - r + r\cdot\sin\theta_0)\cdot r\cdot\sin\theta_0}{4\cdot(R - r + r\cdot\sin\theta_0)^2\cdot r^2}}$$

$$= \sqrt{\left(\frac{(R - r + r\cdot\sin\theta_0) - r\cdot\sin\theta_0}{2\cdot(R - r + r\cdot\sin\theta_0)\cdot r}\right)^2}$$

$$\sqrt{H^2 - K} = \left(\frac{(R - r + r\cdot\sin\theta_0) - r\cdot\sin\theta_0}{2\cdot(R - r + r\cdot\sin\theta_0)\cdot r}\right) \tag{5.26}$$

Hence, the maximum curvature $k_{t,\max}$ of the cutting surface of the tool at a CC is calculated to be

$$k_{t,\max} = H + \sqrt{H^2 - K}$$

$$= \frac{1}{2}\cdot\left(\frac{(R - r + r\cdot\sin\theta_0) + r\cdot\sin\theta_0}{(R - r + r\cdot\sin\theta_0)\cdot r}\right) + \frac{1}{2}\cdot\left(\frac{(R - r + r\cdot\sin\theta_0) - r\cdot\sin\theta_0}{(R - r + r\cdot\sin\theta_0)\cdot r}\right)$$

$$= \frac{1}{2}\cdot\left(\frac{2(R - r + r\cdot\sin\theta_0)}{(R - r + r\cdot\sin\theta_0)\cdot r}\right)$$

$$\Rightarrow \quad k_{t,\max} = \frac{1}{r} \tag{5.27}$$

Similarly the minimum curvature $k_{t,\min}$ is calculated to be

$$
\begin{aligned}
k_{t,\min} &= H - \sqrt{H^2 - K} \\
&= \frac{1}{2}\cdot\left(\frac{(R-r+r\cdot\sin\theta_0)+r\cdot\sin\theta_0}{(R-r+r\cdot\sin\theta_0)\cdot r}\right) - \frac{1}{2}\cdot\left(\frac{(R-r+r.\sin\theta_0)-r\cdot\sin\theta_0}{(R-r+r\cdot\sin\theta_0)\cdot r}\right) \\
&= \frac{1}{2}\cdot\left(\frac{2\cdot r\cdot\sin\theta_0}{(R-r+r\cdot\sin\theta_0)\cdot r}\right)
\end{aligned}
$$

$$
\Rightarrow k_{t,\min} = \frac{\sin\theta_0}{R-r+r\cdot\sin\theta_0} \tag{5.28}
$$

Meanwhile, the direction of the maximum curvature $\mathbf{t}_{s,max}$ in the tool coordinate system is $\mathbf{t}_{s,max} = d\varphi_{\max}\cdot\mathbf{CS}_{\varphi}(\varphi,\theta) + d\theta_{\max}\cdot\mathbf{CS}_{\theta}(\varphi,\theta)$, where

$$
\begin{aligned}
\begin{bmatrix} d\varphi_{\max} \\ d\theta_{\max} \end{bmatrix} &= \begin{bmatrix} k_{t,\max}\cdot g_{12} - d_{12} \\ d_{11} - k_{t,\max}\cdot g_{11} \end{bmatrix} \\
&= \begin{bmatrix} \dfrac{1}{r}\cdot 0 - 0 \\ (R-r+r.\sin\theta_0)\cdot\sin\theta_0 - \dfrac{1}{r}(R-r+r.\sin\theta_0)^2 \end{bmatrix} \\
&= \begin{bmatrix} 0 \\ (R-r+r.\sin\theta_0)\cdot\sin\theta_0 - \dfrac{1}{r}(R-r+r.\sin\theta_0)^2 \end{bmatrix}
\end{aligned}
$$

Substituting these values

$$
\begin{aligned}
\mathbf{t}_{s,max} &= d\varphi_{\max}\cdot\mathbf{CS}_{\varphi}(\varphi,\theta) + d\theta_{\max}\cdot\mathbf{CS}_{\theta}(\varphi,\theta) \\
&= 0\cdot\begin{bmatrix} 0 \\ R-r+r.\sin\theta_0 \\ 0 \end{bmatrix} + \left((R-r+r.\sin\theta_0)\cdot\sin\theta_0 - \frac{1}{r}(R-r+r.\sin\theta_0)^2\right)\cdot\begin{bmatrix} r\cdot\cos\theta_0 \\ 0 \\ r\cdot\sin\theta_0 \end{bmatrix}
\end{aligned}
$$

$$
\Rightarrow \quad \mathbf{t}_{s,max} = \left((R-r+r.\sin\theta_0)\cdot\sin\theta_0 - \frac{1}{r}(R-r+r.\sin\theta_0)^2\right)\cdot r\cdot\begin{bmatrix} \cos\theta_0 \\ 0 \\ \sin\theta_0 \end{bmatrix} \tag{5.29}
$$

The unit vector $\hat{\mathbf{t}}_{s,max}$ in the maximum curvature direction $\mathbf{t}_{s,max}$ is given by

$$\hat{\mathbf{t}}_{s,max} = \mathbf{t}_{s,max} \Big/ \left|\mathbf{t}_{s,max}\right|$$

$$\Rightarrow \hat{\mathbf{t}}_{s,max} = \begin{bmatrix} \cos\theta_0 \\ 0 \\ \sin\theta_0 \end{bmatrix} \tag{5.30}$$

Similarly, the principal direction of the minimum curvature $\mathbf{t}_{s,min}$ is $\mathbf{t}_{s,min} = d\varphi_{\min} \cdot \mathbf{CS}_{\varphi}(\varphi,\theta) + d\theta_{\min} \cdot \mathbf{CS}_{\theta}(\varphi,\theta)$, where

$$\begin{bmatrix} d\varphi_{\min} \\ d\theta_{\min} \end{bmatrix} = \begin{bmatrix} k_{s,\min} \cdot g_{21} - d_{21} \\ d_{11} - k_{s,\min} \cdot g_{11} \end{bmatrix} = \begin{bmatrix} \left(\dfrac{\sin\theta_0}{R - r + r.\sin\theta_0}\right) \cdot 0 - 0 \\ (R - r + r.\sin\theta_0) \cdot \sin\theta_0 - \dfrac{\sin\theta_0}{R - r + r.\sin\theta_0}\left(R - r + r.\sin\theta_0\right)^2 \end{bmatrix}$$

$$\Rightarrow \begin{bmatrix} d\varphi_{\min} \\ d\theta_{\min} \end{bmatrix} = \begin{bmatrix} 0 \\ 0 \end{bmatrix}$$

Since this cannot represent any direction, so the other set of equation is used i.e.

$$\begin{bmatrix} d\varphi_{\min} \\ d\varphi_{\min} \end{bmatrix} = \begin{bmatrix} k_{s,\min} \cdot g_{22} - d_{22} \\ d_{21} - k_{s,\min} \cdot g_{21} \end{bmatrix} = \begin{bmatrix} \left(\dfrac{\sin\theta_0}{R - r + r.\sin\theta_0}\right) \cdot r^2 - r \\ 0 - \left(\dfrac{\sin\theta_0}{R - r + r.\sin\theta_0}\right) \cdot 0 \end{bmatrix}$$

$$\Rightarrow \begin{bmatrix} d\varphi_{\min} \\ d\varphi_{\min} \end{bmatrix} = \begin{bmatrix} \left(\dfrac{\sin\theta_0}{R - r + r.\sin\theta_0}\right) \cdot r^2 - r \\ 0 \end{bmatrix} \tag{5.31}$$

$$\mathbf{t}_{s,\min} = d\varphi_{\min} \cdot \mathbf{CS}_{\varphi}(\varphi,\theta) + d\theta_{\min} \cdot \mathbf{CS}_{\theta}(\varphi,\theta)$$

$$= \left(\left(\frac{\sin\theta_0}{R - r + r.\sin\theta_0} \right) \cdot r^2 - r \right) \cdot \begin{bmatrix} 0 \\ R - r + r.\sin\theta_0 \\ 0 \end{bmatrix} + 0 \cdot \begin{bmatrix} r \cdot \cos\theta_0 \\ 0 \\ r \cdot \sin\theta_0 \end{bmatrix}$$

$$\Rightarrow \mathbf{t}_{s,\min} = \left(\left(\frac{\sin\theta_0}{R - r + r.\sin\theta_0} \right) \cdot r^2 - r \right) \cdot \begin{bmatrix} 0 \\ R - r + r.\sin\theta_0 \\ 0 \end{bmatrix} \tag{5.32}$$

The unit vector $\hat{\mathbf{t}}_{s,\min}$ in the minimum curvature direction $\mathbf{t}_{s,\min}$ is given by

$$\hat{\mathbf{t}}_{s,\min} = \mathbf{t}_{s,\min} / \left| \mathbf{t}_{s,\min} \right|$$

$$\Rightarrow \hat{\mathbf{t}}_{s,\min} = \begin{bmatrix} 0 \\ 1 \\ 0 \end{bmatrix} \tag{5.33}$$

So, the maximum curvature of this cutting surface at the CC point can be found as $k_{t,\max} = 1/r$; and its direction $\hat{\mathbf{t}}_{t,\max}$ is $\begin{bmatrix} \cos\theta_0 & 0 & \sin\theta_0 \end{bmatrix}^T$ in the tool coordinate system (see Figure 5.2). Meanwhile, the minimum curvature is $k_{t,\min} = \sin\theta_0 / \left(R - r + r \cdot \sin\theta_0 \right)$; and its direction $\hat{\mathbf{t}}_{t,\min}$ is $\begin{bmatrix} 0 & 1 & 0 \end{bmatrix}^T$ in the same system. A feature of the cutting surface is that all the normal curvatures are positive as shown in the example of Figure 5.3. Figure 5.3 shows the curvature plot along all the tangent directions at a point ($\theta_0 = 45^\circ$) on a bull-nose end-mill ($R = 10\ mm$ and $r = 2\ mm$).

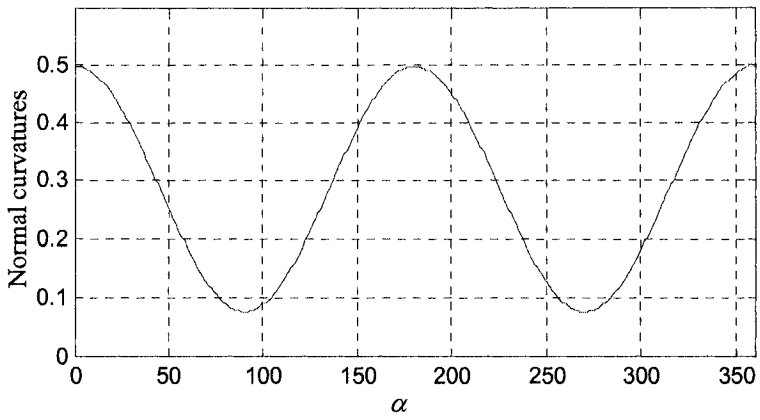

Figure 5.3. Normal curvatures at a point on the cutting surface of a torus end-mill.

For ball-nose end-mills ($R = r$), the principal curvatures are the same as $k_{\max} = k_{\min} = 1/R$, and for the normal curvatures are all equal to $1/R$ as well.

Chapter 6 Comprehensive Curvature Analysis for Single Surface Machining

Evaluating the geometric mis/match between the cutting surface and the part surface in the vicinity of a CC point cannot be completely done by only comparing their principal curvatures, because their principal directions may not necessarily coincide with each other. To make a correct evaluation, the normal curvatures of these surfaces should be compared in every tangent direction. However, the principal directions of the cutting surface are represented in the tool coordinate system whereas the principal directions of the part surface are represented in the part coordinate system; and since the part coordinate system has been used as a reference, so the principal directions of the cutting surface should be converted into the part coordinate system.

6.1 Transformation Matrix for Converting the Principal Directions of the Cutting Surface

According to the position relationship between the part and the tool coordinate systems, the transformation matrix R for converting the principal directions of the cutting surface should be found such that $\mathbf{T}_{t,max} = [R] \cdot \hat{\mathbf{t}}_{t,max}$ and $\mathbf{T}_{t,min} = [R] \cdot \hat{\mathbf{t}}_{t,min}$.

where

$\mathbf{T}_{t,max}$ is the direction of maximum curvature represented in the part coordinate system

$\hat{\mathbf{t}}_{t,max}$ is the direction of maximum curvature represented in the tool coordinate system

$\mathbf{T}_{t,min}$ is the direction of minimum curvature represented in the part coordinate system

$\hat{\mathbf{t}}_{t,min}$ is the direction of minimum curvature represented in the tool coordinate system

$R = \begin{bmatrix} a_x & b_x & c_x \\ a_y & b_y & c_y \\ a_z & b_z & c_z \end{bmatrix}$ is the transformation matrix

a_x, a_y, a_z are respectively the X, Y and Z components of a unit vector along the x axis of the tool coordinate system(x-y-z). Similarly b_x, b_y, b_z are the X, Y and Z components of a unit vector along the y axis and c_x, c_y, c_z are those of the z axis.

In order to determine the elements of the mapping matrix, first of all a relation between the part and the tool coordinate system has been established as shown in Figure 6.1

Let $(\mathbf{x}_w - \mathbf{y}_w - \mathbf{z}_w)$ represent the principal axes of the tool coordinate system $(\mathbf{x} - \mathbf{y} - \mathbf{z})$ in terms of the part coordinate system

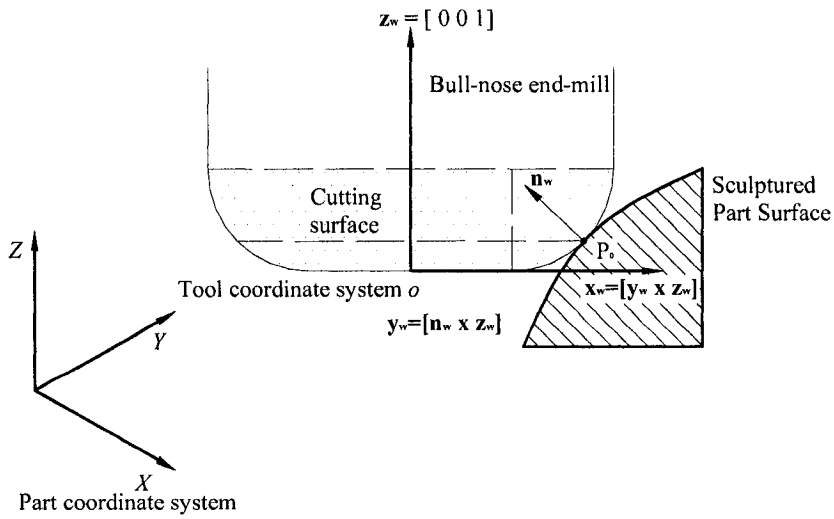

Figure 6.1. Relationship between part coordinate system and tool coordinate system.

Based on the definition of the tool coordinate system

- The z axis of the tool coordinate system is vertically upwards, so $\mathbf{z}_w = [0 \quad 0 \quad 1]^T$
- $\mathbf{y}_w$ axis is perpendicular to the plane formed by the unit surface normal $\hat{\mathbf{n}}$ and the $\mathbf{z}_w$ axis, so it can be calculated by the cross product of $\hat{\mathbf{n}}$ and the $\mathbf{z}_w$ axis. Mathematically,

$$\mathbf{y}_w = \hat{\mathbf{n}} \times \mathbf{z}_w$$

$$\mathbf{y}_w = \begin{vmatrix} \hat{i} & \hat{j} & \hat{k} \\ n_x & n_y & n_z \\ 0 & 0 & 1 \end{vmatrix} = \hat{i}(n_y) - \hat{j}(n_x) + \hat{k}(0) = \begin{bmatrix} n_y \\ -n_x \\ 0 \end{bmatrix} \tag{6.1}$$

- $\mathbf{x}_w$ is given by the cross product of $\mathbf{y}_w$ *and* $\mathbf{z}_w$

$$\mathbf{x}_w = \mathbf{y}_w \times \mathbf{z}_w$$

$$\mathbf{x}_w = \begin{vmatrix} \hat{i} & \hat{j} & \hat{k} \\ n_y & -n_x & 0 \\ 0 & 0 & 1 \end{vmatrix} = \hat{i}(-n_x) - \hat{j}(n_y) + \hat{k}(0) = \begin{bmatrix} -n_x \\ -n_y \\ 0 \end{bmatrix} \tag{6.2}$$

The unit vector $\hat{\mathbf{x}}_w$ and $\hat{\mathbf{y}}_w$ in the direction of $\mathbf{x}_w$ and $\mathbf{y}_w$ axis respectively are calculated to be

$$\mathbf{x}_w = \begin{bmatrix} \frac{-n_x}{\sqrt{(n_x^2 + n_y^2)}} & \frac{-n_y}{\sqrt{(n_x^2 + n_y^2)}} & 0 \end{bmatrix}^T \text{ and } \mathbf{y}_w = \begin{bmatrix} \frac{n_y}{\sqrt{(n_x^2 + n_y^2)}} & \frac{-n_x}{\sqrt{(n_x^2 + n_y^2)}} & 0 \end{bmatrix}^T$$

The unit vectors in the direction of the $(X - Y - Z)$ axis in the world coordinate system are respectively, $\hat{\mathbf{i}} = [1 \quad 0 \quad 0]^T$, $\hat{\mathbf{j}} = [0 \quad 1 \quad 0]^T$ and $\hat{\mathbf{k}} = [0 \quad 0 \quad 1]^T$. Based on the relation between the tool and part coordinate system the elements of the transformation matrix can be calculated as

a_x is the X component of a unit vector along the x axis of the tool coordinate system

$$a_x = \hat{\mathbf{x}}_{\mathbf{w}}^{\mathbf{T}} \cdot \mathbf{i} = \begin{bmatrix} \frac{-n_x}{\sqrt{(n_x^2 + n_y^2)}} & \frac{-n_y}{\sqrt{(n_x^2 + n_y^2)}} & 0 \end{bmatrix} \cdot \begin{bmatrix} 1 \\ 0 \\ 0 \end{bmatrix} = \begin{bmatrix} \frac{-n_x}{\sqrt{(n_x^2 + n_y^2)}} \end{bmatrix} \tag{6.3}$$

a_y is the Y component of a unit vector along the x axis of the tool coordinate system

$$a_y = \hat{\mathbf{x}}_{\mathbf{w}}^{\mathbf{T}} \cdot \mathbf{j} = \begin{bmatrix} \frac{-n_x}{\sqrt{(n_x^2 + n_y^2)}} & \frac{-n_y}{\sqrt{(n_x^2 + n_y^2)}} & 0 \end{bmatrix} \cdot \begin{bmatrix} 0 \\ 1 \\ 0 \end{bmatrix} = \begin{bmatrix} \frac{-n_y}{\sqrt{(n_x^2 + n_y^2)}} \end{bmatrix} \tag{6.4}$$

a_z is the Z component of a unit vector along the x axis of the tool coordinate system

$$a_z = \hat{\mathbf{x}}_{\mathbf{w}}^{\mathbf{T}} \cdot \mathbf{j} = \begin{bmatrix} \frac{-n_x}{\sqrt{(n_x^2 + n_y^2)}} & \frac{-n_y}{\sqrt{(n_x^2 + n_y^2)}} & 0 \end{bmatrix} \cdot \begin{bmatrix} 0 \\ 0 \\ 1 \end{bmatrix} = [0] \tag{6.5}$$

b_x is the X component of a unit vector along the y axis of the tool coordinate system

$$b_x = \hat{\mathbf{y}}_{\mathbf{w}}^{\mathbf{T}} \cdot \hat{\mathbf{i}} = \begin{bmatrix} \frac{n_y}{\sqrt{(n_x^2 + n_y^2)}} & \frac{-n_x}{\sqrt{(n_x^2 + n_y^2)}} & 0 \end{bmatrix} \cdot \begin{bmatrix} 1 \\ 0 \\ 0 \end{bmatrix} = \begin{bmatrix} \frac{n_y}{\sqrt{(n_x^2 + n_y^2)}} \end{bmatrix} \tag{6.6}$$

b_y is the Y component of a unit vector along the y axis of the tool coordinate system

$$b_y = \hat{\mathbf{y}}_{\mathbf{w}}^{\mathbf{T}} \cdot \hat{\mathbf{j}} = \begin{bmatrix} \frac{n_y}{\sqrt{(n_x^2 + n_y^2)}} & \frac{-n_x}{\sqrt{(n_x^2 + n_y^2)}} & 0 \end{bmatrix} \cdot \begin{bmatrix} 0 \\ 1 \\ 0 \end{bmatrix} = \begin{bmatrix} \frac{-n_x}{\sqrt{(n_x^2 + n_y^2)}} \end{bmatrix} \tag{6.7}$$

b_z is the Z component of a unit vector along the y axis of the tool coordinate system

$$b_z = \hat{\mathbf{y}}_{\mathbf{w}}^{\mathbf{T}} \cdot \hat{\mathbf{k}} = \begin{bmatrix} \frac{n_y}{\sqrt{(n_x^2 + n_y^2)}} & \frac{-n_x}{\sqrt{(n_x^2 + n_y^2)}} & 0 \end{bmatrix} \cdot \begin{bmatrix} 0 \\ 0 \\ 1 \end{bmatrix} = [0] \tag{6.8}$$

c_x is the X component of a unit vector along the z axis of the tool coordinate system

$$c_x = \hat{\mathbf{z}}_{\mathbf{w}}^{\mathrm{T}} \times \hat{\mathbf{i}} = \begin{bmatrix} 0 & 0 & 1 \end{bmatrix} \cdot \begin{bmatrix} 1 \\ 0 \\ 0 \end{bmatrix} = \begin{bmatrix} 0 \end{bmatrix} \tag{6.9}$$

c_y is the Y component of a unit vector along the z axis of the tool coordinate system

$$c_y = \hat{\mathbf{z}}_{\mathbf{w}}^{\mathrm{T}} \times \hat{\mathbf{j}} = \begin{bmatrix} 0 & 0 & 1 \end{bmatrix} \cdot \begin{bmatrix} 0 \\ 1 \\ 0 \end{bmatrix} = \begin{bmatrix} 0 \end{bmatrix} \tag{6.10}$$

c_z is the Z component of a unit vector along the z axis of the tool coordinate system

$$c_z = \hat{\mathbf{z}}_{\mathbf{w}}^{\mathrm{T}} \times \hat{\mathbf{k}} = \begin{bmatrix} 0 & 0 & 1 \end{bmatrix} \cdot \begin{bmatrix} 0 \\ 0 \\ 1 \end{bmatrix} = \begin{bmatrix} 1 \end{bmatrix} \tag{6.11}$$

Plugging the above values of the elements of the transformation matrix, the

$$[R] = \frac{1}{\sqrt{n_x^2 + n_y^2}} \cdot \begin{bmatrix} -n_x & n_y & 0 \\ -n_y & -n_x & 0 \\ 0 & 0 & \sqrt{n_x^2 + n_y^2} \end{bmatrix} \tag{6.12}$$

With the help of the transformation matrix the direction of maximum curvature of the cutting surface of the tool can be determined in terms of the part coordinate system

$$\mathbf{T}_{t,\max} = [R] \cdot \hat{\mathbf{t}}_{t,\max} = \frac{1}{\sqrt{n_x^2 + n_y^2}} \cdot \begin{bmatrix} -n_x & n_y & 0 \\ -n_y & -n_x & 0 \\ 0 & 0 & \sqrt{n_x^2 + n_y^2} \end{bmatrix} \cdot \begin{bmatrix} \cos\theta_0 \\ 0 \\ \sin\theta_0 \end{bmatrix}$$

$$\Rightarrow \mathbf{T}_{t,\max} = \begin{bmatrix} \left(-n_x \cdot \cos\theta_0\right) \Big/ \sqrt{n_x^2 + n_y^2} \\ \left(-n_y \cdot \cos\theta_0\right) \Big/ \sqrt{n_x^2 + n_y^2} \\ \sin\theta_0 \end{bmatrix} \tag{6.13}$$

Similarly, the direction of minimum curvature of the cutting surface of the tool can be determined in terms of the part coordinate system

$$\mathbf{T}_{t,\min} = [R]\cdot\hat{\mathbf{t}}_{t,\min} = \frac{1}{\sqrt{n_x^2+n_y^2}}\cdot\begin{bmatrix} -n_x & n_y & 0 \\ -n_y & -n_x & 0 \\ 0 & 0 & \sqrt{n_x^2+n_y^2} \end{bmatrix}\cdot\begin{bmatrix} 0 \\ 1 \\ 0 \end{bmatrix}$$

$$\Rightarrow \mathbf{T}_{t,\min} = \begin{bmatrix} n_y/\sqrt{n_x^2+n_y^2} \\ -n_x/\sqrt{n_x^2+n_y^2} \\ 0 \end{bmatrix} \tag{6.14}$$

Thus, in the part coordinate system, the direction of the maximum curvature $\mathbf{T}_{t,\max}$ is $\left[\left(-n_x\cdot\cos\theta_0\right)/\sqrt{n_x^2+n_y^2} \quad \left(-n_y\cdot\cos\theta_0\right)/\sqrt{n_x^2+n_y^2} \quad \sin\theta_0\right]^T$, and the direction of the minimum curvature $\mathbf{T}_{t,\min}$ is $\left[n_y/\sqrt{n_x^2+n_y^2} \quad -n_x/\sqrt{n_x^2+n_y^2} \quad 0\right]^T$. The values of the principal curvatures are the same in the two coordinate systems. The direction of the maximum curvature of the cutting surface $\mathbf{T}_{t,\max}$ is designated as a reference to identify the tangent directions (see Figure 6.2).

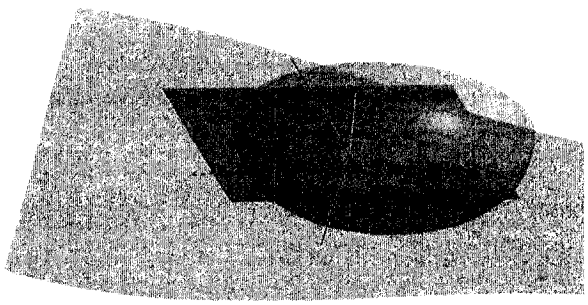

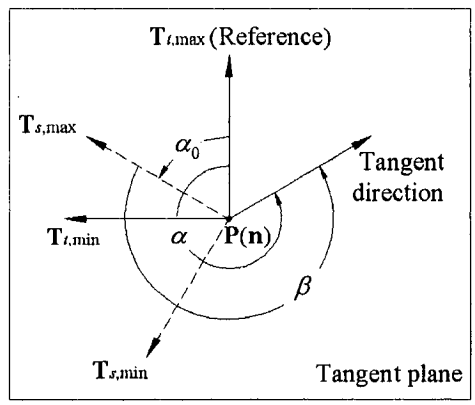

Figure 6.2. Principal directions of the toroidal cutting surface and the part surface.

According to Euler's formula, the cutting-surface normal curvature along any tangent direction can calculated, the tangent direction is represented with angle α measured positive counter-clockwise from the direction of the maximum curvature $\mathbf{T}_{t,\max}$, and can be calculated as

$$k_t(\alpha) = \frac{1}{r} \cdot \cos^2 \alpha + \frac{\sin\theta_0}{R - r + r \cdot \sin\theta_0} \cdot \sin^2 \alpha \qquad \alpha \in [0,\ 2\pi] \tag{6.15}$$

For the normal curvatures of the part surface, given in Equation (5.20), the angle β of a tangent direction is measured from the maximum curvature direction $\mathbf{T}_{s,\max}$ of the part surface. To find the normal curvatures of the cutting and the part surfaces in a direction, the angle α_0 between the directions of the maximum curvatures of these two surfaces should be found.

$$\alpha_0 = \arccos\left(\frac{\mathbf{T}_{s,\max} \cdot \mathbf{T}_{t,\max}}{\left|\mathbf{T}_{s,\max}\right| \cdot \left|\mathbf{T}_{t,\max}\right|} \right) \tag{6.16}$$

where α_0 is measured in counter-clockwise from $\mathbf{T}_{t,\max}$ and is between 0 and π. Therefore, the relationship between α and β is $\beta = 2\pi + \alpha - \alpha_0$ $(0 \le \alpha \le \alpha_0)$ or $\beta = \alpha - \alpha_0$ $(\alpha_0 < \alpha \le 2\pi)$. Based on this angle, for an interior surface point, the normal curvature of the part surface in a direction measured from $\mathbf{T}_{t,\max}$ can be calculated as

$$k_s(\beta) = k_{s,\max} \cdot \cos^2(\alpha - \alpha_0) + k_{s,\min} \cdot \sin^2(\alpha - \alpha_0) \qquad \alpha \in [0,\ 2\pi] \tag{6.17}$$

where angle α starts from $\mathbf{T}_{t,\max}$ and is positive in counter-clockwise direction

With Eqs. (6.15) and (6.17), the normal curvatures of the cutting and part surfaces can be calculated in the same direction, and they can be analyzed to detect local gouging at a CC point using the following conditions. Curvature Conditions for Different Shape Machining with Ball- and Bull-Nose End-Mills

To facilitate the curvature comparison between the cutter and the different shapes of the local area around the CC point on the part surface i.e. based on the values of the principal curvatures of the cutting surface of the tool and the part surface, the different curvature conditions are provided in the following cases.

6.1.1 Case 1: $k_{t,\max} \geq k_{t,\min} \geq 0 \geq k_{s,\max} \geq k_{s,\min}$

First, at a convex CC point on the part surface the normal curvatures are negative in all the tangent directions but the normal curvatures of the cutting surface are always positive in all tangent directions. Hence, the condition for this case is

$$k_{t,\max} \geq k_{t,\min} \geq 0 \geq k_{s,\max} \geq k_{s,\min} \tag{6.18}$$

The curvature comparison along all the tangent directions can be omitted, because no matter what the phase difference (α_0) is, the normal curvature of the cutting surface of the tool will always be greater than that of the part surface in all the tangent directions i.e. $\beta \in [0, 2\pi]$ and hence local gouging does not occur when the cutter contacts the convex CC point on the part surface. An example of the above case is illustrated in Figure 6.3.

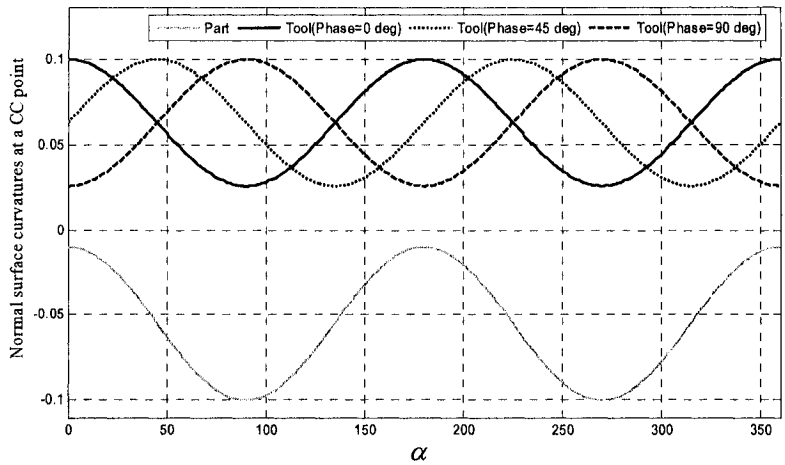

Figure 6.3. Normal curvature comparisons for an example for case (1).

In Figure 6.3 the principal curvatures of the part surface at a CC point are -0.01 and $-0.1\ mm^{-1}$ respectively and that of the cutting surface of the tool are 0.1 and $0.0261\ mm^{-1}$ respectively. Three different normal curvature plots of the cutting surface of the tool with the same principal curvatures but with a phase difference of 0^0, 45^0 and 90^0 respectively are plotted as shown in Figure 6.3 i.e. it can be seen that irrespective of the phase difference the normal curvatures of the cutting surface of the tool are always greater than that of the part surface in all tangent directions and hence local gouging will not occur at this CC point , therefore is no need of curvature comparison in all tangent directions.

6.1.2 Case 2: $k_{t,\max} \geq k_{t,\min} \geq k_{s,\max} \geq k_{s,\min}$

Since all part-surface curvatures at a concave CC point and some at a saddle CC point are positive, the curvature comparison between the tool and the concave/saddle part surfaces should be conducted in detail. In one extreme case, if, at a CC point, the curvature conditions are such that as in Equation (6.19).

$$k_{t,\max} \geq k_{t,\min} \geq k_{s,\max} \geq k_{s,\min} \tag{6.19}$$

In this extreme case all the normal curvatures of the cutting surface are larger than those of the part surface, local gouging does not occur at this point. An example of this case is explained with the help of Figure 6.4.

In Figure 6.4 principal curvatures of the part surface are 0.05 and -0.03 mm^{-1} and that of the cutting surface of the tool are 0.06 and 0.1 mm^{-1} at a CC point. It can be seen from the figure that irrespective of the phase difference, if the condition of Equation (6.19) is met, the normal curvature of the cutting surface of the tool will be greater than that of the part surface in all tangent directions and hence there will be no local gouging at that CC point and therefore there is no need of detailed curvature comparison in this extreme case as well.

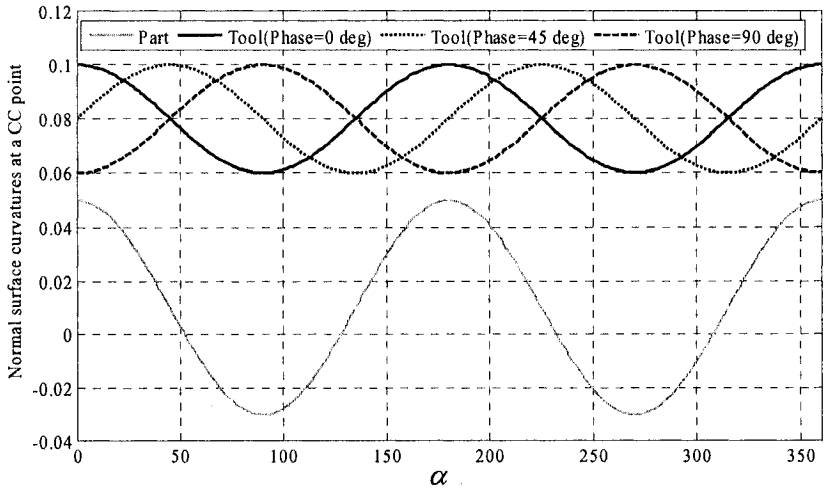

Figure 6.4. Normal curvature comparisons for an example for case (2).

6.1.3 Case 3: $k_{s,\max} \geq k_{s,\min} > k_{t,\max} \geq k_{t,\min}$

In another extreme case of a concave or saddle CC point on the part surface could be as shown in Equation (6.20).

$$k_{s,\max} \geq k_{s,\min} > k_{t,\max} \geq k_{t,\min} \tag{6.20}$$

In this extreme case, the normal curvatures of the cutting surface are smaller than those of the part surface in all the tangent directions i.e. $\beta \in [0, 2\pi]$ and the tool will over-cut the part surface in all tangent directions. An example of the above case is illustrated with the help of Figure 6.5.

In Figure 6.5 the principal curvatures of the part surface are *0.1* and *0.05* mm^{-1} and that of the cutting surface of the tool are *0.04* and *0.01* mm^{-1}. It can be seen from the figure that irrespective of the phase difference, if the condition of Equation (6.20) is met, the normal curvatures of the cutting surface of the tool will always be less than that of the part surface and hence the tool will overcut the part surface at that CC point in all tangent direction and therefore detailed curvature comparison in not required.

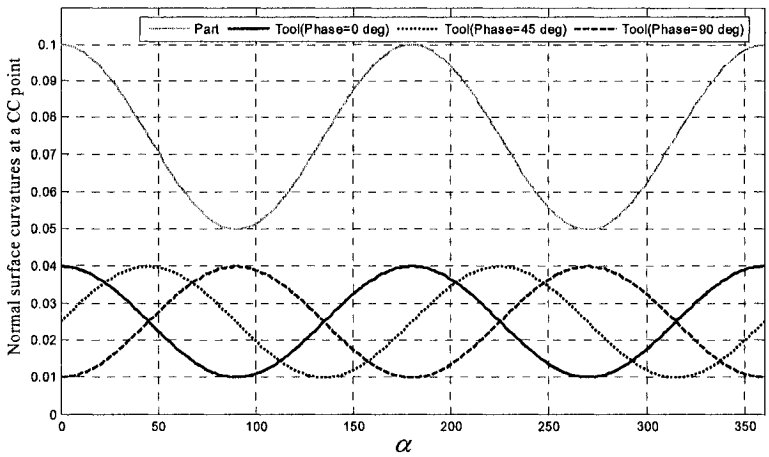

Figure 6.5. Normal curvature comparisons for an example for case (3).

6.1.4 Case 4: $k_{s,max} \geq k_{t,max} > k_{t,min} \geq k_{s,min}$

In one specific case at a concave or saddle CC point on the part surface, the principal curvatures of the part surface and the cutting surface of the tool a could be related as shown in Equation (6.21).

$$k_{s,\max} \geq k_{t,\max} \geq k_{t,\min} \geq k_{s,\min} \tag{6.21}$$

In this specific case, local gouging will occur but not necessarily in all the tangent directions. The tangent directions in which gouging will occur will depend on the phase difference(α_0). An example of this case is illustrated with the help of Figure 6.6. In this example the principal curvatures of the part surface are 0.1 and 0.01 mm^{-1} and that of the cutting surface of the tool is 0.08 and 0.03 mm^{-1}. It can be seen from Figure 6.6 that irrespective of the different phase differences, gouging does occur in some tangent directions.

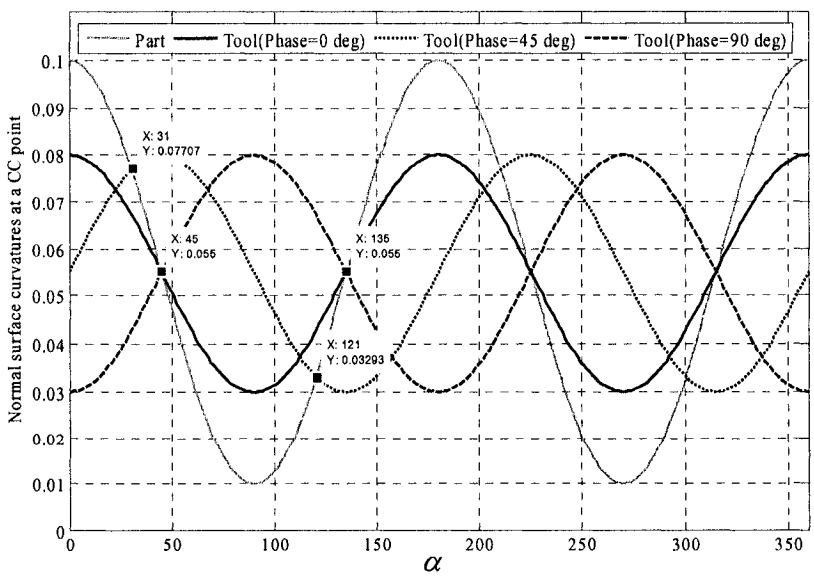

Figure 6.6. Normal curvature comparisons for an example for case (4).

For example when the phase difference is 0^0 and 90^0, gouging occurs in the tangent directions from 0^0-45^0,135^0-225^0 and 315^0-360^0 but the gouging is more when the phase difference is 90^0 than that compared to that of 0^0. When the phase difference is 45^0, gouging occurs in the tangent directions from 0^0-31^0, 121^0-211^0 and 301^0-360^0. So in order to know the tangent directions in which gouging will occur, the detailed curvature comparison has to be done.

6.1.5 Case 5: $k_{t,max} \geq k_{s,max} > k_{s,min} \geq k_{t,min}$

In other specific case, if the principal curvatures are such that as in Equation (6.21)

$$k_{t,\max} \geq k_{s,\max} \geq k_{s,\min} \geq k_{t,\min} \tag{6.21}$$

In this specific case as well, local gouging will occur in some tangent directions. The tangent directions in which gouging will occur will depend on the phase difference(α_0). And hence detailed curvature analysis has to be performed. An example of this case is illustrated with the help of. Figure 6.7.

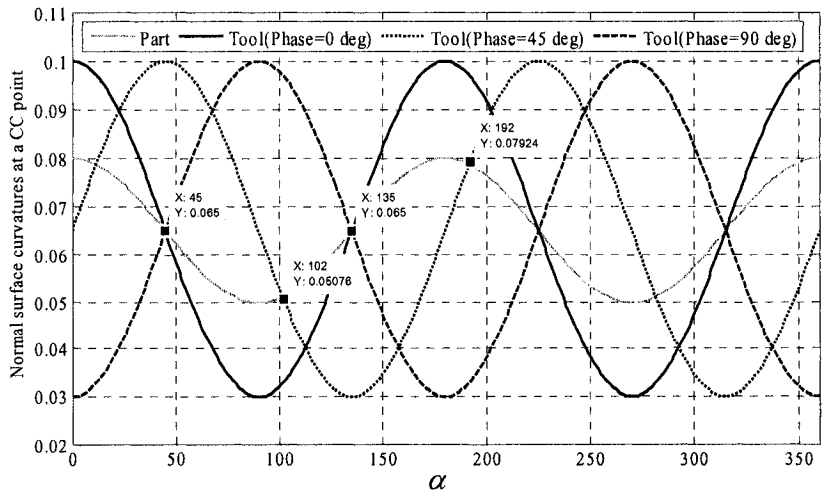

Figure 6.7. Normal curvature comparisons for an example for case (5).

In this example the principal curvatures of the part surface are 0.08 and 0.05 mm^{-1} and that of the cutting surface of the tool is 0.1 and 0.03 mm^{-1}.It can be seen from Figure 6.7 gouging does occur in some tangent directions for all the three different phase differences. For example when the phase difference is 0^0, gouging occurs in the tangent directions from 45^0-135^0 and 225^0-315^0, when the phase difference is 45^0,gouging occurs from 0^0-12^0,101^0-191^0 and 281^0-360^0 and when the phase difference is 90^0,gouging occurs in the tangent directions 0^0-45^0,135^0-225^0 and 315^0-360^0. So also in this case in order to know the tangent directions in which gouging will occur, the detailed curvature comparison has to be done.

6.1.6 Case 6: $k_{t,\max} \geq k_{s,\max} > k_{t,\min} \geq k_{s,\min}$

If the principal curvatures of the part and cutting surface of the tool are related as given by Equation (6.22)

$$k_{t,\max} \geq k_{s,\max} \geq k_{t,\min} \geq k_{s,\min} \tag{6.22}$$

This is a very special case in which the cutter may or may not gouge the part surface; thus the detailed curvature comparison is needed. An example of this case is illustrated with the help of Figure 6.8.

In this example the principal curvatures of the part surface are *0.08* and *0.02* mm^{-1} and that of the cutting surface of the tool are *0.1* and *0.05* mm^{-1}. It can be seen that the condition of Equation (6.22) has been met. It can seen from the figure that if the phase difference between the two normal curvatures is zero, then the normal surface curvature of the tool will always be greater than that of the part surface in all tangent directions and

hence gouging will not occur in this case. But if the phase difference is 45^0, it can be seen from figure that in some tangent directions ($0\text{-}5^0$,$135\text{-}185^0$ and $315\text{-}360^0$ approx.) that the normal curvature of the tool is less than that of the part surface and hence there will be gouging in these tangent directions. And similarly when the phase difference is 90^0, gouging will occur in the tangent directions from $0\text{-}31^0$,$148.1\text{-}211^0$ and $328.1 - 360^0$ respectively.

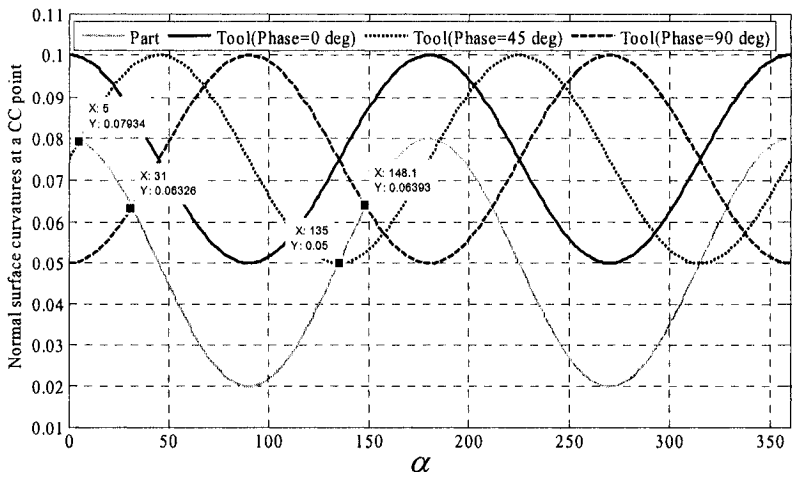

Figure 6.8. Normal curvature comparisons for an example for case (6).

For these types of cases, a mathematical model for its comparison, an optimization problem, can be formulated as

$$f(\alpha)=\frac{1}{r}\cos^2\alpha+\frac{\sin\theta_0}{R-r+r\cdot\sin\theta_0}\sin^2\alpha-k_{s,\max}\cos^2(\alpha-\alpha_0)-k_{s,\min}\sin^2(\alpha-\alpha_0) \qquad (6.23)$$

where $\alpha\in[0,\ 2\pi]$. An existing global optimization method can be employed to find the minimum of $f(\alpha)$. If this minimum is positive or equal to zero in its domain, gouging is free at this point; otherwise, it will occur.

Therefore, in order to detect gouging first of all the principal curvatures of the part and cutting surface are calculated and if any of the conditions of the Eqs. (6.18) – (6.20) are met then there is no need to calculate the normal curvatures but if the conditions of Eqs. (6.21)-(6.22) is met then gouging will occur in some tangent directions and in order to find these tangent directions the normal curvatures of the surfaces need to be compared but if the condition of Equation (6.22),then gouging may or may not occur and in that case Equation.(6.23) is used to detect gouging. This comprehensive curvature analysis can be quickly carried out at every CC point in order to detect local gouging, and if the tool over-cuts the surface at a CC point, a warning message will be sent suggesting to use a smaller tool.

6.2 Verification of Comprehensive Curvature Analysis

To verify this new approach to analyzing the tool-and-part surface curvatures for local gouging detection, a part with a NURBS surface is adopted in this example, and a bull-nose end-mill with a radius of 12 *mm* and a corner radius of 4 *mm* is used for CNC machining. Figure 6.9 shows this cutter is machining part surface at a CC point. By conducting the comprehensive curvature analysis, local gouging on the surface is detected at this CC point

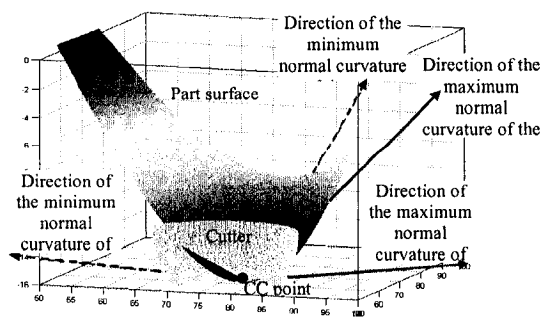

Figure 6.9. Bull-nose end-mill cuts a part surface at a CC point in 3-axis CNC milling.

At this CC point, the maximum and the minimum curvatures of the part surface are calculated to be $k_{s,\max} = 0.0575$ and $k_{s,\min} = 0.0109\ mm^{-1}$, respectively; and those of the cutting surface of the tool are $k_{t,\max} = 0.25$ and $k_{t,\min} = 0.0246\ mm^{-1}$, respectively. From the above values of the principal curvatures, it can be seen that $k_{t,\max} \geq k_{s,\max} \geq k_{t,\min} \geq k_{s,\min}$ and hence the condition of Equation (6.21) is met, and the optimization problem should be solved. To demonstrate the normal curvatures of the tool and the part surfaces along all the tangent directions, they are plotted in Figure 6.10. In this figure, the normal curvatures of the cutting surface of the tool are less then that of the part surface in two zones i.e. in the tangent directions, whose angles are between 68° to 107° and 248° to 287°, the angles are measured anticlockwise positive and from the maximum curvature direction of the cutting surface of the tool . So it can be seen that gouging occurs in two zones, first in the tangent direction whose angles are from 68° to107° i.e. for a period of 39° (107° - 68°) and the second in the tangent directions from 248° to 287° i.e. for a period of 43° (287° - 248°) . These two zones are represented by angles δ and γ in Figure 6.9 respectively.

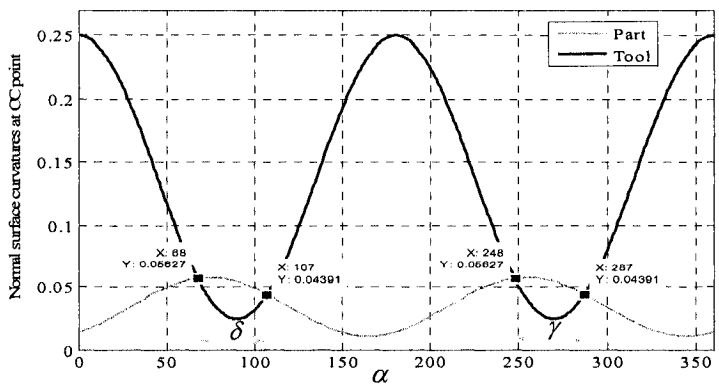

Figure 6.10. Normal curvatures of the part and the cutting surface at a CC point.

To verify this result, the neighbourhood of the CC point in is enlarged and projected from a viewpoint inside the cutter along the surface normal direction. This is shown in

Figure 6.11. In this figure, the lighter and darker regions represent the tool and the part surfaces, respectively. The two regions of the part surface come out of the tool surface at the CC point, which means the end-mill is cutting inside the part surface. With respect to the direction of the maximum curvature of the part surface, the left and right-hand side gouging regions are within the ranges, δ and γ, which are well approximate to the calculated result.

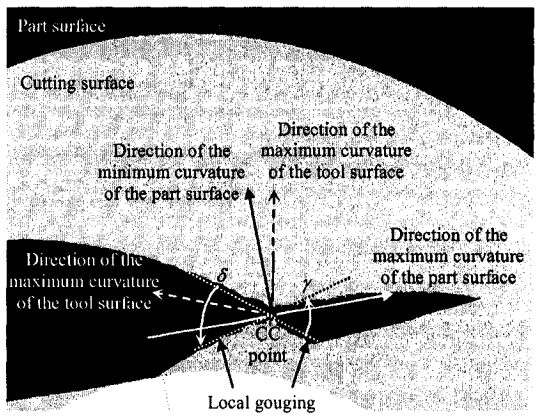

Figure 6.11. Local gouging at the CC point.

6.3 Curvature Analysis for Flat End-Mills

The way of curvature analysis is different when using flat end-mills, compared to that when using bull- or ball-nose end-mills. This is because the toroidal/spherical cutting surface of the bull-/ball-nose end-mills degenerates into a planar cutting circle of the flat end-mills ($r = 0$). To conduct the curvature analysis between the cutting circle and the local part surface at the CC point, first, the intersection curve between the plane of this

circle and the part surface can be identified; second, the curvature of this curve at the CC point should be calculated; and third, this curvature is compared with the curvature of the cutting circle, $1/R$.

However, the curvature of the intersection curve is not equal to the normal curvature of the part surface along the tangent direction of this curve. By using Meusnier's theorem, the curvature of the intersection curve can be computed as

$$k = \frac{1}{\cos\eta}\left(k_{s,\max}\cdot\cos^2\beta_0 + k_{s,\min}\cdot\sin^2\beta_0\right) \tag{6.24}$$

where angle β_0 is the angle between $\mathbf{T}_{s,\max}$ and $\mathbf{T}_{t,\min}$, and angle η is the angle between the tool axis and the surface normal **n** (see Figure 6.12). To compare the tool-and-part surface curvatures, if this curvature k is less than $1/R$, the local surface is free of gouging; otherwise, it will be gouged.

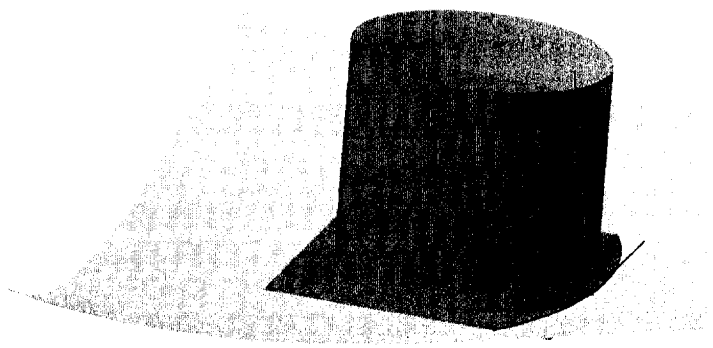

Figure 6.12. Illustration of sculptured surface machining using a flat end-mill.

Chapter 7 Practical Tool Size Determination

One of the main applications of the comprehensive curvature analysis is to determine a practical tool size for machining a CC point on the part surface for 3-axis CNC local gouge free machining. An algorithm is proposed to select a practical tool size based on the concept that local gouging occurs when the normal curvatures of the cutting surface of the tool is less then that of the part surface at a CC point. A practical tool size means that a tool of standard sizes that are available in the market or available in the machine shop.

For a CC point on the part surface, its principal curvatures, their directions and the normal curvatures can be calculated. Furthermore the principal directions of the cutting surface of the tool and the hence the phase difference between the maximum curvature directions can be calculated. From the list of the available tool sizes in the machine shop at Concordia University the principal curvatures and the normal curvatures of the cutting surface of the tool and compared with that of the part surface for gouging check in each tangent direction. Based on this idea, the tool size determination is divided into three different cases which are discussed below. The shank radius ($R_{available}$) of the tools available in machine shop is [30, 25, 20, 18, 16, 12, 10, 8, and 6] *mm*. The corner radius

(r) should be equal or less than the shank radius. The minimum corner radius is generally 2 *mm*.

7.1 Case (a): Machining Impossible

If the normal curvatures of the part surface are such that even the smallest tool available in the machine shop will locally gouge the part surface in any tangent direction, then a message will be send out to modify the original design of the part surface. This is illustrated with the help of an example given in Figure 7.1.

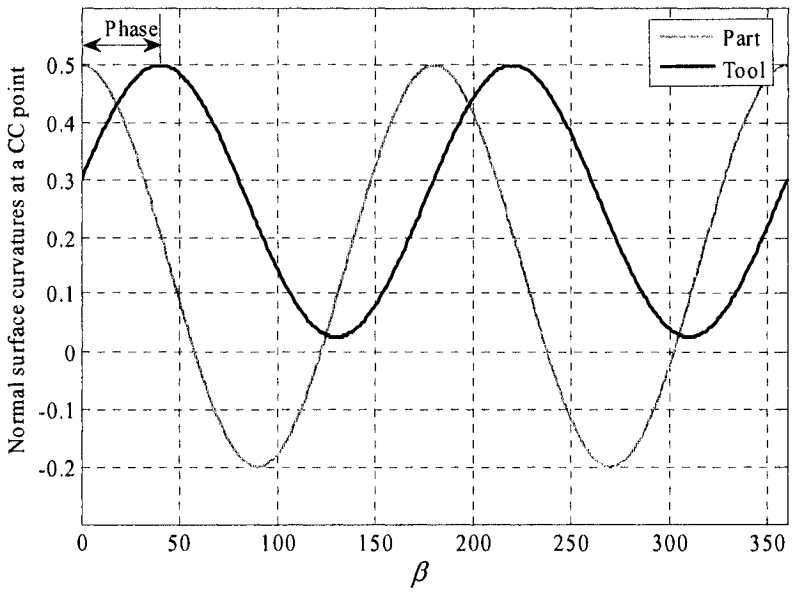

Figure 7.1. An example of case (a)

In this example the principal curvatures of the part surface are 0.5 mm^{-1} and -0.2 mm^{-1}.The phase difference between the maximum curvature directions is 40^0. The smallest tool available in the machine shop is of size R=6 *mm* and r = 2 *mm,* the principal curvatures with this tool is found out to be 0.5 mm^{-1} and 0.024 mm^{-1}. And from the curvature plot it can be seen that the normal curvature of the cutting surface of the tool is

less than that of the part surface in some tangent directions, hence local gouging will occur.

7.2 Case (b): Convex CC Point on the Part Surface

At a convex CC point on the part surface, the principal curvatures are less than zero, whereas at the cutting surface of the tool, all the CC points are concave i.e. the principal curvatures are greater than zero as a result of which local gouging will not occur. And hence the biggest tool available in the machine shop is selected. This is illustrated with the help of Figure 7.2.

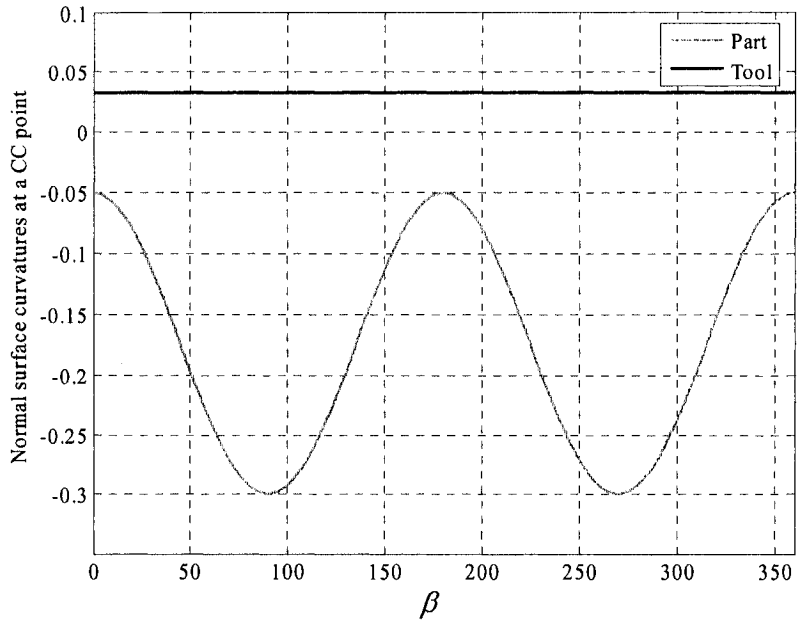

Figure 7.2. An example of case (b)

It can be seen from Figure 7.2, that the normal curvature of the cutting surface of even the biggest tool will be greater than that of the part surface in all tangent directions and hence local gouging will not occur.

7.3 Case(c): Saddle and Concave CC Point on the Part Surface

At a saddle and concave CC point the normal curvature of the part surface in the minimum curvature direction $\left(k_{s,\mathbf{T}_{t,\min}}\right)$ of the cutting surface of the tool is calculated. If for a saddle CC point, this value is negative the steps of case (c (i)) are followed. For the other cases of saddle CC point and for the concave CC point the steps of case (c (ii)) are followed.

7.3.1 Case(c (i))

The following are the steps to select the tool size

1. The biggest shank radius available $\left(R_{temp} = 30\ mm\right)$ is chosen as the temporary shank radius.
2. The temporary corner radius $\left(r_{temp}\right)$ is calculated from the equation given below

$$r_{temp} = \frac{1}{k_{s,\max}}$$

3. Based on the temporary shank and corner radius, the temporary principal curvatures $\left(k_{t,\max\_temp}, k_{s,\min\_temp}\right)$ as well as the temporary normal curvatures $\left(k_{t,temp}\right)$ of the cutting surface of the tool are calculated. These are compared in each tangent direction with the normal curvature of the part surface and if any tangent direction the criteria for local gouging is met, Step (4) is followed to determine another tool size otherwise these temporary tool sizes are taken to be as the final tool size for local gouge free machining.

4. The temporary corner radius is updated by reducing the size by 0.1 *mm* i.e. $r_{temp} = \left(r_{temp} - 0.1\right)\ mm$. Then the local gouging is again checked by Step 3. This process keeps on going until the value of corner radius is 2 *mm* or the tool size is such that there is no local gouging. Even after that if the local gouge free tool size is not determined, then the next biggest shank radius available of the tool sizes is selected as temporary shank radius and Steps (2-4) are again followed until the suitable tool is not selected.

An example is given in Figure 7.3 to illustrate this case

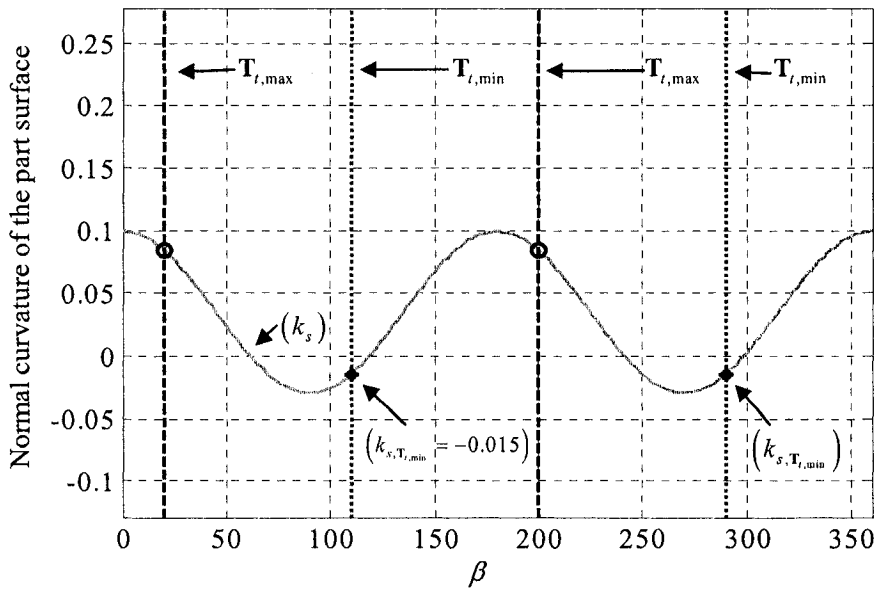

Figure 7.3. An example of case (c (i))

It can be seen from the figure that the condition for this case is met since $k_{s,\mathbf{T}_{t,\min}} = -0.015\ mm^{-1}$.So from Step (1), the temporary shank radius is selected $R_{temp} = 30\ mm$ and the corner radius from Step (2) is calculated to be $r_{temp} = 10\ mm$, based on these values the temporary normal curvatures are calculated and compared .The curvature plot is shown in Figure 7.4.

It can be seen from the normal curvature comparison plot in Figure 7.4 that local gouging condition is met, and hence the corner radius of the tool is updated and local gouging is again checked, the loop goes on until the tool size is such there is no local gouging. For the above example the tool size determined from the algorithm is $R = 30\ mm$ and $r = 5.6\ mm$. The curvature plot is shown in Figure 7.5.

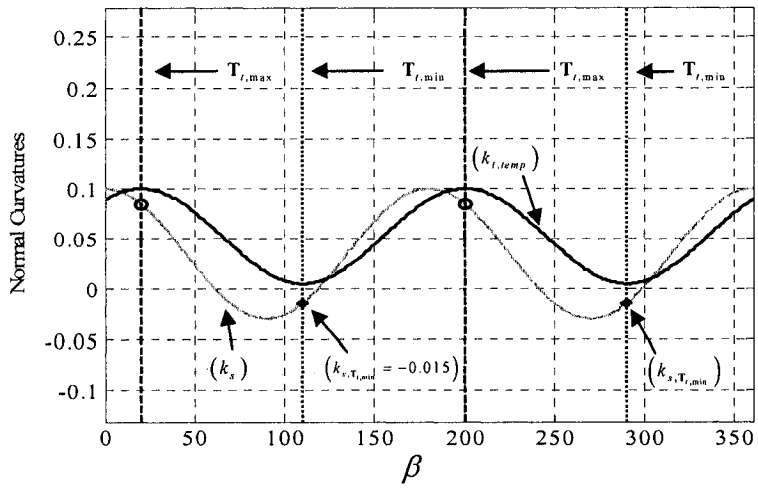

Figure 7.4. An example of case (c (i)) after the first loop.

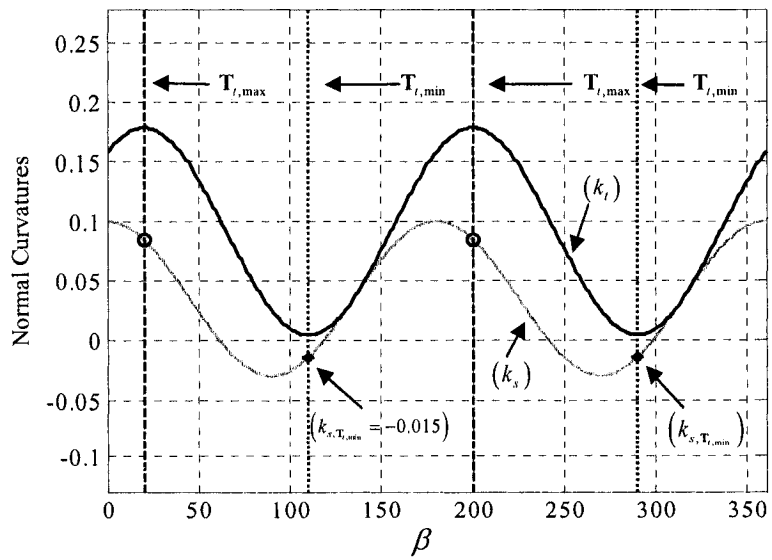

Figure 7.5. Solution for the case (c (i)).

7.3.2 Case(c (ii))

The following are the steps to calculative the tool size

1. The temporary corner radius $\left(r_{temp}\right)$ is calculated from the equation given below

$$r_{temp} = \frac{1}{k_{s,\max}}$$

2. The biggest shank radius $\left(R_{temp}\right)$ is calculated from the following equation

$$k_{s,\mathbf{T}_{t,\min}} = \frac{\sin\theta_0}{R_{temp} - r_{temp} + r_{temp}\cdot\sin\theta_0}$$

3. This value of R_{temp} is updated by the biggest shank radius available which is less than that R_{temp} calculated from Step (2).

4. Based on the temporary shank and corner radius, the temporary principal curvatures $\left(k_{t,\max\_temp}, k_{s,\min\_temp}\right)$ are calculated and then the temporary normal curvatures $\left(k_{t,temp}\right)$ of the cutting surface of the tool are calculated .These are compared in each tangent direction with the normal curvature of the part surface and if any tangent direction the criteria for local gouging is met, Step (5) is followed to determine a suitable tool size otherwise the temporary tool size is taken to be as the final tool size for local gouging free machining.

5. The temporary corner radius is updated by reducing it by 0.1 *mm* i.e. $r_{temp} = \left(r_{temp} - 0.1\right)\ mm$. Then the local gouging is again checked by Step (4). This process keeps on going until the value of corner radius is 2 *mm* or a tool size is such that local gouging would not occur. Even after that if the local gouge free tool size is not determined, then the next biggest shank radius available of the tool sizes is

selected as temporary shank radius and Step (5) is used to calculate temporary corner radius. The Steps (2)-(3) are followed only for the first loop, after that they are always skipped. The procedure is illustrated with the help of Figure 7.6

In this example the principal curvatures of the part surface are 0.1 and 0.01 mm^{-1}.The phase difference between the maximum curvature directions is 20^0 and $k_{s,\mathbf{T}_{t,\min}} = 0.021\ mm^{-1}$. Hence the condition of case(c (ii)) is met. From Step (1), the temporary corner radius $\left(r_{temp}\right)$ is calculated to be 10 *mm* .And from equation in Step (2), the temporary shank radius $\left(R_{temp}\right)$ is calculated to be 13.79 *mm.* From Step (3) this value is updated to 12 *mm.* And then normal curvatures are compared to check for local gouging as shown in Figure 7.7.

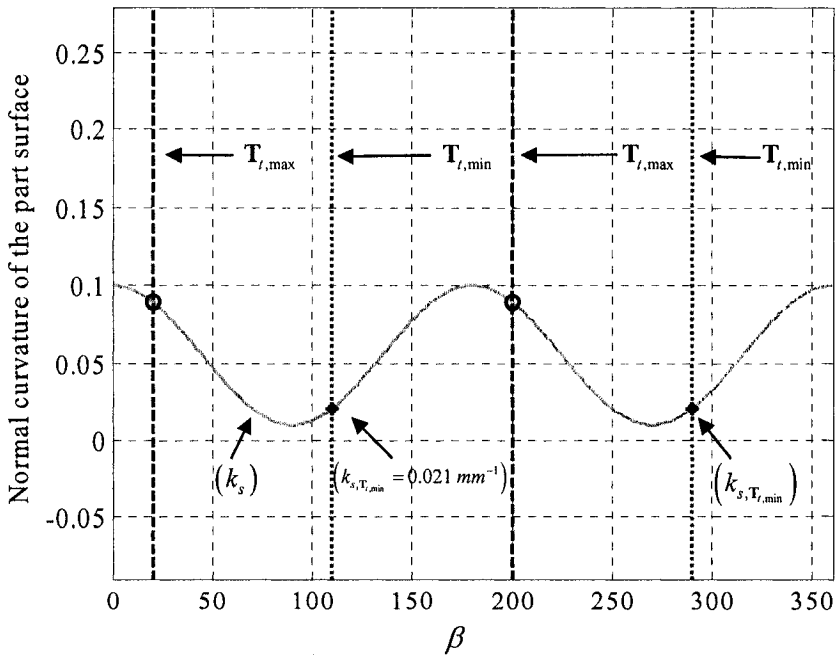

Figure 7.6. An example for case (c (ii))

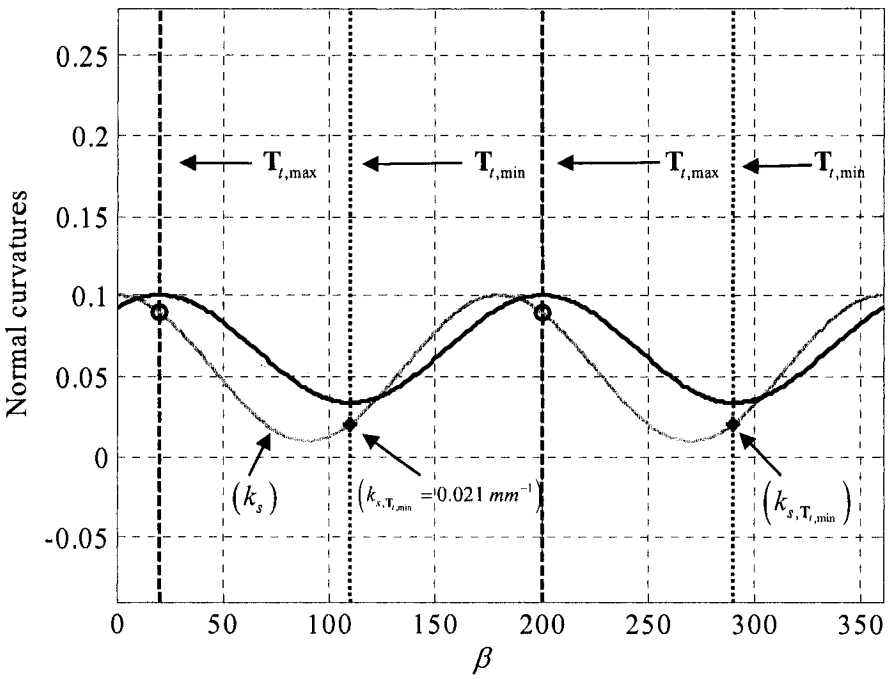

Figure 7.7. An example of case (c (ii)) after the first loop

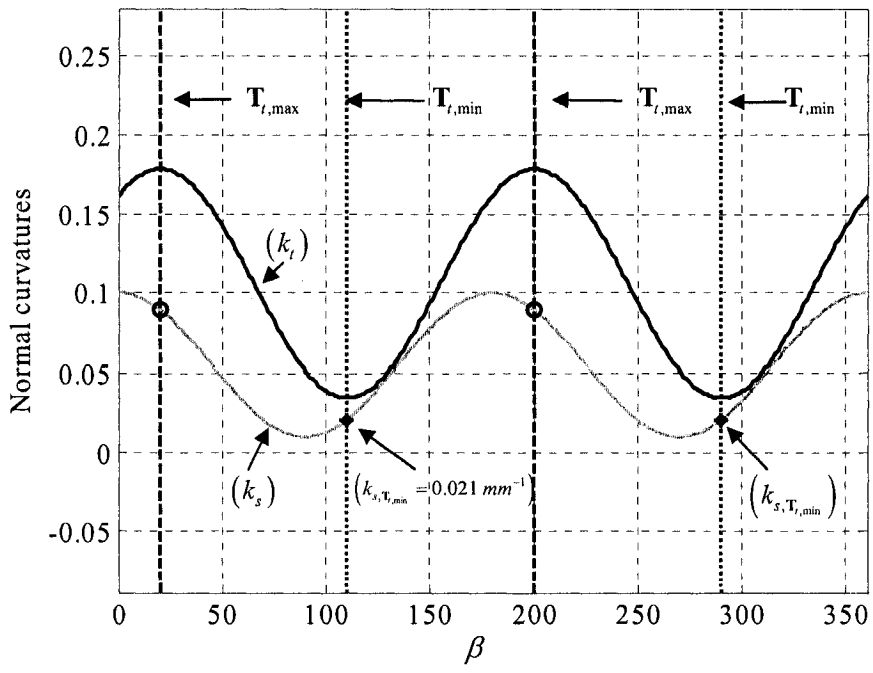

Figure 7.8. Solution for case (c (ii))

It can bee seen that criteria of local gouging has been met, and hence the corner radius of the tool is updated and local gouging is again checked, the loop goes on until the tool size is such there is no local gouging. For the above example the tool size determined from the algorithm is $R = 8\ mm$ and $r = 5.6\ mm$. The curvature plot is shown in Figure 7.8.

With this algorithm the tool size will be determined at one CC point, applying this algorithm over all the CC points would give a list of different tool sizes and the smallest of the shank radius and corner radius from the list of all shank radii and corner radii will be selected. The tool size determined will not locally gouge the part surface at any CC point and hence can be used for CNC machining for these parts.

Chapter 8 Comprehensive Curvature Analysis for Compound Surface Machining

Compound surfaces are widely used in the computer-aided mechanical design, and a compound surface usually consists of several surface patches connected with G^1 or G^2 continuity. The curvature analysis at an interior surface point on the compound surface is the same as the way introduced in Chapter 6 . However, for a CC point on the borders between the patches, the evaluation of the geometric mis/match between the cutting surface and the neighboring patches becomes more difficult, although the governing equations of curvature analysis for a single surface are still effective.

To solve this problem, for Patch 1, the maximum curvature is $k_{s1,\max}$, its principal direction is $\mathbf{T}_{s1,\max}$, and the angle between $\mathbf{T}_{t,\max}$ and $\mathbf{T}_{s1,\max}$ is α_{s1}. The tangents of the patch boundary at the border point, which define the interiors of the neighboring patches, can be calculated as $\mathbf{B}_1$ and $\mathbf{B}_2$ (see Figure 8.1). So the angles between the boundary tangents and the reference axis $\mathbf{T}_{t,\max}$ are α_{B1} and α_{B2}, and the normal curvatures of Patch 1 is

$$k_{s1}(\alpha) = k_{s1,\max} \cdot \cos^2(\alpha - \alpha_{s1}) + k_{s1,\min} \cdot \sin^2(\alpha - \alpha_{s1}) \qquad \alpha \in [0, \alpha_{B1}] \text{ and } [\alpha_{B2}, 2\pi] \qquad (8.1)$$

Similarly, the normal curvature formula for Patch 2 at the border point can be found as (see Figure 8.1)

$$k_{s2}(\alpha) = k_{s2,\max} \cdot \cos^2(\alpha - \alpha_{s2}) + k_{s2,\min} \cdot \sin^2(\alpha - \alpha_{s2}) \qquad \alpha \in [\alpha_{B1}, \alpha_{B2}] \tag{8.2}$$

By applying the technique introduced in Chapter 6 , the curvatures of Patches 1 and 2 can be compared with those of the cutting surface in order to detect gouging for the border points.

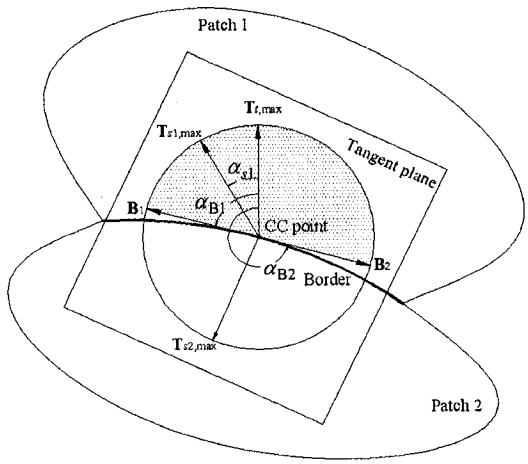

Figure 8.1. Illustration of compound surface machining using a bull-nose end-mill.

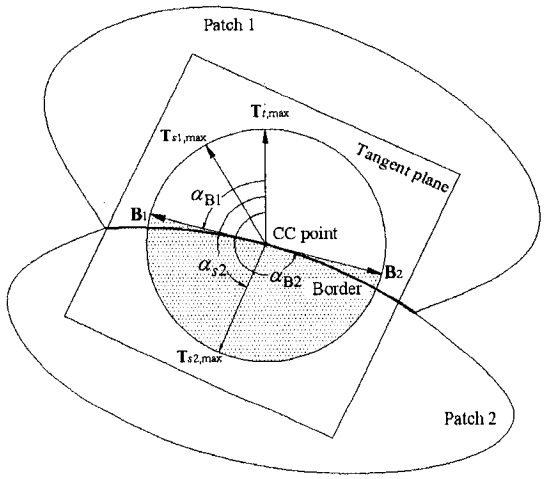

Figure 8.2. Illustration of compound surface machining using a bull-nose end-mill.

This technique can also be applied to compound surfaces with many patches to inspect the border points among the neighboring patches for potential local gouging.

Chapter 9 Applications

One of the main applications of this new approach for comprehensive curvature analysis is to detect local gouging for sculptured surface machining. To demonstrate its validity and efficiency in local gouging detection, this approach has been applied to several examples of sculptured surface machining. These examples are discussed below in detail.

9.1 Gouging Detection on a Horizontal Quarter Cylinder and a NURBS Surface with Similar Shape

In the first example, a horizontally oriented quarter cylindrical part with a radius of 20 *mm* and a length of 80 *mm* is as shown in Figure 9.1 (a), and a free- form part surface (Figure 9.1(b)) with a similar shape are adopted for gouging check. Both of these part surfaces are represented by NURBS surface with the same 3 by 5 control points, which are listed in Table 9-1. The weights of the control points for the free-form part surface are all assigned as one where as the weights for the quarter cylinder are as shown in Equation (9.1).

Table 9-1. Control points of the part surfaces.

	v direction		
u direction	(20,0,0)	(0,0,0)	(0,0,20)
	(20,20,0)	(0,20,0)	(0,20,20)
	(20,40,0)	(0,40,0)	(0,40,20)
	(20,60,0)	(0,60,0)	(0,60,20)
	(20,80,0)	(0,80,0)	(0,80,20)

$$w = \begin{bmatrix} 1 & 0.707 & 1 \\ 1 & 0.707 & 1 \\ 1 & 0.707 & 1 \\ 1 & 0.707 & 1 \\ 1 & 0.707 & 1 \end{bmatrix} \tag{9.1}$$

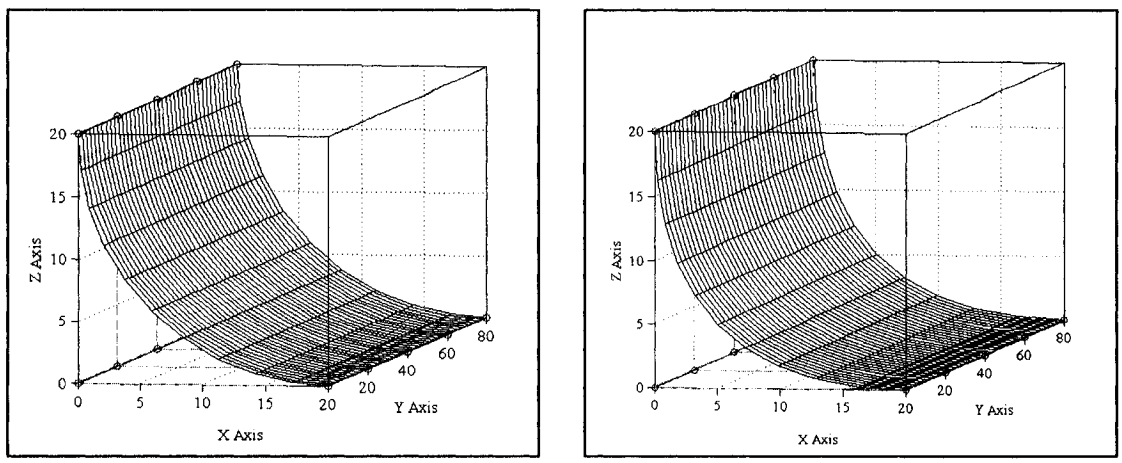

(a) **(b)**

Figure 9.1. A horizontal quarter cylindrical part and a free-form surface part.

The gouging check is applied to both these parts at a CC point with parametric value of $u=3$ and $v=0.5$. In the part coordinate system these parametric values represent CC point (5.85, 60, 5.85) and (5, 60, 5) respectively for the horizontally oriented quarter

cylinder and the free form surface respectively. In order to check gouging the comprehensive curvature analysis has to be applied at the CC point. For demonstration purposes a bull-nose end mill with shank radius of 20 *mm* and corner radius of 15 *mm* is chosen to machine the part surfaces at that point.

9.1.1 Comprehensive curvature analysis on the horizontally oriented quarter cylinder

The principal curvatures of the part surface are calculated to be 0.05 and 0.00 mm^{-1} and that of the cutting surface of the tool are calculated to be 0.07 and .046 mm^{-1}. It can be seen that from the principal curvatures that the condition of Case (6) is met. So the phase difference between the maximum curvature directions has been calculated to be $\alpha_0 = 0^0$, and based on this angle the normal curvatures are calculated in each tangent direction. The normal curvature plot is shown in Figure 9.2 (a). It can be seen that the normal curvature of the cutting surface of the tool is greater than that of the part surface in every tangent direction and hence it can be concluded that gouging will not occur at this CC point. This can be also be visually verified from the Figure 9.3 (a) that the tool does not cut into the part surface.

9.1.2 Comprehensive curvature analysis on free-form part surface

The principal curvatures of the part surface are calculated to be 0.07 and 0.00 mm^{-1} and that of the cutting surface of the tool are calculated to be 0.066 and .046 mm^{-1}. It can be seen that from the principal curvatures that the condition of case (4) is met. So gouging will occur in some tangent directions and hence normal curvatures have to be compared in order in order to know these tangent direction. The phase difference between the

maximum curvature directions has been calculated to be $\alpha_0 = 0^0$. The normal curvature plot is shown in Figure 9.2 (b). It can be seen that the normal curvature of the cutting surface of the tool is greater than that of the part surface in the tangent directions 0^0-16^0,163^0-197^0 and 344^0-360^0 and hence it can be concluded that gouging will occur in these directions at this CC point. This can also be visually verified from the Figure 9.3 (b) that the tool comes out of the part surface in these tangent directions.

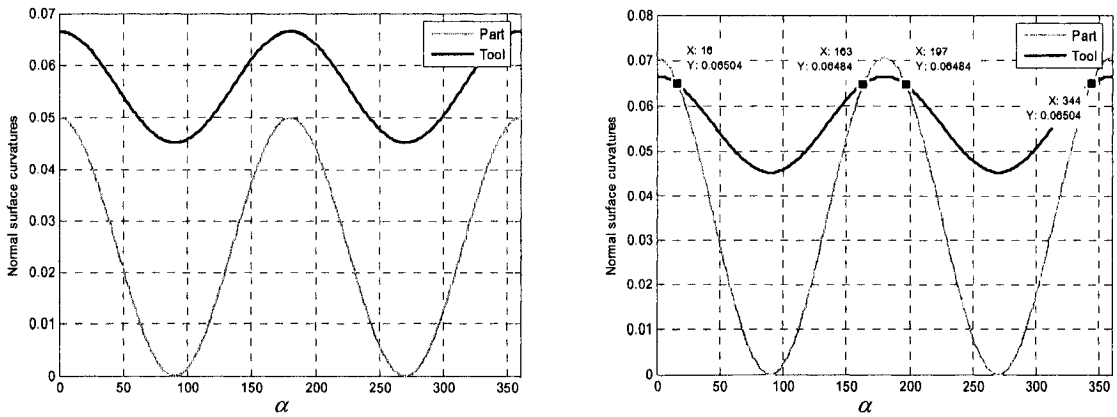

Figure 9.2. Normal curvatures of the part and the cutting surface at a CC point.

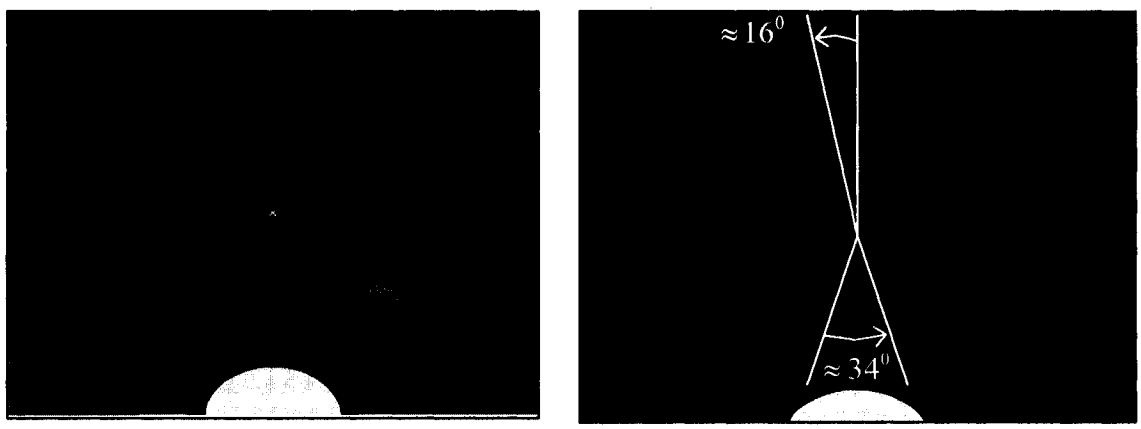

Figure 9.3. Surface and tool interaction at a CC point shown by CATIA.

Therefore it can be concluded that when these parts are machined with the same size tool, there is no gouging in horizontal cylinder whereas there is gouging in the free form part at the same CC point ($u=3$ and $v=0.5$.) although they have a similar shape. This is because of the fact that there curvatures have different values at the CC point.

9.2 Tool size determination for an horizontal quarter cylinder and NURBS surface with similar shape

From the algorithm for the tool size determination, since the principal curvatures of the horizontal quarter cylinder is same at all the CC point, the tool size determined at a CC point will be the same as that for all the other CC points and hence will be the tool size for local gouge free machining. The tool size determined for the horizontal cylinder by applying the practical tool size algorithm is $R=30$ *mm* and $r=20$ *mm*. The principal curvatures of cutting surface of the tool are calculated to be 0.05 mm^{-1} and 0.03 mm^{-1}. The surface and tool interaction as well as the normal curvature plot at a CC point is shown in . It can be seen from that local gouging will not occur at this CC point.

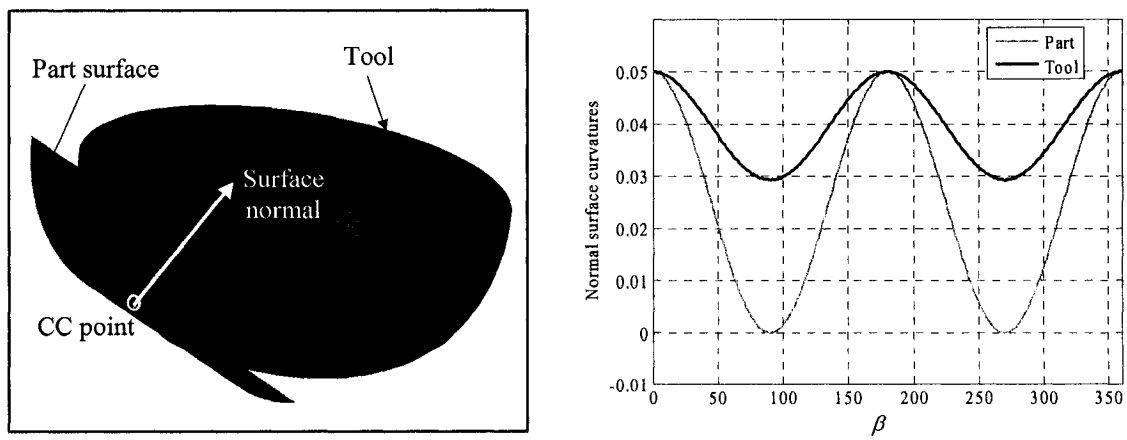

(a) Surface and tool interaction (b) Normal curvature plot

Figure 9.4. Surface and tool interaction and normal curvature plot.

For a NURBS surface of similar shape as that of the horizontally oriented cylinder the principal curvature varies along the different CC points and hence the minimum of the different shank and corner radii will be the tool size. The tool size determined from the practical tool size determination algorithm is calculated to be $R=30\ mm$ and r $=15\ mm$. The principal curvatures of the cutting surface of the tool are calculated to be 0.071 mm^{-1} and 0.028 mm^{-1}. Since the principal curvatures for the part surface varies along different CC point and in order to show the validity of the practical tool size determination algorithm, the surface and tool interaction along with the normal curvature plot is shown at a CC point on the part surface which has the highest value of the principal curvatures. These are shown in Figure 9.5. It can be seen from the figure that gouging does not occur even at a CC point with highest value of principal curvatures and hence it can be concluded that gouging will not occur at any CC point.

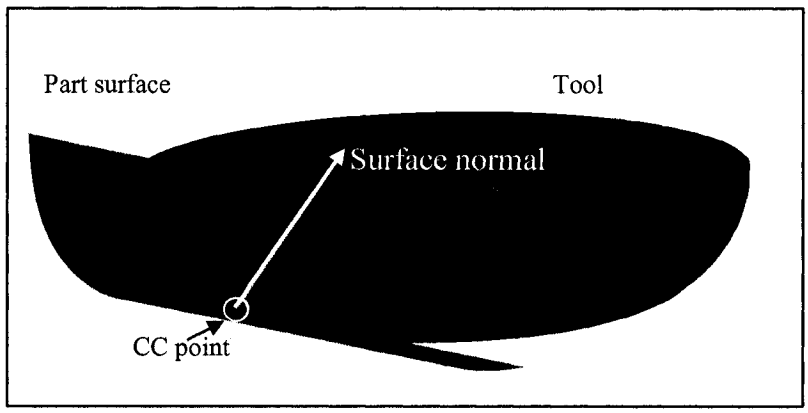

(a) Surface and tool interaction at a CC point.

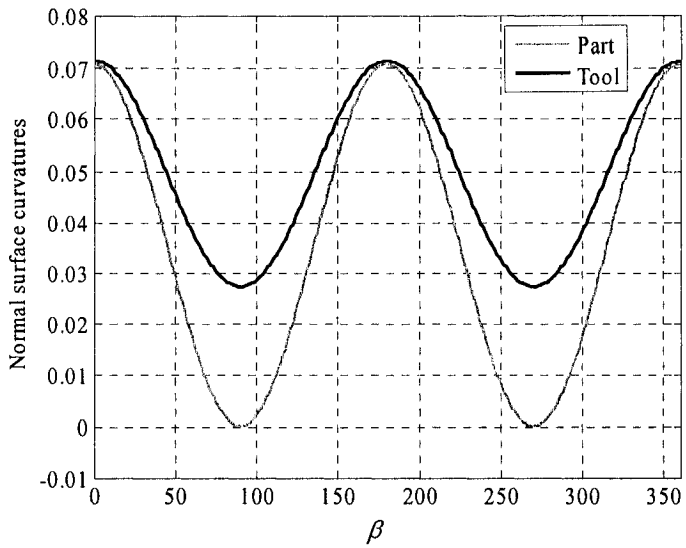

(b) Normal curvature plot at a CC plot.

Figure 9.5. Surface and tool interaction and normal curvature plot.

9.3 Gouging Detection on the Vertical Quarter Cylinder and NURBS Surface with Similar Shape

In the second set of example, both of the parts are the same as in the first set of example, the only difference is that they are vertically oriented instead of horizontally oriented. The control points of these parts are listed in Table 9-2.The tool used to check gouging is of the same size as that used in the first example i.e. R = 20, r = 15 .The CC point for gouging check is $u=3$ and $v=0.5$. In terms of the part coordinate system these points are (5.858, 5.858, 12.5) and (5.0, 5.0, 12.5) for the vertical cylinder and free form part respectively.

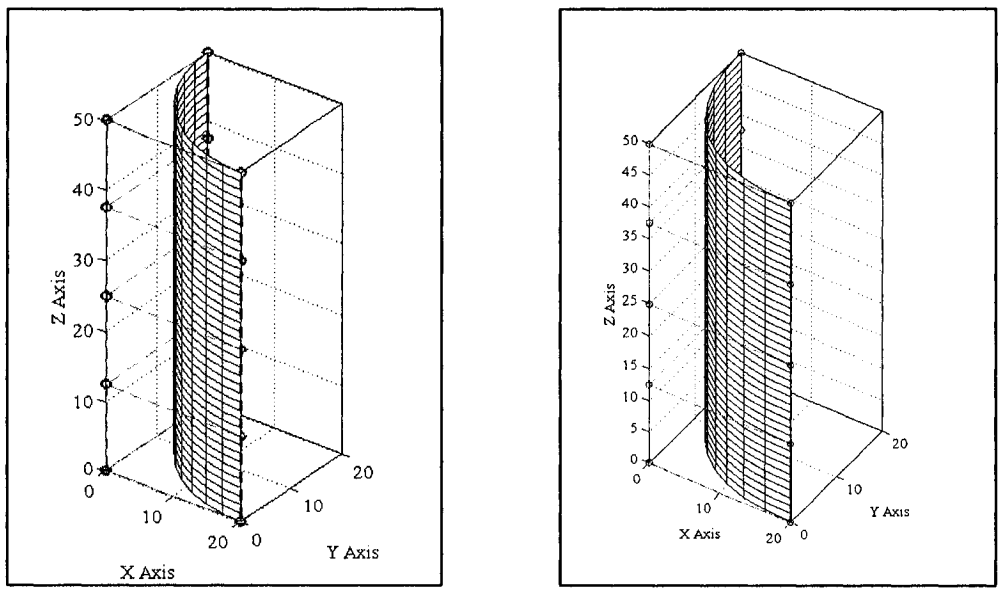

Figure 9.6. A vertical quarter cylindrical part and a free-form surface.

Table 9-2. Control points of the part surfaces.

	v direction		
u direction	(20,0,50)	(0,0,50)	(0,0,50)
	(20,0,37.5)	(0,0,37.5)	(0,20,37.5)
	(20,0,25)	(0,0,25)	(0,20,25)
	(20,0,12.5)	(0,0,12.5)	(0,20,12.5)
	(20,0,0)	(0,0,0)	(0,20,0)

9.3.1 Comprehensive curvature analysis on vertically oriented quarter cylinder

The principal curvatures of the part surface at a CC point are calculated to be 0.05 and 0.00 mm^{-1} and that of the cutting surface of the tool are calculated to be 0.066 and .05 mm^{-1}. From the values of the principal curvatures, the condition for case (2) has been met, and hence no local gouging will occur and therefore detailed curvature analysis can

be omitted. This can be visually verified from the Figure 9.7 (a). This figure is tilted a little bit in order to show that the tool does not gouge the part in any direction. The same figure is shown from a different view i.e. when projected from a viewpoint inside the cutter along the surface normal direction in Figure 9.7 (b).

9.3.2 Comprehensive curvature analysis on free form part surface

The principal curvatures of the part surface are calculated to be 0.07 and 0.00 mm^{-1} and that of the cutting surface of the tool are calculated to be 0.066 and .05 mm^{-1} at the CC point. From the values of the principal curvatures the condition of case (4) is met. So gouging will occur in some tangent directions and hence normal curvatures have to be compared in order in order to know these tangent direction. The phase difference between the maximum curvature directions has been calculated to be $\alpha_0 = 90^0$. The normal curvature plot is shown in Figure 9.8.

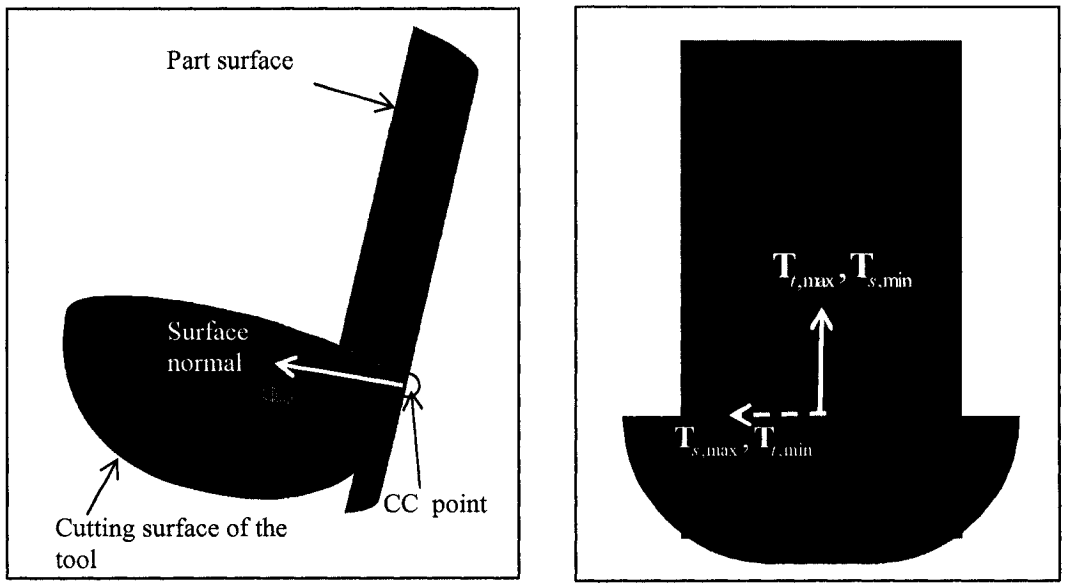

Figure 9.7. Surface and tool interaction at a CC point shown by CATIA

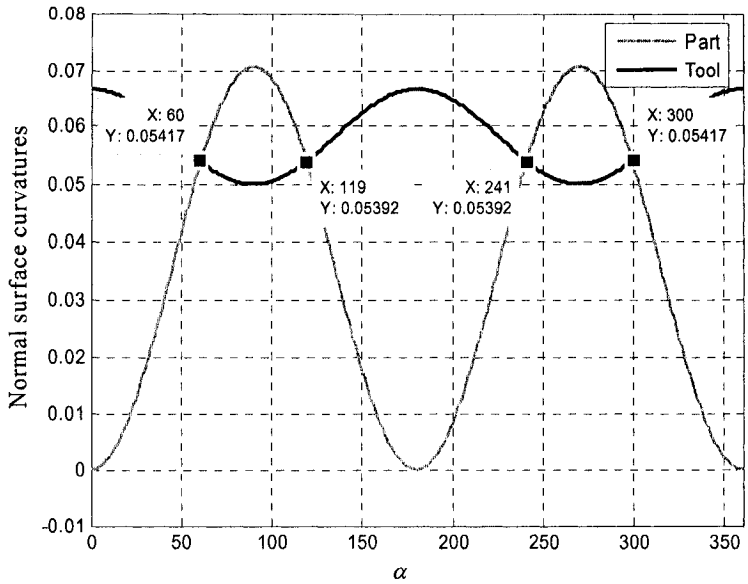

Figure 9.8. Curvature plot for a free-form surface.

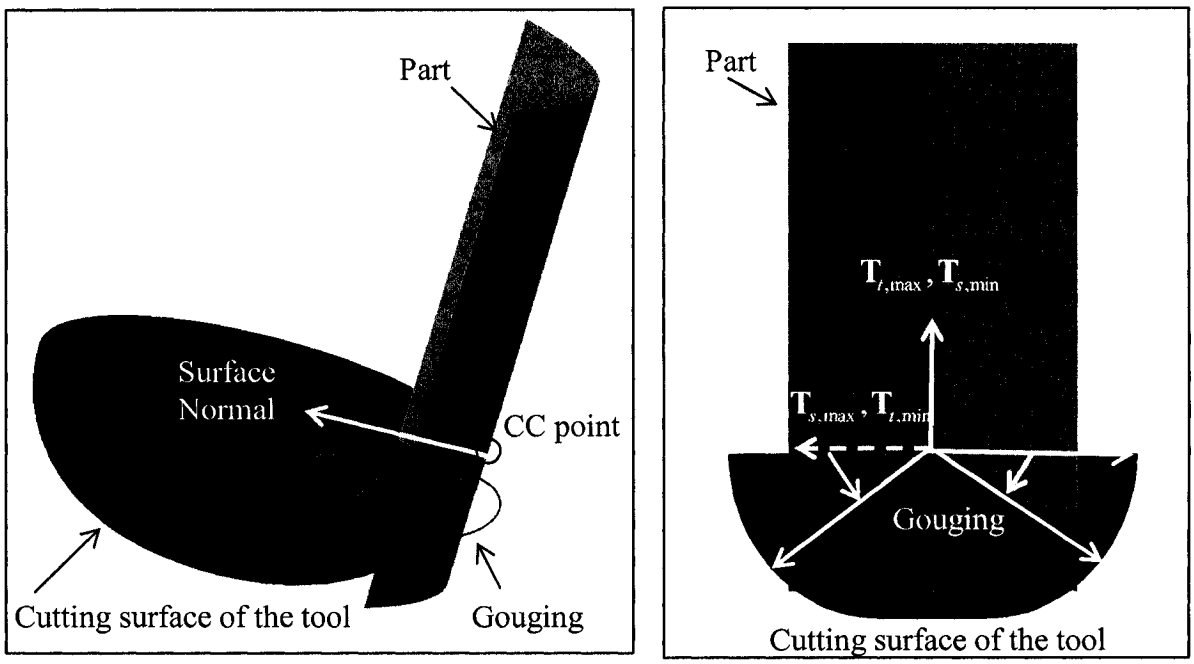

(a) (b)

Figure 9.9. Surface and tool interaction at a CC point shown by CATIA.

This can be clearly seen from Figure 9.9 (a) that the tool is coming out of the part surface in some tangent directions. The exact directions can be seen from a different view i.e. when projected from a viewpoint inside the cutter along the surface normal direction as shown in Figure 9.9.Since the CC point for the cutting surface of the tool is at $\theta_0 = 0$.So there will be no portion of the cutting surface of the tool in the tangent directions from 0^0-90^0 and 270^0-360^0. Hence gouging will occur in some regions in tangent directions from 90^0-270^0 .These regions are shown in Figure 9.9 (b).

9.4 Comprehensive Curvature Analysis on Quarter Horizontal and Vertical Cylinder

In the above two examples, gouging did not occur at the CC points of the horizontal and vertical cylinders. In this example, a different size tool (R = 30, r =10) is adopted to check gouging at the same CC points of the two cylindrical parts. The principal curvatures of these two cylinders are the same and they are 0.05 and 0.00 mm^{-1}.

When machining at the CC point on the horizontal quarter cylinder, the principal curvatures of the cutting surface of the tool are 0.1 and 0.02 mm^{-1} and when machining a vertical cylinder, the principal curvatures are 0.1 and 0.033 mm^{-1}. It can be seen with both the parts, the condition of Case (6) has been met and hence gouging may or may not occur. The phase difference between the maximum curvature directions for the horizontal quarter cylinder and maximum curvature direction of the cutting surface is calculated to be $\alpha_0 = 0^0$. For the vertical cylinder $\alpha_0 = 90^0$ .The normal curvature plots are shown Figure 9.10. It can be seen that in there is no gouging when the bull-nose end mill

machines a CC point on the horizontal quarter cylinder, whereas there will gouging on vertical quarter cylinder when machining with the same size bull nose end although both the part surface have the same principal curvatures. The tool and surface interaction for both the cases have been shown in Figure 9.11. It can be visually verified from the figure that the tool is not coming out of the horizontal quarter cylinder but it is coming out (gouging) from the vertical quarter cylinder.

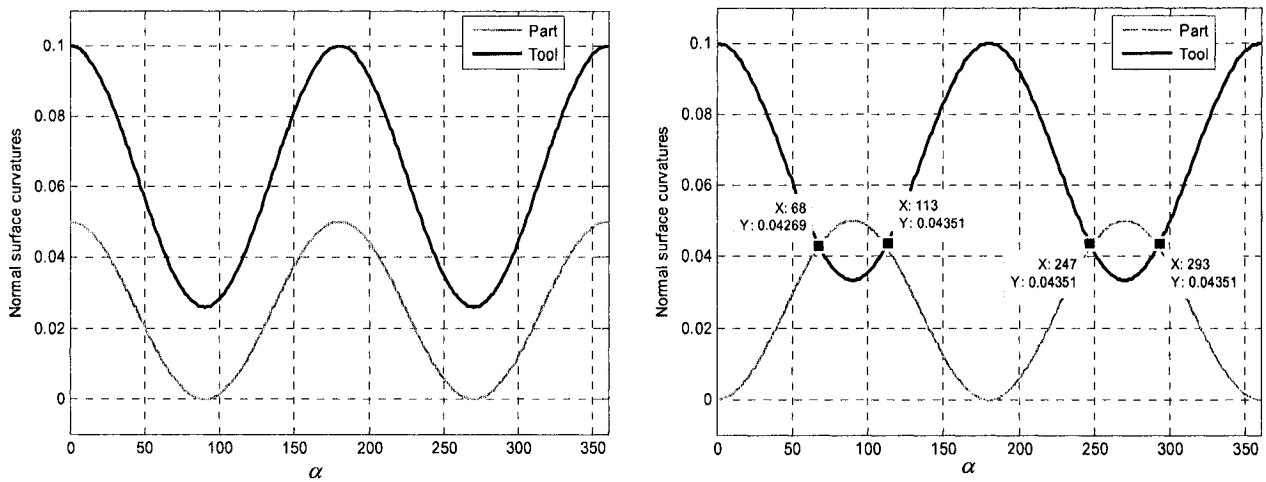

(a) Horizontal quarter cylinder (b) Vertical quarter cylinder

Figure 9.10. Comparison of normal curvature plots.

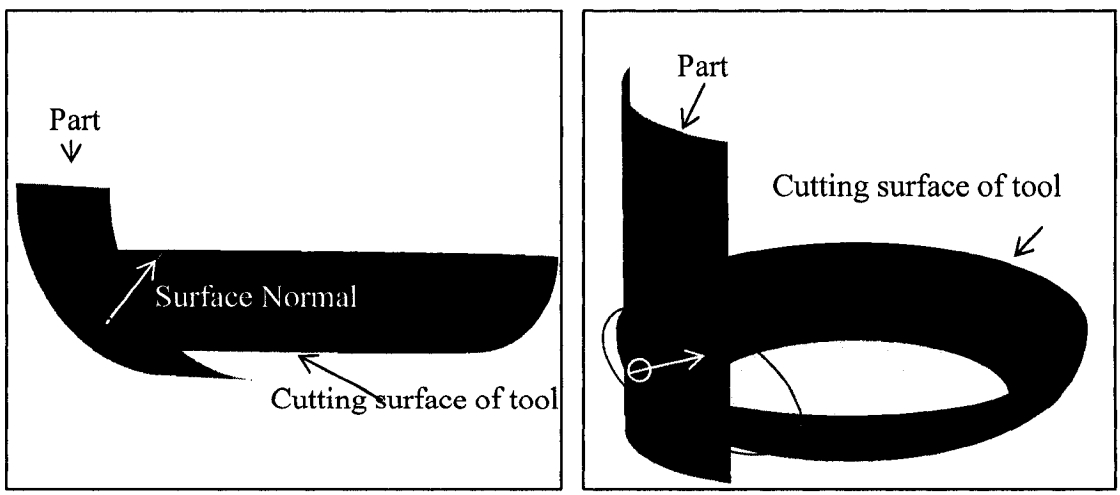

(a) Horizontal quarter cylinder (b) Vertical quarter cylinder

Figure 9.11. Surface and tool interaction at a CC point shown by CATIA.

9.5 Tool Size Determination for a Vertical Quarter Cylinder and NURBS Surface with Similar Shape

Similar to the case of horizontally oriented cylinder, the principal curvatures of the vertically oriented cylinder are the same at all the CC point, so the tool size determined for any CC point will be valid for all the other CC point. The tool size determined for the vertical cylinder by applying the practical tool size algorithm is $R=16\ mm$ and $r=16\ mm$. The principal curvatures of cutting surface of the tool will be the same and equal to 0.063 mm^{-1}. If the comparison of the principal curvatures is done, the condition of case (2) is met and can be concluded even without the normal curvature comparison that local gouging will not occur .The surface and tool interaction at a CC point in Figure 9.12

For the part surface with a similar shape, the principal curvature value changes at different CC points and hence the smallest of the shank radii and corner radii is taken as the tool size. Since the principal curvatures for the part surface varies along different CC point and in order to show the validity of the practical tool size determination algorithm, the principal curvature of the part surface having the largest value is compared with the principal curvatures of the cutting surface of the tool. For this part surface the tool size determined is $R=12\ mm$ and $r=11\ mm$. The principal curvatures are calculated to be 0.091 mm^{-1} and 0.083 mm^{-1}.Similar to the above the condition of case(2) has been met hence it can be concluded that gouging will not occur as can be also be seen from Figure 9.12 (b) and there is no need of normal curvature comparison.

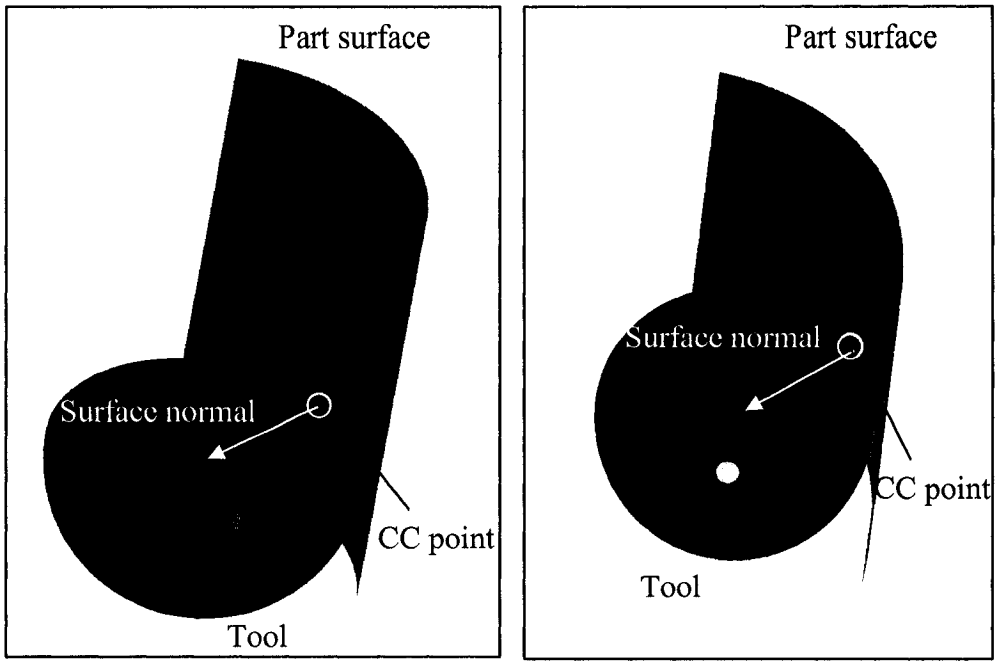

(a) Vertical quarter cylinder (b) Similar NURBS surface

Figure 9.12. Surface and tool interaction at a CC point shown by CATIA.

9.6 Comprehensive Curvature Analysis on Compound Surfaces

Compound surfaces are widely used in the computer-aided mechanical design, and a compound surface usually consists of several surface patches connected with G^1 and G^2 continuity. In this example a compound sculptured surface with two patches and with a G^1 (Tangent Continuity) is adopted. This is designed with the help of CATIA software and then with the help of IGES files, the control points are obtained which are then plugged into the MATLAB program to detect gouging for a compound surface on the border points. The compound surface is shown in Figure 9.13.Local gouging is checked at a CC point on the part surface with two different size bull nose end-mill.

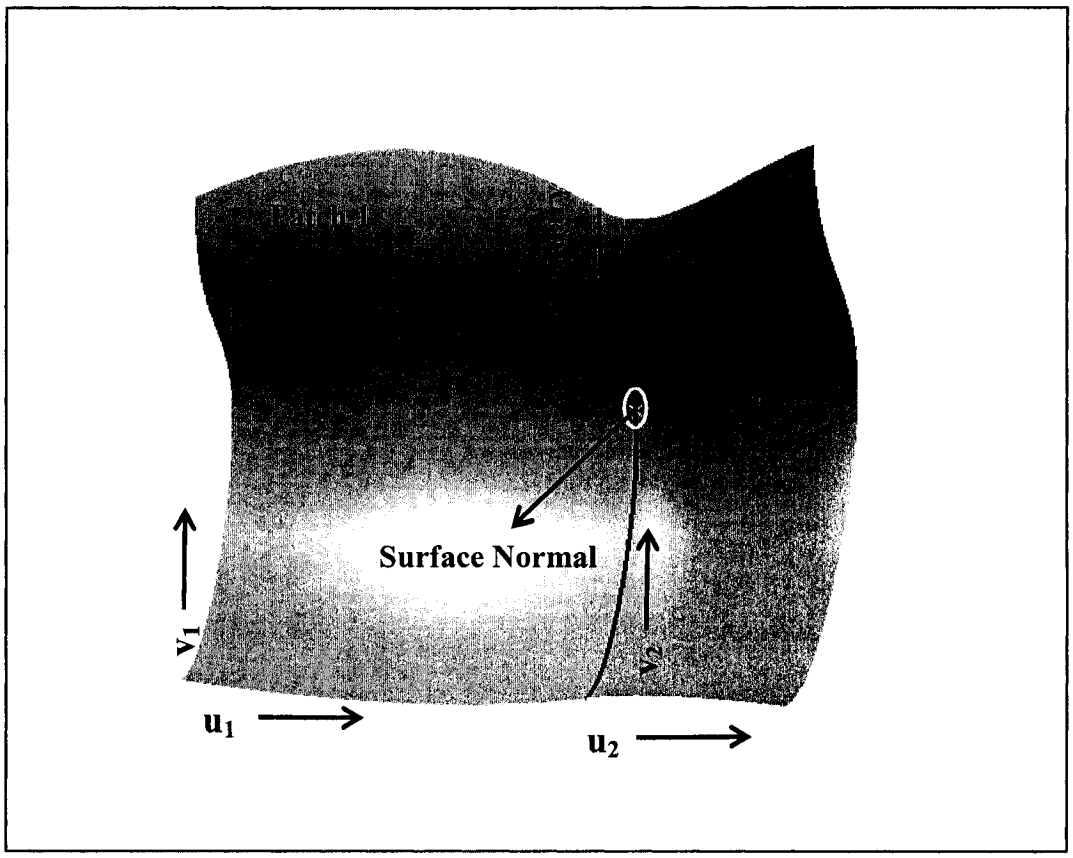

Figure 9.13. Compound surface with two patches.

With both the tool all the values to be calculated will be the same at that CC point except the principal curvatures of the cutting surface of the tool. The common values are calculated and listed in Table 9-3. The tangent of the patch boundary is calculated to be $\mathbf{B}_1 = -\mathbf{B}_2 = \begin{bmatrix} -0.728 & 0 & -0.685 \end{bmatrix}^T$.

Table 9-3. Calculated parameters of compound surface.

Parameters of the part Surface	Patch 1	Patch 2
Number of control points $(u\ (row) \times \mathrm{v}\ (\mathrm{column}))$	(13 × 5)	(12 × 4)
Order $(k = u$ curve , $l = v$ curve$)$	$k_1 = 4\ ,\ l_1 = 2$	$k_2 = 4\ ,\ l_2 = 4$
Range of parameter	$u_1 \in [0,10]\ ,\ \mathrm{v}_1 \in [0,4]$	$u_2 \in [0,9]\ ,\ \mathrm{v}_2 \in [0,1]$
Parametric value at CC point	$u_{1,cc} = 5.7\ ,\ \mathrm{v}_{1,cc} = 4$	$u_{2,cc} = 4.563\ ,\ \mathrm{v}_{2,cc} = 0$
CC point in part coordinate system	$(69.108, 0, -17.235)$	$(69.108, 0, -17.235)$
Maximum curvature at CC point	$k_{s1,\max} = 0.0454\ mm^{-1}$	$k_{s2,\max} = 0.0444\ mm^{-1}$
Minimum Curvature at CC point	$k_{s1,\min} = -0.0122 mm^{-1}$	$k_{s1,\min} = -0.1158\ mm^{-1}$
Maximum curvature direction at CC point on the part surface	$\mathbf{T}_{s1,\max} = \begin{bmatrix} -0.723 \\ 0.027 \\ -.690 \end{bmatrix}$	$\mathbf{T}_{s2,\max} = \begin{bmatrix} -0.732 \\ 0.025 \\ -.681 \end{bmatrix}$
Minimum curvature direction at CC point of the part surface	$\mathbf{T}_{s1,\min} = \begin{bmatrix} -0.188 \\ -0.969 \\ 0.159 \end{bmatrix}$	$\mathbf{T}_{s2,\min} = \begin{bmatrix} -0.162 \\ -0.972 \\ 0.171 \end{bmatrix}$

Table 9-4. Calculated values of the bull-nose end mill.

Parameter	Value
Maximum curvature direction at CC point on the cutting surface of the tool	$\mathbf{T}_{t,\max} = [0.662 \quad -0.245 \quad .708]$
Minimum curvature direction at CC point on the cutting surface of the tool	$\mathbf{T}_{t,\min} = [0.346 \quad 0.9381 \quad 0]$
Angles between boundary tangents (B1, B2) reference axis $\mathbf{T}_{t,\max}$	$\alpha_{B1} = 165^0$, $\alpha_{B2} = 345^0$
Angle between $\mathbf{T}_{t,\max}$ and $\mathbf{T}_{s1,\max}$	$\alpha_{s1} = 167^0$
Angle between $\mathbf{T}_{t,\max}$ and $\mathbf{T}_{s2,\max}$	$\alpha_{s2} = 165^0$

9.6.1 Gouging check with a bull nose end-mill (R = 25 mm, r = 12 mm)

In order to check gouging at a border point, a bull nose end mill adopted with a shank radius of 25 *mm* (R) and a corner radius (r) of 12 *mm*. The principal curvatures of cutting surface of the tool at the CC point are calculated to be 0.083 and 0.033 mm^{-1}. Comparing the values of the principal curvatures of the cutting surface of the tool and the two patches that the condition of Case (6) has been met and hence normal curvatures have to be compared in each tangent direction to check gouging.

Plugging the above calculated values in Equation (8.1) and Equation (8.2), and by representing the angles in degrees, we have

$$k_{s1}(\alpha) = 0.045 \cdot \cos^2(\alpha - 167^0) - 0.0122 \cdot \sin^2(\alpha - 167^0) \qquad \alpha \in [0^0, 165^0] \text{ and } [345^0, 360^0] \tag{9.2}$$

$$k_{s2}(\alpha) = 0.044 \cdot \cos^2(\alpha - 165^0) - 0.116 \cdot \sin^2(\alpha - 165^0) \qquad \alpha \in [165^0, 345^0] \tag{9.3}$$

The normal curvatures of the cutting surface of the tool is calculated to be

$$k_t(\alpha) = 0.08 \cdot \cos^2(\alpha) + 0.033 \cdot \sin^2(\alpha) \quad \alpha \in [0^0, 360^0] \tag{9.4}$$

A mathematical model for its comparison, can be formulated as

$$f_1(\alpha) = k_t(\alpha) - k_{s1}(\alpha) \quad \alpha \in [0^0, 165^0] \text{ and } [345^0, 360^0] \tag{9.5}$$

$$f_2(\alpha) = k_t(\alpha) - k_{s2}(\alpha) \quad \alpha \in [165^0, 345^0] \tag{9.6}$$

If the value of the function is negative in any tangent direction, gouging will occur in those directions otherwise, there will be no local gouging. For this case both the functions are positive in their domain and hence gouging will not occur. The same result can be obtained by plotting the normal curvatures of the cutting surface of the tool and the compound surface as in Figure 9.13 .It can be seen from the curvature plot that the normal curvature plot of the tool is greater than that of the compound part surface in all directions and hence there will be no local gouging. This can also be visually that the tool does not overcut the compound part surface at the CC point verified from Figure 9.15

9.6.2 Gouging check with a bull nose end-mill (R = 35 mm, r = 25 mm)

In this example a bigger size tool is adopted for gouge check at the same CC point at the boundary of the compound surface. The only values that are different from that of previous example are that of the principal curvature of the cutting surface of the tool and they are calculated to be $k_{t,\max} = 0.04\ mm^{-1}$ and $k_{t,\min} = 0.026\ mm^{-1}$.

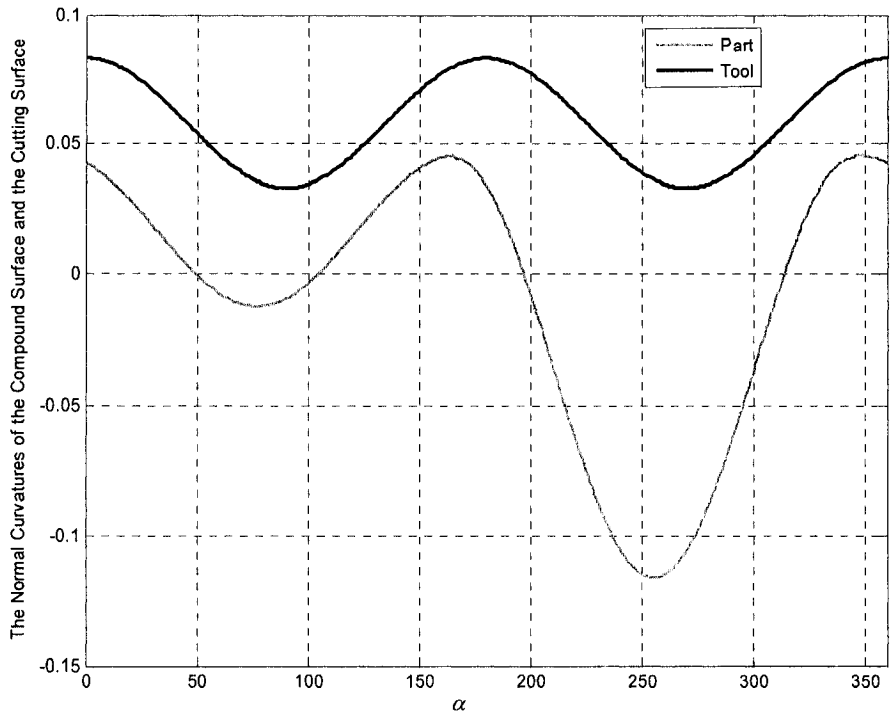

Figure 9.14. Normal curvature plot for compound surface and tool.

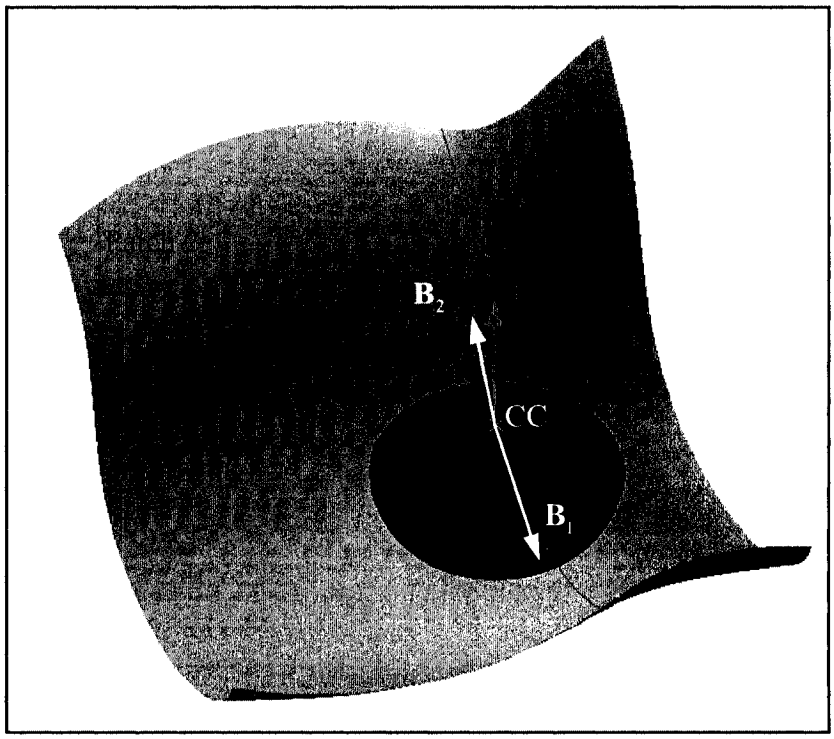

Figure 9.15. Tool and compound surface interaction at boundary.

The only difference would be in the value of Equation (9.3), and will become

$$k_t(\alpha) = 0.04 \cdot \cos^2(\alpha) + 0.026 \cdot \sin^2(\alpha) \quad \alpha \in [0^0, 360^0] \tag{9.6}$$

Similarly the mathematical model for its comparison, can be formulated as

$$f_1(\alpha) = k_t(\alpha) - k_{s1}(\alpha) \quad \alpha \in [0^0, 165^0] \text{ and } [345^0, 360^0] \tag{9.7}$$

$$f_2(\alpha) = k_t(\alpha) - k_{s2}(\alpha) \quad \alpha \in [165^0, 345^0] \tag{9.8}$$

For this case, the values of the function f_1 becomes negative in the tangent directions 0^0-4^0,141^0-165^0 and 345^0-360^0,whereas the function f_2 becomes negative in the tangent directions 165^0-177^0 and 336^0-345^0. And hence gouging will occur in these tangent directions. The same result can be seen from the curvature plot in Figure 9.16 and from Figure 9.17-Figure 9.18.

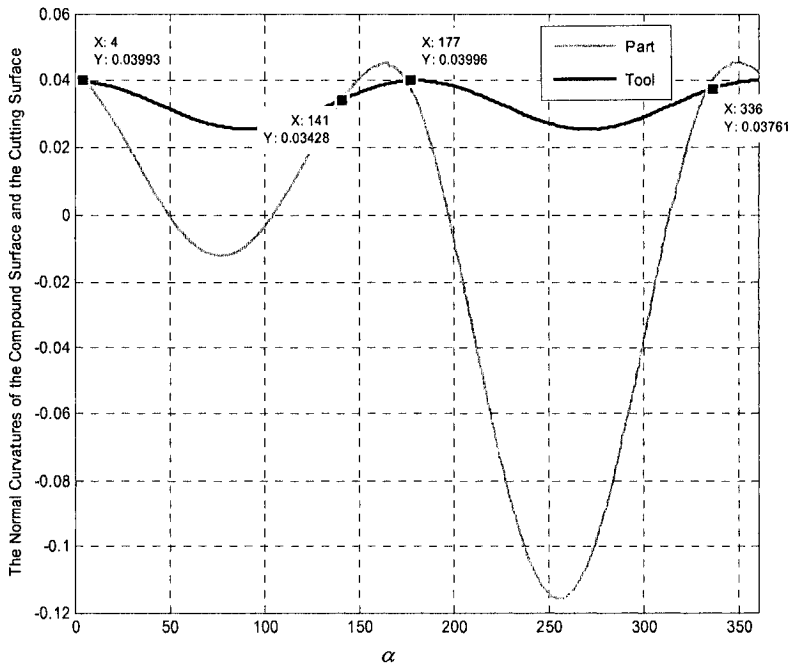

Figure 9.16. Normal curvature plot for compound surface and tool.

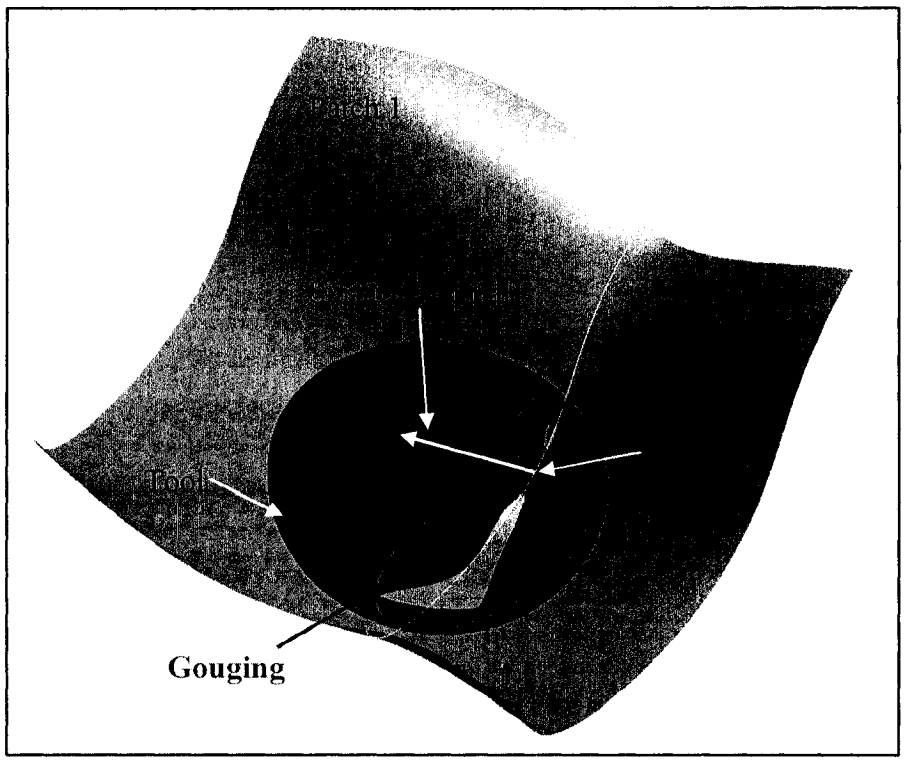

Figure 9.17. Tool and compound surface interaction.

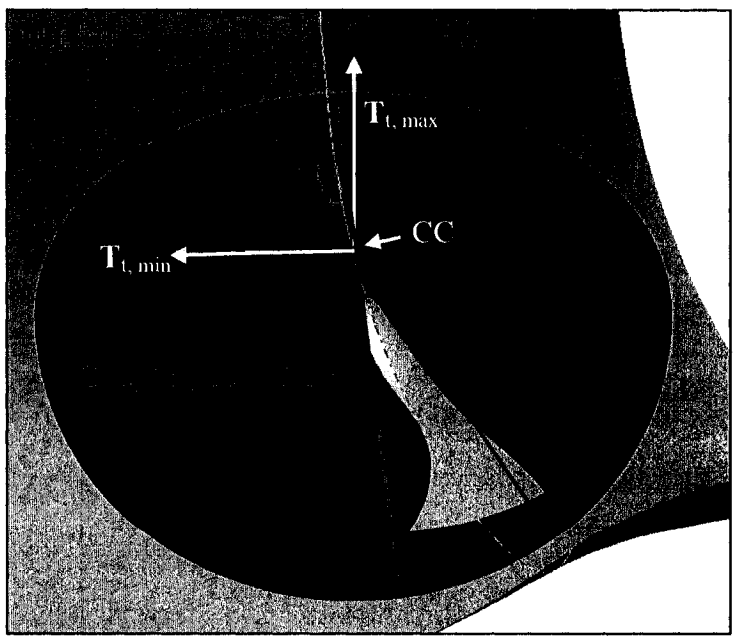

Figure 9.18. Local gouging on compound surface.

Chapter 10 Summary and Contributions

My thesis work provides a practical, accurate solution to local gouging detection and cutter size determination for 3-axis milling of sculptured surfaces, which is summarized in this section. In this work, first, I have reviewed a number of published literatures related with local gouging detection, and then I become familiar with the current ways to check local gouging. With extensive study on computer-aided geometric design and differential geometry, I fully understand the advantages and shortcomings of these methods; all of them are neither accurate nor practical due to lots of assumptions and approximations in them.

In order to overcome the shortcomings of the current methods, a new approach for comprehensive normal curvature analysis has been proposed to conduct accurate local gouging detection. The main idea of this approach includes (1) rough check based on the principal curvatures of the cutting and part surfaces at the CC points, and (2) detail check, if necessary, by comparing the normal curvatures of these surfaces along all tangent directions.

Second, the technical procedure of this approach is established, which contains four main steps. (1) The principal curvatures of the cutting and part surfaces are calculated. (2) The principal directions of the cutting surface are calculated, if required, and then transformed from the tool coordinate system to the part coordinate system. (3) The principal directions of the part surface are found in the part coordinate system. (4) Based on Euler's formula, the normal curvatures of the cutting and part surfaces are calculated and compared in all tangent directions in order to check against the criteria for local gouging. This new technique is applicable to single sculptured surfaces, more importantly, it is effective to inspect for local gouging on the borders of compound surfaces, where this defect always occurs. Furthermore, this approach has been employed to determine optimal, standard tool sizes for 3-axis finish milling of sculptured surfaces.

Next, a program system using MATLAB is made to implement this innovative approach. In the structure of the system, the program to detect local gouging at a CC point given the control points, weights and orders of a NURBS surface and the cutter size is the basis. Another advanced program is written to detect local gouging on the compound surfaces including their borders. A supplementary program is developed to determine tool sizes for effective surface machining.

Finally, to demonstrate its validity and robustness, this approach has been applied to some examples of different and typical surfaces. By using dominating CAD/CAM software - CATIA, I design all these surfaces with NURBS surface modeling and save

them in IGES format. After retrieving all the surface information from the IGES files, I feed it into my program system to get the results, which are presented in Chapter 9.

This research work significantly contributes to the scientific research on multi-axis CNC machining, and some of the highlights are listed here.

- Based on the comprehensive curvature analysis, local gouging can be detected quickly, accurately and completely for 3-axis finish machining of sculptured surface.
- Local gouging can be detected on the border points of a compound surface.
- Gouging can be detected for the regular tools, namely, torus , ball and flat end-mills.
- A practical tool size can be determined for machining without local gouging.
- A fundamental understanding has been raised that local gouging not only occurs along the principal directions of the cutting and part surfaces but also along other tangent directions.

Although this work solves the problem in local gouging detection, it is constrained to sculptured surfaces without global gouging during machining. A powerful approach can be obtained by combining this approach with an established method for global gouging detection, which can completely solve the gouging problem. The future work will be carried out on this topic. In all, my research has laid a solid foundation for gouging detection in 3-axis finish machining, and this work could be developed for 5-axis CNC machining.

Chapter 11 Bibliography

[1] A. Rao, R. Sarma, "On local gouging in five-axis sculptured surface machining using flat-end tools," *Computer-Aided Design*, 32 (2000) 409-420.

[2] A. Hatna, R.J. Grieve, "Pre-processing approach for cutter interference removal," *International Journal of Production Research*, 39(3) (2001) 435-460.

[3] D.C.H. Yang, Z. Han, "Interference detection and optimal tool selection in 3-axis NC machining of free-form surfaces," *Computer-Aided Design*, 31(5) (1999) 371-377.

[4] D.M. Etter, D.C. Kuncicky, *Introduction to MATLAB 6*, Prentice Hall, 2002.

[5] D. Yu, J. Deng, Z. Duan, J. Liu, "Generation of gouge-free cutter location paths on freeform surfaces for non-spherical cutters," *Computers in Industry*, 28 (1996) 81-94.

[6] G. Glaeser, J. Wallner, H. Pottmann, "Collision-free 3-axis milling and selection of cutting tools," *Computer-Aided Design*, 31 (1999) 225-232.

[7] H. Pottmann, J. Wallner, G. Glaeser, B. Ravani, "Geometric criteria for gouge-free three-axis milling of sculptured surfaces," *Transactions of ASME, Journal of Mechanical Design*, 121 (1999) 241-248.

[8] I. Zeid, *Mastering CAD/CAM*, McGraw Hill Higher Education, 2005.

[9] J.H. Yoon, H. Pottmann, Y.S. Lee, "Locally optimal cutting positions for 5-axis sculptured surface machining," *Computer-Aided Design,* 35 (2003) 69-81.

[10] J.H. Yoon, "Tool tip gouging avoidance and optimal tool positioning for 5-axis sculptured surface machining," *International Journal of Production Research*, 41(10) (2003) 2125-2142.

[11] J.H. Oliver, D.A. Wysocki, E.D. Goodman, "Gouge detection algorithm for sculptured surface NC generation," *Transactions of ASME, Journal of Engineering for Industry*, 115 (1993) 139-144.

[12] K.K. George, N.R. Babu, "On the effective tool path planning algorithms for sculptured surface manufacture," *Computers and Industrial Engineering*, 28(4) (1995) 823-838.

[13] K. Lee, *Principals of CAD/CAM/CAE Systems*, Addison Wesley Longman,1999.

[14] L. Zhou, Y.J. Lin, "An effective global gouge detection in tool-path planning for free-form surface machining," *The International Journal of Advanced Manufacturing Technology*, 18 (2001) 461-473.

[15] S.C. Lin, *Computer Numerical Control*, Delmar Publishers,1994.

[16] S.J. Chapman, *MATLAB Programming for Engineers,* Thomson Learning.

[17] X.C. Wang, Y. Yu, "An approach to interference-free cutter position for five-axis free-form surface side finishing milling", *Journal of Material Processing Technology*, 123 (2002) 191-196.

[18] X.M. Ding, J.Y.H. Fuh, K.S. Lee, "Interference detection for 3-axis mold machining," *Computer-Aided Design,* 33 (2001) 561-569.